Perseverance MEDA Atmospheric Pressure Observations - Initial Results

Ari-Matti Harri[1], Mark Paton[1], Maria Hieta[1], Jouni Polkko[1], Claire Newman[2], Jorge Pla-García[3], Joonas Leino[1], Terhi Mäkinen[1], Janne Kauhanen[1], Iina Jaakonaho[1], Agustín Sánchez-Lavega[4], Ricardo Hueso[5], Maria Genzer[1], Ralph D. Lorenz[6], Mark T Lemmon[7], Alvaro Vicente-Retortillo[3], Leslie Tamppari[8], Daniel Viúdez-Moreiras[9], Manuel de la Torre Juarez[10], Hannu Savijärvi[11], Jose Antonio Rodríguez-Manfredi[12], and German Martinez[13]

[1]Finnish Meteorological Institute
[2]Aeolis Research
[3]Centro de Astrobiología (CSIC-INTA)
[4]Universidad del Pais Vasco UPV/EHU
[5]UPV/EHU
[6]Johns Hopkins University Applied Physics Lab
[7]Space Science Institute
[8]Jet Propulsion Laboratory
[9]Centro de Astrobiología (INTA-CSIC)
[10]Jet Propulsion Laboratory- California Institute of Technology, Pasadena, CA, USA
[11]University of Helsinki
[12]Centro de Astrobiología
[13]Lunar and Planetary Institute

May 25, 2023

Abstract

The Mars2020 Perseverance Rover landed successfully on the Martian surface on the Jezero Crater floor (18.44°N, 77.45°E) at Martian solar longitude, L_s, $\sim$5 in February 2021. Since then it has produced highly valuable environmental measurements with a versatile scientific payload including the MEDA (Mars Environmental Dynamics Analyzer) suite of environmental sensors. One of the MEDA systems is the PS pressure sensor system which weighs 40 grams and has an estimated absolute accuracy of better than 3.5 Pa and a resolution of 0.13 Pa. We present initial results from the first 414 sols of Martian atmospheric surface pressure observations by the PS whose performance was found to meet its specifications. Observed sol-averaged atmospheric pressures follow an anticipated pattern of pressure variation in the course of the advancing season and are consistent with data from other landing missions. The observed diurnal pressure amplitude varies by $\sim$2-5 \% of the sol-averaged pressure, with absolute amplitude 10-35 Pa in an approximately direct relationship with airborne dust. During a regional dust storm, which began at $L_s~135^\circ$ the diurnal pressure amplitude roughly doubles. The diurnal pressure variations were found to be remarkably sensitive to the seasonal evolution of the atmosphere. In particular analysis of the diurnal pressure signature revealed diagnostic information likely related to the regional scale structure of the atmosphere. Comparison of Perseverance pressure observations to data from other landers reveals the global scale seasonal behaviour of Mars' atmosphere.

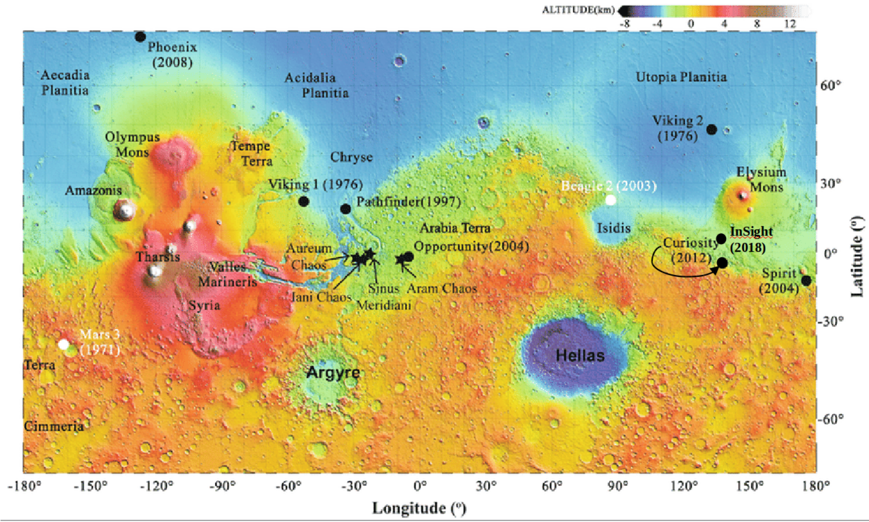

ALTITUDE(km)
-8 -4 0 4 8 12
Phoenix (2008)
Aecadia Planitia
Acidalia Planitia
Utopia Planitia
Olympus Mons
Tempe Terra
Chryse
Viking 2 (1976)
Viking 1 (1976)
Pathfinder(1997)
Beagle 2 (2003)
Elysium Mons
Amazonis
Arabia Terra
Opportunity(2004)
Isidis
Curiosity (2012)
InSight (2018)
Tharsis
Valles Marineris
Aureum Chaos
Iani Chaos
Sinus Meridiani
Aram Chaos
Spirit (2004)
Syria
Mars 3 (1971)
Terra
Argyre
Hellas
Cimmeria
60°
30°
0°
-30°
-60°
Latitude (°)
-180° -150° -120° -90° -60° -30° 0° 30° 60° 90° 120° 150° 180°
Longitude (°)

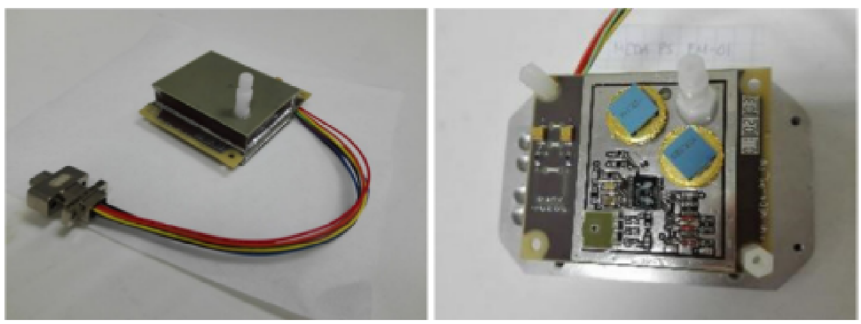

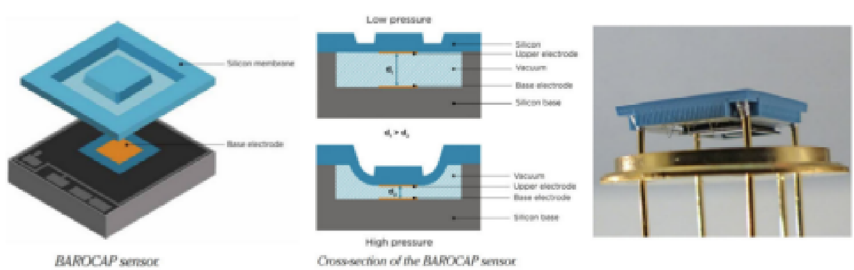

Silicon membrane
Base electrode
Low pressure
Silicon
Upper electrode
Vacuum
Base electrode
Silicon base
High pressure
BAROCAP sensor
Cross-section of the BAROCAP sensor

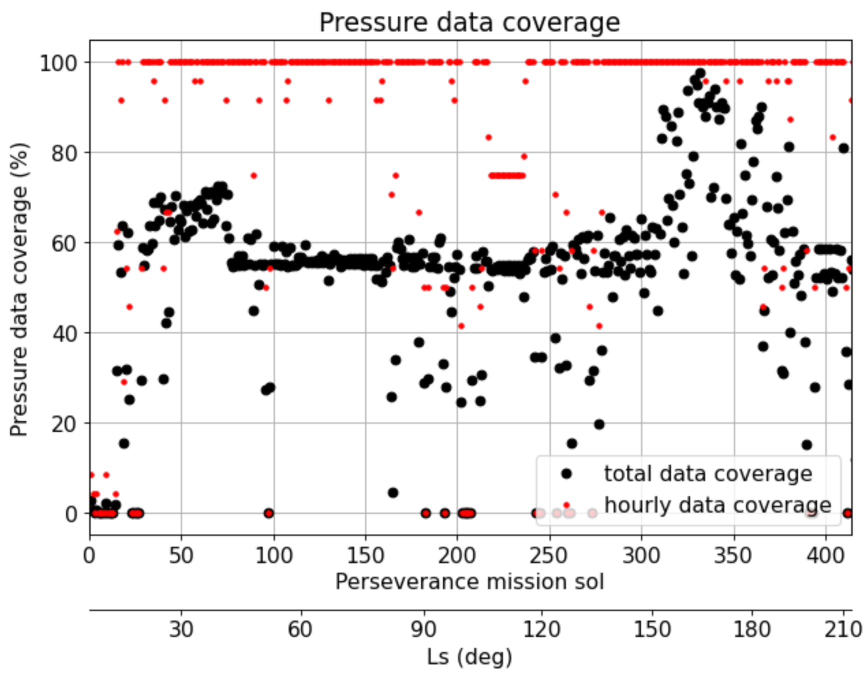
Pressure data coverage
Pressure data coverage (%)
100
80
60
40
20
0
0
50
100
150
200
250
300
350
400
Perseverance mission sol
30
60
90
120
150
180
210
Ls (deg)
total data coverage
hourly data coverage

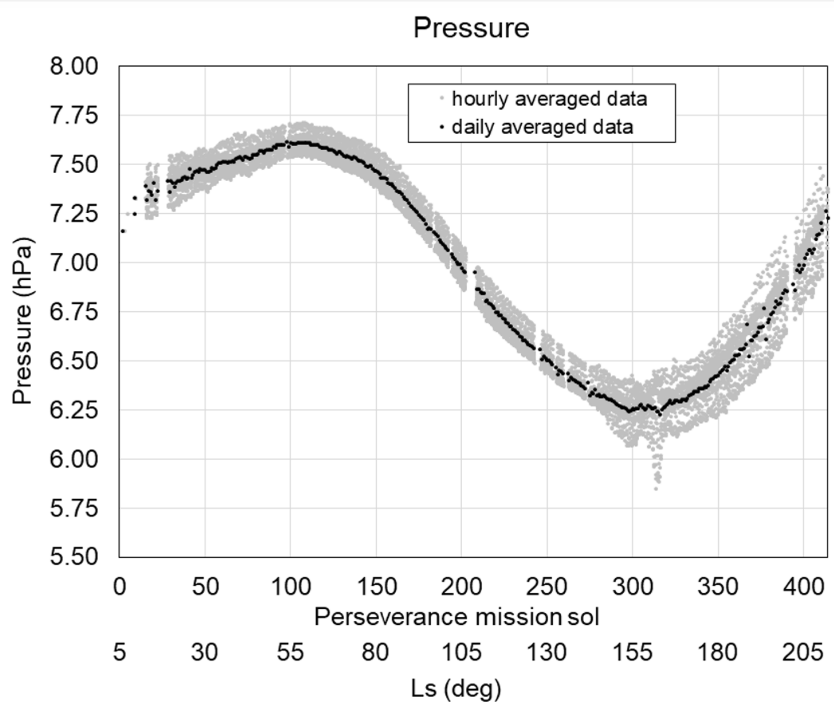
Pressure
Pressure (hPa)
8.00
7.75
7.50
7.25
7.00
6.75
6.50
6.25
6.00
5.75
5.50
hourly averaged data
daily averaged data
0
50
100
150
200
250
300
350
400
Perseverance mission sol
5
30
55
80
105
130
155
180
205
Ls (deg)

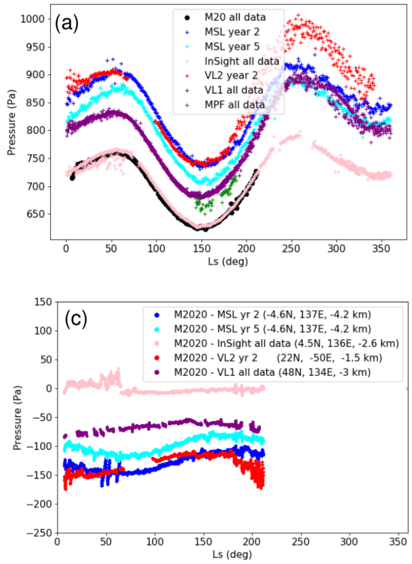
(a)
M20 all data
MSL year 2
MSL year 5
InSight all data
VL2 year 2
VL1 all data
MPF all data
Pressure (Pa)
Ls (deg)
(b)
Perseverance
MSL
InSight
VL2
VL1
Pressure (Pa)
Ls (deg)
(c)
M2020 - MSL yr 2 (-4.6N, 137E, -4.2 km)
M2020 - MSL yr 5 (-4.6N, 137E, -4.2 km)
M2020 - InSight all data (4.5N, 136E, -2.6 km)
M2020 - VL2 yr 2 (22N, -50E, -1.5 km)
M2020 - VL1 all data (48N, 134E, -3 km)
Pressure (Pa)
Ls (deg)
(d)
M2020 - MSL (-4.6N, 137E, -4.2 km)
M2020 - InSight (4.5N, 136E, -2.6 km)
M2020 - VL2 (48N, 134E, -3 km)
M2020 - VL1 (22N, -50E, -1.5 km)
Pressure (Pa)
Ls (deg)

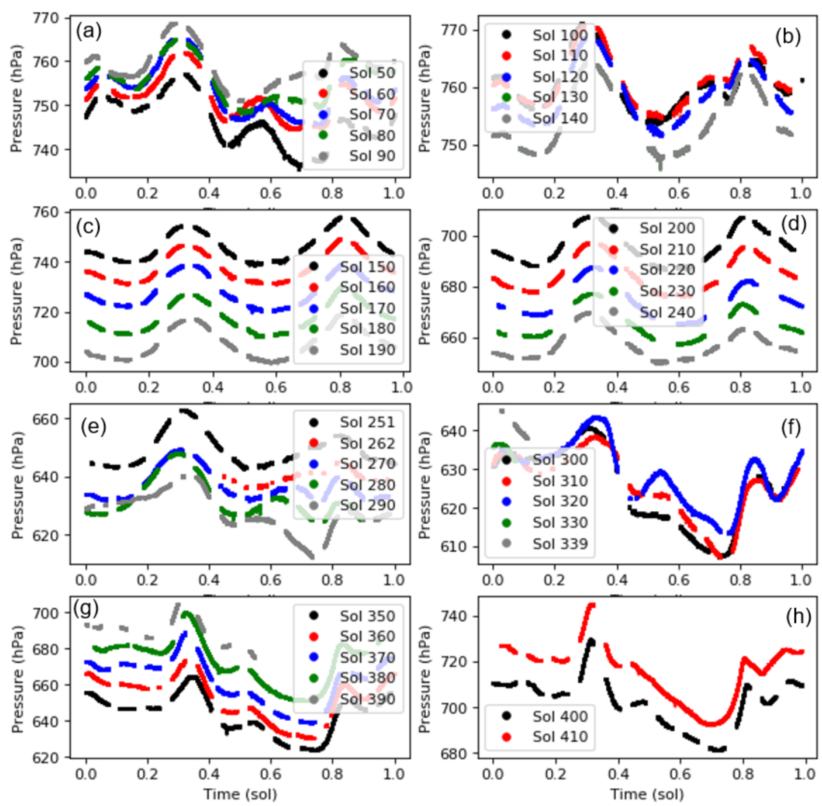
(a)
Sol 50
Sol 60
Sol 70
Sol 80
Sol 90
(b)
Sol 100
Sol 110
Sol 120
Sol 130
Sol 140
(c)
Sol 150
Sol 160
Sol 170
Sol 180
Sol 190
(d)
Sol 200
Sol 210
Sol 220
Sol 230
Sol 240
(e)
Sol 251
Sol 262
Sol 270
Sol 280
Sol 290
(f)
Sol 300
Sol 310
Sol 320
Sol 330
Sol 339
(g)
Sol 350
Sol 360
Sol 370
Sol 380
Sol 390
(h)
Sol 400
Sol 410
Pressure (hPa)
Time (sol)

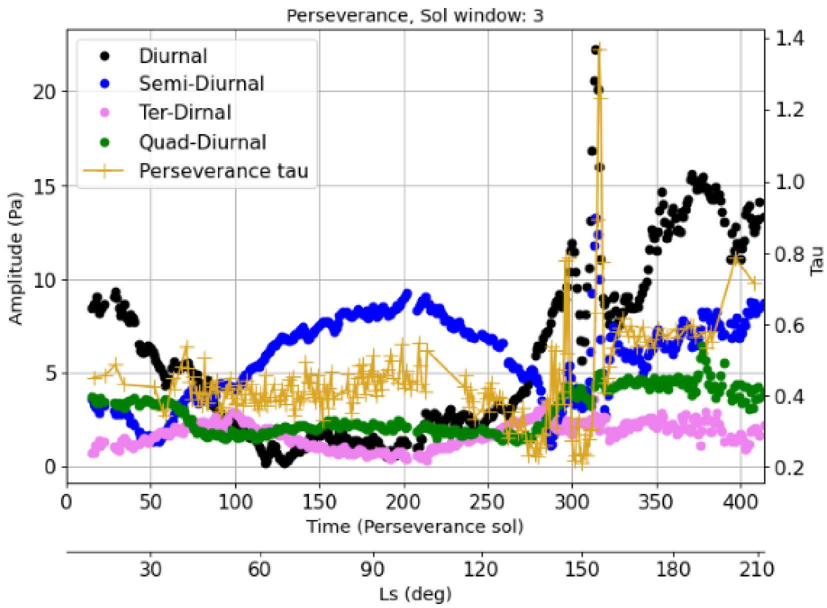
Perseverance, Sol window: 3
Diurnal
Semi-Diurnal
Ter-Dirnal
Quad-Diurnal
Perseverance tau
Amplitude (Pa)
Tau
Time (Perseverance sol)
Ls (deg)

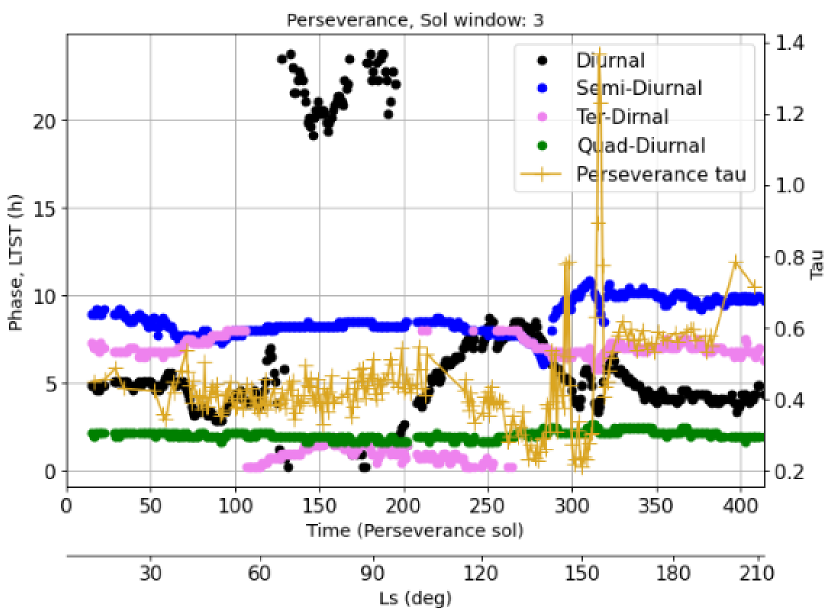
Perseverance, Sol window: 3
Diurnal
Semi-Diurnal
Ter-Dirnal
Quad-Diurnal
Perseverance tau
Phase, LTST (h)
Tau
Time (Perseverance sol)
Ls (deg)

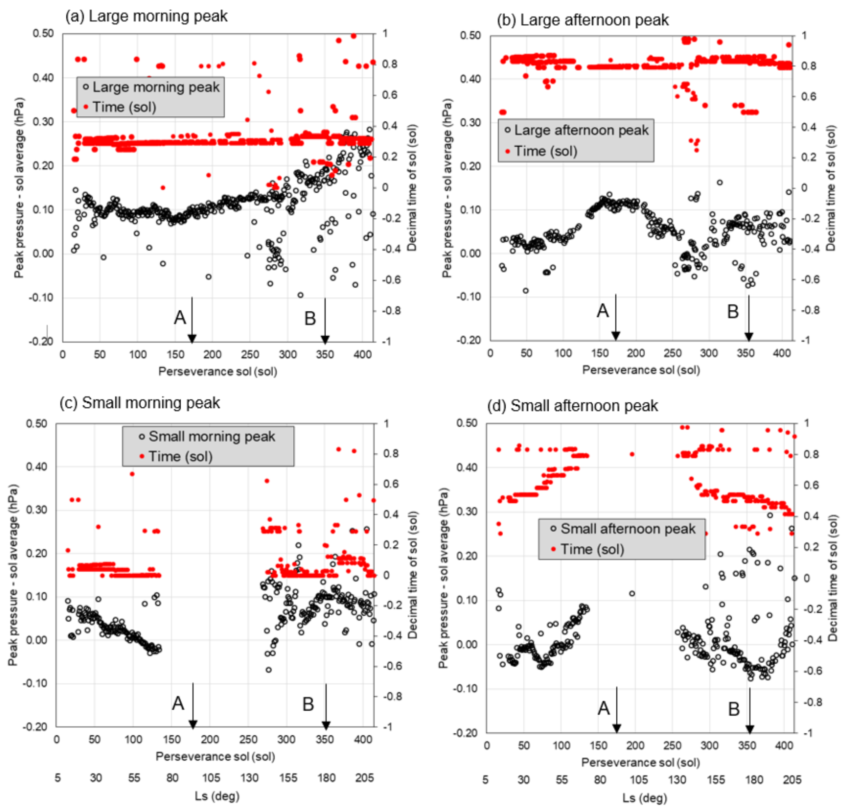

(a) Large morning peak
Large morning peak
Time (sol)
Peak pressure - sol average (hPa)
Decimal time of sol (sol)
Perseverance sol (sol)
A
B
(b) Large afternoon peak
Large afternoon peak
Time (sol)
(c) Small morning peak
Small morning peak
Time (sol)
Ls (deg)
(d) Small afternoon peak
Small afternoon peak
Time (sol)

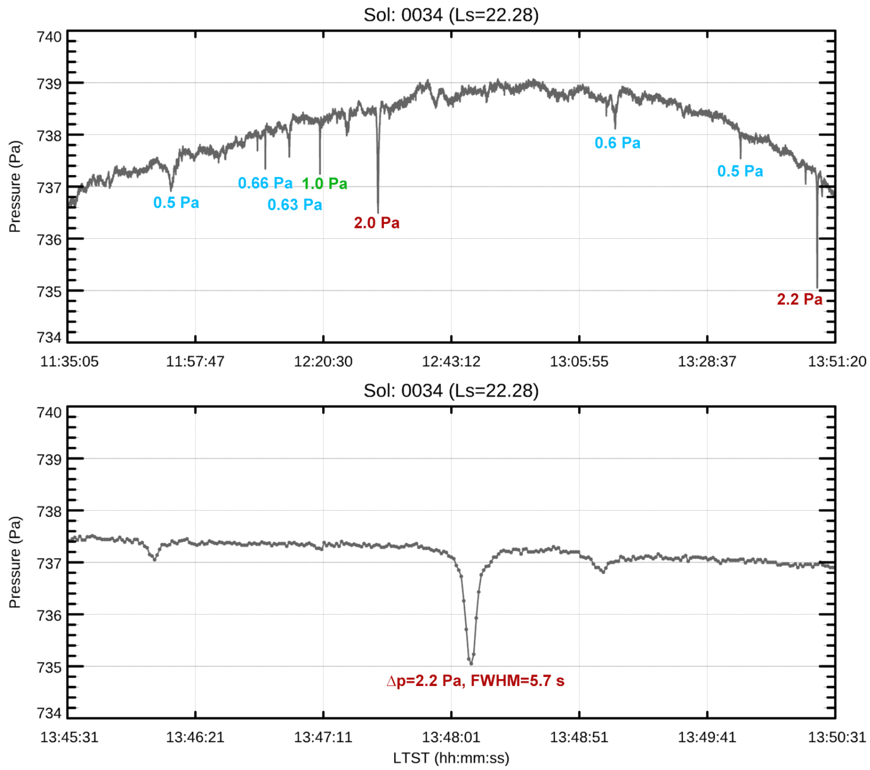
Sol: 0034 (Ls=22.28)
Pressure (Pa)
740
739
738
737
736
735
734
0.5 Pa
0.66 Pa
1.0 Pa
0.63 Pa
2.0 Pa
0.6 Pa
0.5 Pa
2.2 Pa
11:35:05
11:57:47
12:20:30
12:43:12
13:05:55
13:28:37
13:51:20
Sol: 0034 (Ls=22.28)
Pressure (Pa)
Δp=2.2 Pa, FWHM=5.7 s
13:45:31
13:46:21
13:47:11
13:48:01
13:48:51
13:49:41
13:50:31
LTST (hh:mm:ss)

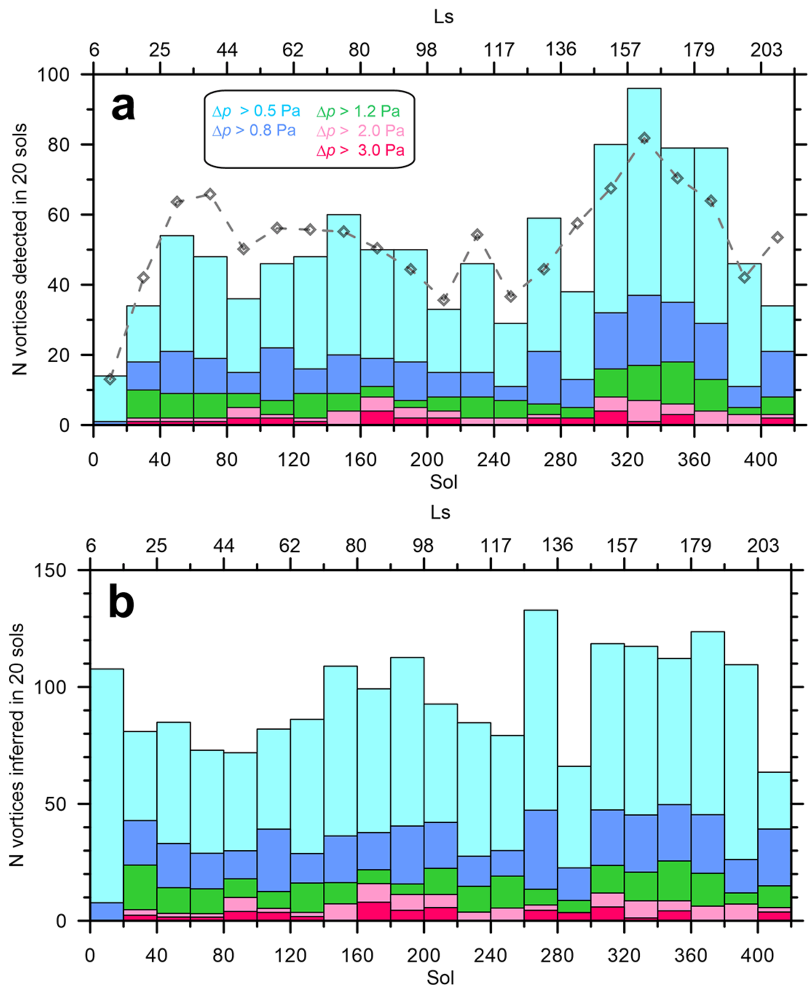

a
Δp > 0.5 Pa
Δp > 0.8 Pa
Δp > 1.2 Pa
Δp > 2.0 Pa
Δp > 3.0 Pa
N vortices detected in 20 sols
Coverage (%)
Ls
Sol
b
N vortices inferred in 20 sols
Ls
Sol

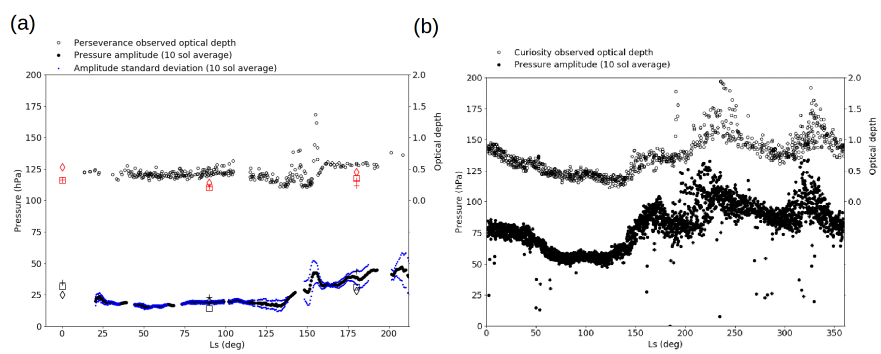

(a)
Perseverance observed optical depth
Pressure amplitude (10 sol average)
Amplitude standard deviation (10 sol average)
Pressure (hPa)
Optical depth
Ls (deg)
(b)
Curiosity observed optical depth
Pressure amplitude (10 sol average)
Pressure (hPa)
Optical depth
Ls (deg)

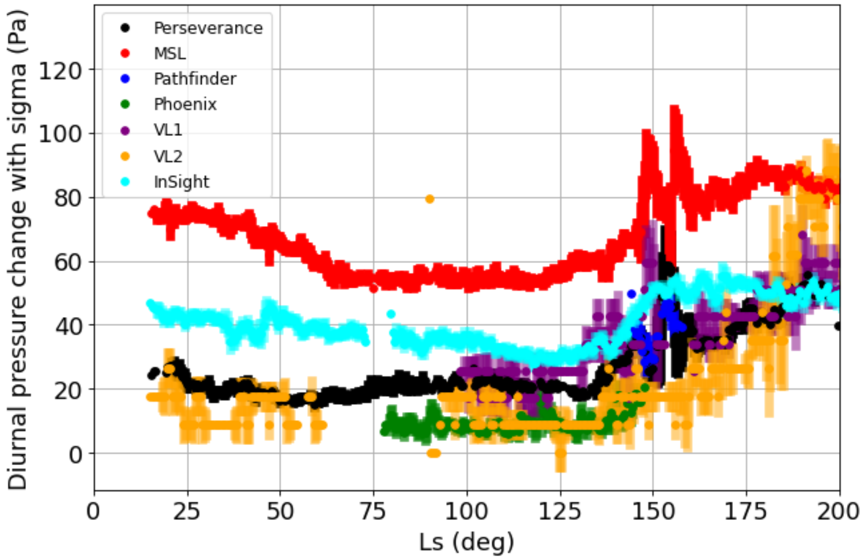
Perseverance
MSL
Pathfinder
Phoenix
VL1
VL2
InSight
Diurnal pressure change with sigma (Pa)
Ls (deg)

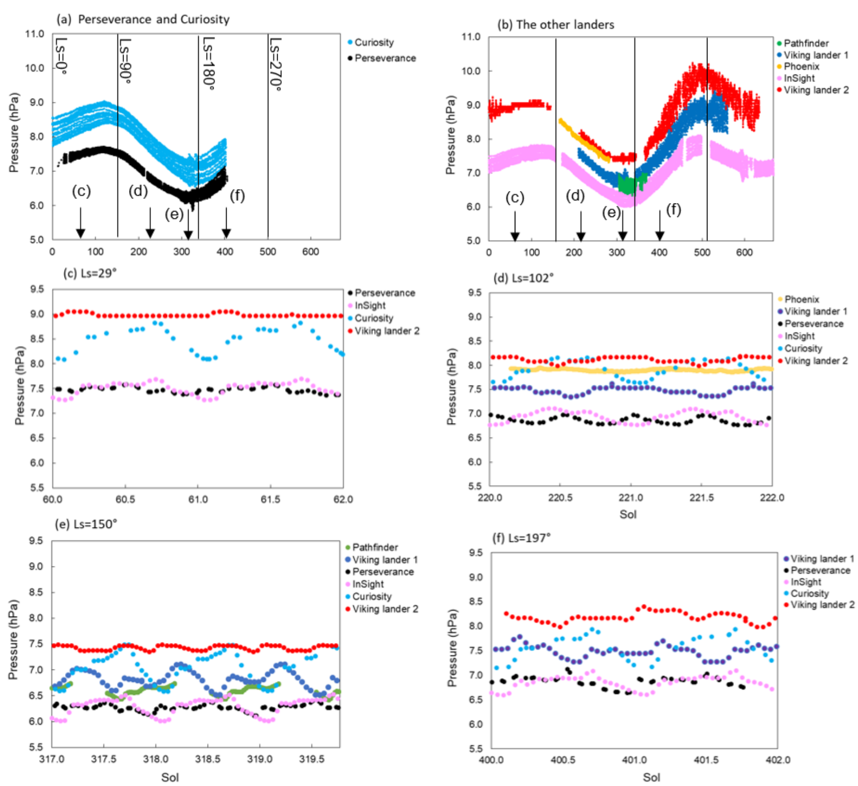
(a) Perseverance and Curiosity
Ls=0°
Ls=90°
Ls=180°
Ls=270°
Curiosity
Perseverance
Pressure (hPa)
(b) The other landers
Pathfinder
Viking lander 1
Phoenix
InSight
Viking lander 2
(c) Ls=29°
Perseverance
InSight
Curiosity
Viking lander 2
(d) Ls=102°
Phoenix
Viking lander 1
Perseverance
InSight
Curiosity
Viking lander 2
Sol
(e) Ls=150°
Pathfinder
Viking lander 1
Perseverance
InSight
Curiosity
Viking lander 2
Sol
(f) Ls=197°
Viking lander 1
Perseverance
InSight
Curiosity
Viking lander 2
Sol

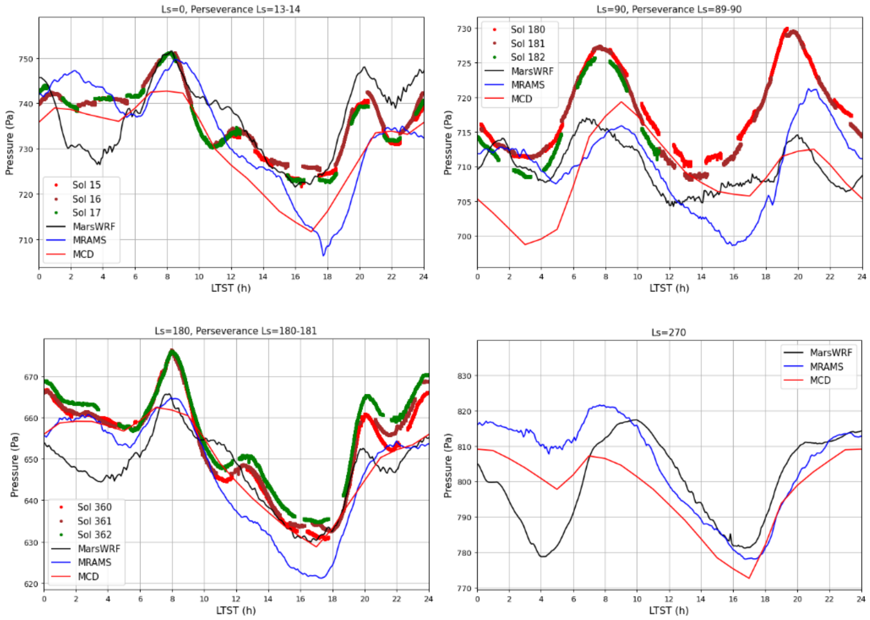
Ls=0, Perseverance Ls=13-14
Sol 15
Sol 16
Sol 17
MarsWRF
MRAMS
MCD
Pressure (Pa)
LTST (h)
Ls=90, Perseverance Ls=89-90
Sol 180
Sol 181
Sol 182
MarsWRF
MRAMS
MCD
Pressure (Pa)
LTST (h)
Ls=180, Perseverance Ls=180-181
Sol 360
Sol 361
Sol 362
MarsWRF
MRAMS
MCD
Pressure (Pa)
LTST (h)
Ls=270
MarsWRF
MRAMS
MCD
Pressure (Pa)
LTST (h)

Perseverance MEDA Atmospheric Pressure Observations - Initial Results

Ari-Matti Harri[1*], Mark Paton[1], Maria Hieta[1], Jouni Polkko[1], Claire Newman[2], Jorge Pla-Garcia[3], Joonas Leino[1], Terhi Mäkinen[1], Janne Kauhanen[1], Iina Jaakonaho[1], Agustin Sánchez-Lavega[4], Ricardo Hueso[4], Maria Genzer[1], Ralph Lorenz[5], Mark Lemmon[6], Alvaro Vicente-Retortillo[3], Leslie K. Tamppari[7], Daniel Viudez-Moreiras[3], Manuel de la Torre-Juarez[7], Hannu Savijärvi[1], Javier A. Rodríguez-Manfredi[3], German Martinez[8]

[1]Finnish Meteorological Institute, Helsinki, Finland
[2]Aeolis Research, Chandler, AZ, USA
[3]Centro de Astrobiología (INTA-CSIC), Madrid, Spain
[4]UPV/EHU, Bilbao, Spain
[5]Johns Hopkins Applied Physics Laboratory, Laurel, MD, USA
[6]Space Science Institute, College Station, TX, USA
[7]Jet Propulsion Laboratory/California Institute of Technology, Pasadena, CA, USA
[8]Lunar and Planetary Institute, Houston, TX, USA

Key Points:

- The atmospheric pressure observations by Perseverance Rover have proved to be of excellent quality fulfilling expectations
- Jezero crater pressure exhibits significant differences to other Martian areas likely due to varying regional geography and solar forcing
- Overall, the diurnal and seasonal atmospheric pressure cycles at Jezero Crater follow an anticipated pattern of pressure variation

*P.O. Box 503, 00101 Helsiki, Finland

Corresponding author: Ari-Matti Harri, `Ari-Matti.Harri@fmi.fi`

Abstract

The Mars2020 Perseverance Rover landed successfully on the Martian surface on the Jezero Crater floor (18.44°N, 77.45°E) at Martian solar longitude, L_s, $\sim$5 in February 2021. Since then it has produced highly valuable environmental measurements with a versatile scientific payload including the MEDA (Mars Environmental Dynamics Analyzer) suite of environmental sensors. One of the MEDA systems is the PS pressure sensor system which weighs 40 grams and has an estimated absolute accuracy of better than 3.5 Pa and a resolution of 0.13 Pa. We present initial results from the first 414 sols of Martian atmospheric surface pressure observations by the PS whose performance was found to meet its specifications. Observed sol-averaged atmospheric pressures follow an anticipated pattern of pressure variation in the course of the advancing season and are consistent with data from other landing missions. The observed diurnal pressure amplitude varies by $\sim$2-5 % of the sol-averaged pressure, with absolute amplitude 10-35 Pa in an approximately direct relationship with airborne dust. During a regional dust storm, which began at L_s 135° the diurnal pressure amplitude roughly doubles. The diurnal pressure variations were found to be remarkably sensitive to the seasonal evolution of the atmosphere. In particular analysis of the diurnal pressure signature revealed diagnostic information likely related to the regional scale structure of the atmosphere. Comparison of Perseverance pressure observations to data from other landers reveals the global scale seasonal behaviour of Mars' atmosphere.

Plain Language Summary

The Mars2020 Perseverance Rover successfully arrived at Mars in February 2021. It landed during an early Martian spring afternoon in a crater north of Mars' equator called Jezero crater. The rover is equipped with meteorological instruments that have so far produced extensive and valuable data for understanding the Martian atmosphere. One of the meteorological instruments is an accurate and precise pressure sensor. The pressure sensor has revealed large changes in the pressure over the seasons that are related to large changes in the actual mass of the Martian atmosphere. This is in line with seasonal pressure changes measured during previous Mars missions and can be explained as the freezing of the atmosphere onto the Martian poles and its subsequent thaw. On a shorter time scale the pressure sensor revealed complex pressure changes over a Martian day. These variations are thought to be related to atmospheric dust whose ubiquitous nature is known to have a strong influence on the Martian climate. As the seasons progressed the daily pressure variations morphed to exhibit different patterns likely related to the large-scale regional changes in the atmosphere. Comparison of Perseverance pressure observations to other landers revealed the global nature of the atmosphere.

1 Introduction

The Mars2020 Perseverance Rover landed successfully on the Martian surface on the Jezero Crater floor (18.44°N, 77.45°E) at the Martian solar longitude, $L_s, 5°$ in February 2021. Since then, it has produced highly valuable environmental measurements with a versatile scientific payload including the MEDA (Mars Environmental Dynamics Analyzer) suite of environmental sensors (Rodriguez-Manfredi et al., 2021). One of the MEDA sensor systems is the pressure sensor (PS) whose observations and initial results utilizing the data acquired during the first 414 sols of the mission ($L_s 5 - 212°$) will be addressed in this manuscript.

Martian atmospheric investigations through spacecraft observations began in the early to middle 1960s as reported by, *e.g.*, Kliore et al. (1969, 1973) and later by Kieffer et al. (1973, 1977); Snyder and Moroz (1992); Zurek (1992); Zurek et al. (1992a). Surface pressure of the atmosphere was firstly estimated using remote sensing methods, both ground based by *e.g.* (Young, 1969) and from spacecraft starting from Mariner as reported by, *e.g*, (Kliore et al., 1965). The Viking landers in 1974-77 provided the first time series of *in situ* atmospheric observations that turned out to be a treasure trove of data covering multiple Martian years (Kieffer et al., 1977; Tillman et al., 1979; Zurek, 1978, 1981). Thereafter Mars Pathfinder (M. P. Golombek et al., 1999; Schofield et al., 1997), the Phoenix lander (Taylor et al., 2008; Savijärvi & Määttänen, 2010), the Mars Science Laboratory aka Curiosity Rover (Gómez-Elvira et al., 2012), the InSight lander (M. Golombek et al., 2020) and the Perseverance Rover (Rodriguez-Manfredi et al., 2021) have continued *in situ* investigations of the Martian atmosphere including accurate atmospheric pressure observations.

During the years of *in situ* and remote observations, Martian atmospheric observations have been accompanied and supplemented by increasingly sophisticated and varied modeling efforts in a range of spatial and temporal scales already since late 1960s (Leovy & Mintz, 1969; Pollack et al., 1981, 1990; Haberle et al., 1993; Barnes et al., 1993; Forget et al., 1999; Richardson et al., 2007; Savijärvi & Kauhanen, 2008; Newman et al., 2017; Richardson & Newman, 2018; Newman et al., 2019). Pressure observations from surface stations have prompted investigations of the CO2 cycle and its connection to the poles, ice and dust e.g. Guo et al. (2009); Kahre and Haberle (2010). The characacterisation of pressure changes due to large scale circulations (Wilson & Hamilton, 1996; Basu et al., 2004) and local meteorology (Toigo & Richardson, 2003; Rafkin et al., 2016) have been predicted and characterised using computer models.

Data assimilation using orbital data is an important activity to enable realistic predictions using atmospheric models and verifying the physics (Rogberg et al., 2010; Lee et al., 2011; Montabone et al., 2014). Better understanding of the behaviour of the Martian atmosphere can help develop better predictions e.g. Battalio and Lora (2021). A network of surface pressure stations could could be key to characterising fast evolving weather systems and dust lifting events (Newman et al., 2021). Our current understanding of the Martian atmosphere and its processes is still understandably far less detailed than our understanding of our own terrestrial atmosphere, but the Martian atmospheric phenomena are presently clearly much better understood than those of any other solar system atmospheres.

Some of the earlier Martian landing vehicles have operated at similar latitudes or elevations to Perseverance, resulting in similarities in terms of climate zone or annual mean atmospheric pressure. Figure 1 shows the locations of Martian landing vehicles with Martian topography, giving a clear idea of the differences in the altitude and type of terrain of the landing sites. In terms of longitude, however, Perseverance seems to be relatively isolated, which has implications when comparing to data from other landed missions. Perseverance observations also have particular significance because they mean that for the first time, we have four *in situ* sets of meteorological observations being carried out at the same time at different locations on the Martian surface (including observations by MSL, InSight, Perseverance, and also China's Zhurong rover, data from which are not currently publicly available). We will present several interesting initial discoveries based on these facts, in addition to the independent Perseverance pressure observations.

In addition to this article there are two companion articles in this journal utilizing the pressure data focusing on atmospheric dynamics (Sánchez-Lavega et al., 2023) and small-scale thermal vortices (Hueso et al., 2023).

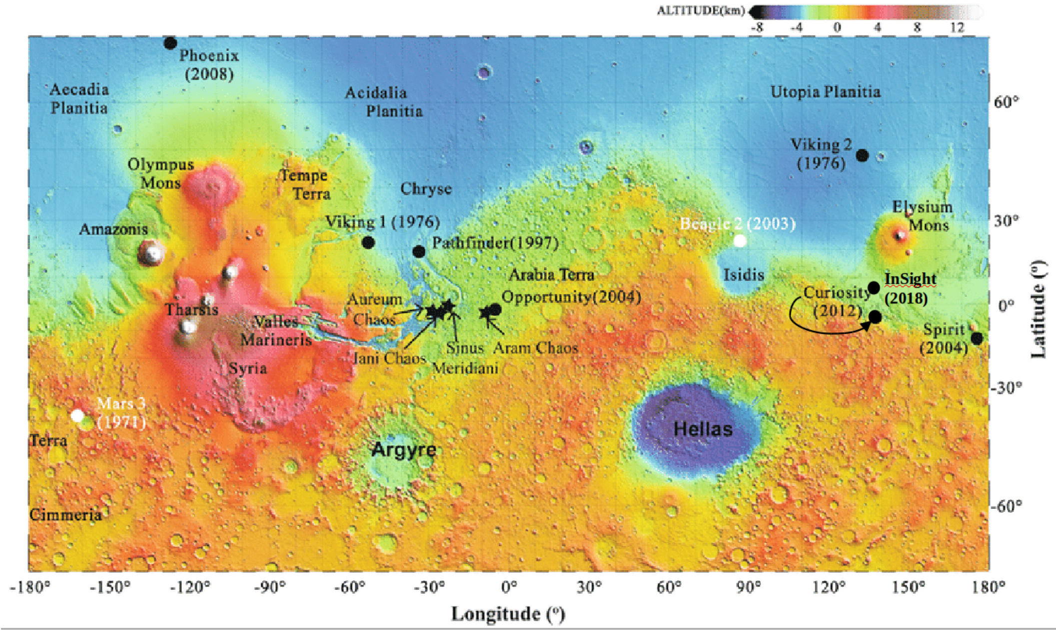

Figure 1. Landing sites of the seven spacecraft having provided *in situ* atmospheric data depicted on a topographic map of Mars (NASA JPL, 2021).

2 Brief MEDA PS device specification and performance

Instrument description. The Perseverance pressure measurement device (MEDA PS) is based on the silicon-micro-machined pressure sensor head (Barocap®) and transducer technology developed by Vaisala Inc. The Barocap® version used by MEDA PS is optimized for the Martian near-surface atmospheric pressure. Changing ambient pressure is changing the sensor head capacitance by varying the distance of the sensor head capacitor plates. Besides being pressure dependent, the Barocap® capacitance is also sensitive to temperature, and thus accurate temperature measurements close to the sensor head are necessary. The supporting housekeeping temperature measurements are provided by Vaisala's Thermocap® sensor heads.

MEDA PS consists of two transducers, each having its controlling ASIC (application specific integrated circuit) and 8 channels containing the Barocap sensor heads, Thermocap sensor heads and constant reference capacitors. Two types of Barocap sensors are used: the NGM type with high stability and relatively long warm-up time and the less stable but faster RSP2M type as a backup. Hence, the primary sensor for scientific investigations is the NGM type Barocap on transducer 1 channel 8 and the secondary sensor the RSP2M Barocap on transducer 1 channel 6. We provide a calibrated pressure reading for both sensor heads in the DER and CAL type data products in the PDS archive (Rodriguez-Manfredi & de la Torre Juarez, 2021) that are optimal for most investigations.

Calibration and performance. MEDA PS has been calibrated at the Finnish Meteorological Institute (FMI) laboratories over the expected operational pressure and temperature ranges. The calibration has been performed in stable temperatures from -45°C to +55°C and stable pressure points ranging from 0 hPa to 14 hPa, which extend well beyond the pressure and temperature ranges prevailing within the electronics compartment housing the MEDA PS on Mars itself. Cali-

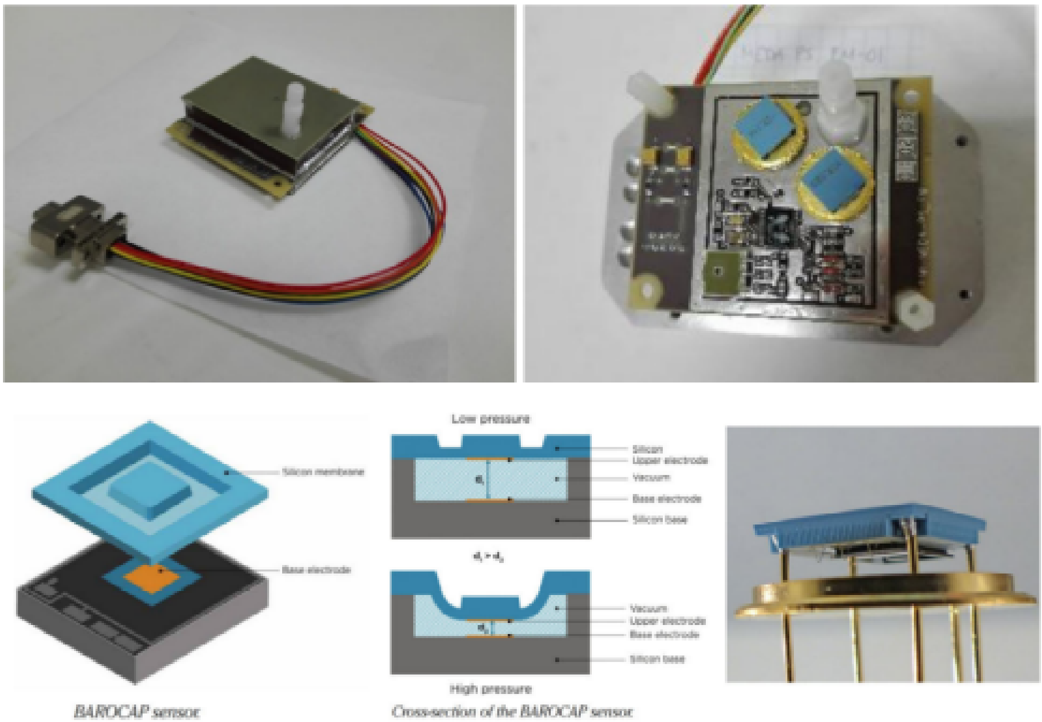

Figure 2. MEDA PS device within its Faraday cage made out of thin conductive foil (ltop eft pane) and the instrument with its pressure sensor heads and part of the electronics visible without the Faraday cover (top right pane). The structure of the silicon micromachined sensor head is shown on the lower row.

bration measurements were also performed in changing pressure and temperature conditions. The Barocap sensors are known to have small changes in the temperature dependence or sensor offset when introduced to a new electrical and thermal environment, and thus calibration checks were performed at all stages after the sensor-level calibration. The calibration checks were performed after integration to the MEDA electronics compartment (MEDA ICU), during the final rover-level thermal vacuum test, during the interplanetary cruise and soon after landing on Mars. The RSP2M Barocaps are also periodically cross-checked against the primary Barocap for possible drift compensation.

The estimated MEDA PS uncertainty based on the sensor- and rover-level measurements was analyzed to be better than 3.5 Pa. This includes the effects of the short-term repeatability, environmental effects and the pressure reference accuracy. The resolution of the primary Barocap, restricted mostly by the electronics noise, is 0.13 Pa in nominal measurement mode, and 0.1 Pa in high-resolution mode, as determined in sensor-level measurements. According to the test data, the time response of MEDA PS is equal to or less than 1 s, having almost no effect on the measurements at the nominal sampling rate of 1 Hz. The effect of the warm-up time of the NGM Barocaps has been removed by the calibration.

The system resources required by the whole MEDA PS package are dimensions $62\times50\times17$ mm, mass 43 g and power consumption less than 15 mW. The MEDA PS detailed specification available before the launch of the Perseverance Rover is described in detail by (Rodriguez-Manfredi et al., 2021). The MEDA PS is located inside the MEDA Instrument Control Unit (ICU) in the rover body, with a filter-protected tube connecting it to the outside environment and conveying ambient pressure to be measured. The MEDA PS device is depicted in Figure 2 illustratating the pressure sensor head and its encapsulation of the full pressure device in a Faraday cage giving shielding against electromagnetic interference.

During the first 414 Martian sols of Perseverance operations MEDA PS has been functioning as expected. The temperature dependence of the Barocap sensors was checked and corrected at the beginning of the operations against the primary Barocap, which is known to be very stable based on the test data. In the first drift offset check performed after 150 sols, the drift of the secondary Barocap was less than 0.3 Pa and slightly larger for the other RSP2M Barocaps.

3 MEDA PS observation strategy and pressure data coverage

MEDA has been designed for flexible operations that are being conducted according to the scheduling by the Perseverance rover. MEDA measures for five minutes at the top of each hour in local mean solar time (LMST) in every mission sol, other than during exceptional circumstances. In addition, on average, MEDA is operating continuously for every other hour. That enables us to generate data sets with averaged pressure measurements approximately at 1-hour intervals, as well as data sets with pressure observations at 1 second intervals for a period of one hour or a few hours in a row for *e.g.* turbulence-related studies. There are also periods, when MEDA is only able to measure for five minutes per hour (or sometimes fifteen or twenty minutes per hour) or is doing no measurements at all for a few hours, due to Perseverance resource allocation reasons.

In the present investigations we use data sets with 1-hour intervals. The 1-hour data sets are not complete but they do have gaps due to scheduling of Perseverance and MEDA operations. Figure 3 illustrates how well the observed data sets cover each Perseverance sol. in the average about 50-70 % of the 24 hour of a sol throughout the season with some periods having 100 % coverage and few sols have

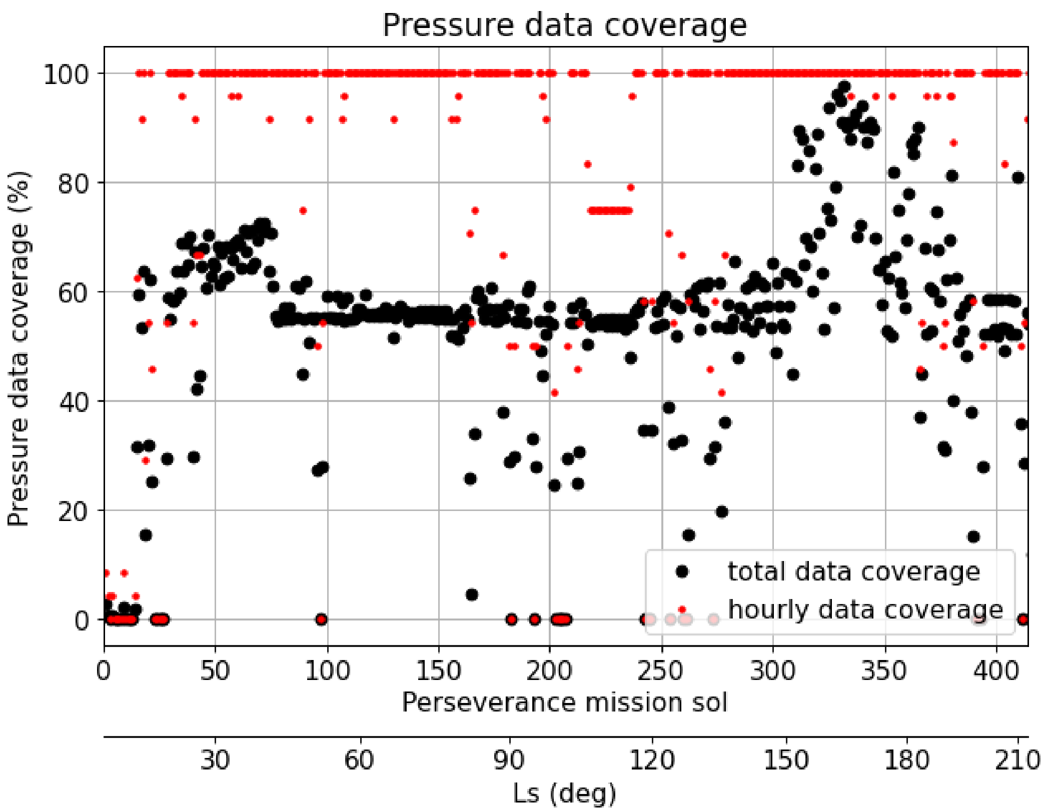

Figure 3. The coverage of atmospheric pressure observations made by the MEDA PS instrument. The black dots depict the overall percentage of pressure readings once per second in a sol, red dots the percentage of the pressure readings available at 1-hour intervals.

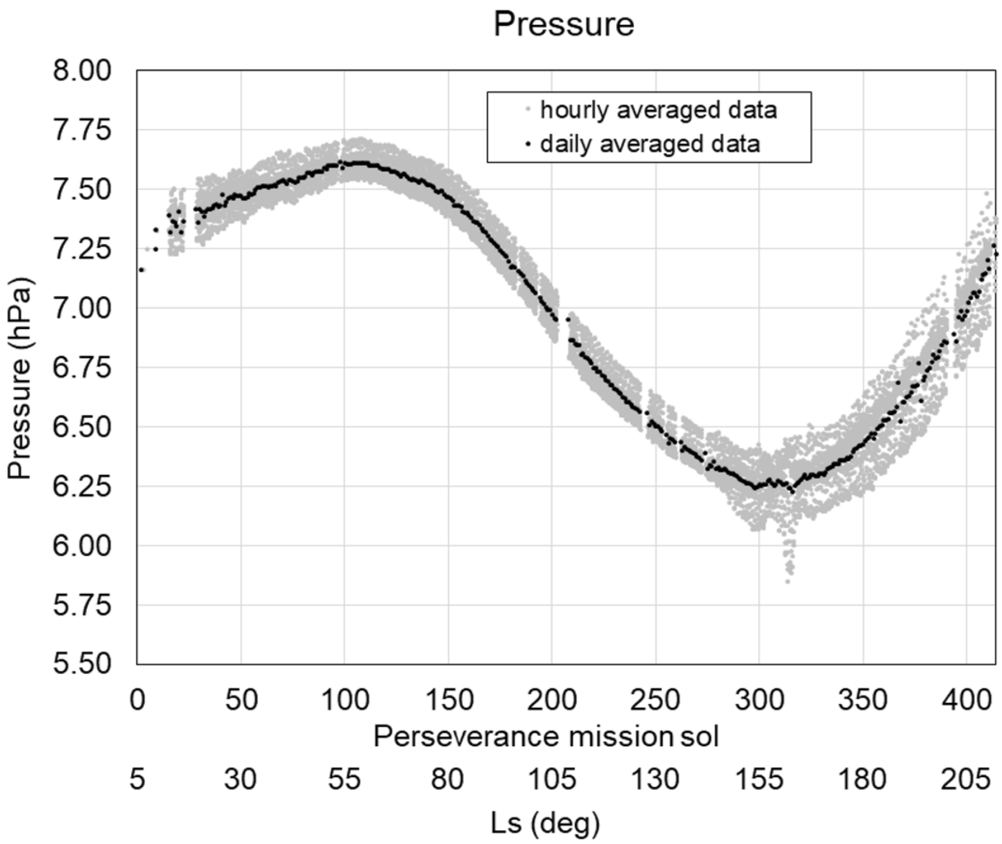

Figure 4. The sol averaged pressure data and the diurnal pressure amplitude (approximate total peak-to-peak range based on observations once per hour) for Perseverance during the period of the first 414 sols corresponding to approximately solar longitude range of L_s $5 - 212°$.

no pressure data at all. The gaps in the 1-hour data set take place more or less randomly around the 24 hour Martian sol. The data coverage of this level allows good characterisation of both the diurnal and seasonal variations in the pressure.

4 Changes in Jezero crater atmospheric pressure with seasonal cycle

The condensation and sublimation of CO2 in the polar regions during winter and spring causes planetwide seasonal variations in the surface pressure, which were first detected by the Viking landers as reported by, *e.g.*, Kieffer et al. (1977); Tillman et al. (1979). The seasonal CO2 cycle, which is largely controlled by the polar heat balance (Paige & Ingersoll, 1985, e.g.,), can clearly be seen in the seasonal variation of daily average surface pressure.

This is nicely demonstrated at the Jezero crater site by the Perseverance Rover measurements. The daily averaged atmospheric surface pressure during the first 414 sols of the Perseverance mission is depicted in Figure 4. The figure also includes the range of diurnal pressure variation plotted on both sides of the average pressure line with a gray color. Hence the gray area illustrates the approximate total range of diurnal pressure variation around the average pressure of a sol. The minimum pressure peak at around Ls 153 shown in Figure 4 was likely caused by a regional dust storm (Lemmon et al., 2022).

In seasonal-to-annual time scales the CO2 condensation-sublimation cycle at the polar regions gives rise to a seasonal pressure variation on the order of as much as 30 % of the local surface pressure (Kieffer et al., 1977; Tillman et al., 1979, e.g.,). The observed sol-averaged atmospheric pressure during the 414 first Perseverance sols, from the landing time at early Northern springtime to Northern fall, follows an anticipated pattern of total pressure variation in the course of the advancing season. The data has the first maximum in late spring roughly on Perseverance sol 110 and a minimum on sol 310, whereas by the Perseverance sol 414 (corresponding to approximately L_s 212°) the atmospheric pressure is climbing higher than the first maximum toward the annual maximum. When comparing Perseverance with concurrent observations by the Curiosity Rover and the Insight lander as well as with the historical Viking Landers data, we can see distinct differences in the amplitude of the seasonal pressure variations that are due to different surface elevations.

The sol-averaged MEDA PS atmospheric pressure data together with the hourly-averaged pressure depicted in Figure 4 is nicely showing the evolution of the atmospheric pressure over first 414 Perseverance sols at the Jezero crater site. In the beginning of the data set the pressure is going down during the Northern spring and summer seasons and turning to an increasing leg during the late summer. The diurnal amplitude, shown approximately by the gray area in Figure 4, shows a clear increase during periods with increased amounts of airborne dust starting approximately from Perseverance sol 270 and staying high until sol 414 (when our investigation period ends). There seems to be a direct relationship between the range of diurnal pressure variation and the amount of airborne dust as has been earlier discovered by, *e.g.*, Zurek (1978, 1981); Paige and Ingersoll (1985).

The seasonal dependence of the Martian atmospheric pressure drives the atmosphere to the extent that about one third of the mass of the Martian atmosphere is deposited on the polar caps during Northern and Southern winters and evaporated back to the atmosphere during summertime. This results in the characteristic atmospheric pressure pattern having two local maxima and minima during a Martian year, with the maxima occurring approximately at solar longitudes L_s 60° and L_s 260°. This pattern can clearly be seen in Figure 5, which compares the sol-averaged pressure of Perseverance with Curiosity Rover, Insight Lander, Viking Landers and the Pathfinder mission. Table 1 gives the basic characteristics of each mission.

Investigations of the seasonal pressure cycle together with observations from other Martian landing missions enhance our understanding of the CO2 cycle, the annual heat balance of the polar caps and the global scale atmospheric circulation of Mars (Paige & Ingersoll, 1985; Guo et al., 2009). Major drivers behind the seasonal variation are solar radiation and surface and subsurface thermal properties (Wood and Paige, 1992). Atmospheric dust loading and regional circulation will influence short scale variations (Haberle et al., 1993; Hess et al., 1980). The annually averaged atmospheric pressure is largely depending on the elevation of the site and hence the atmospheric pressures are differing between observation sites (Hess et al., 1980; Richardson & Newman, 2018).

In order to investigate the relative evolution of the pressure cycle at different latitudes figures 5 (c) and 5 (d) show the differences in pressure between the Perseverance landing site and the other four landers, excluding Pathfinder. In figures 5 (c) and (d) a more negative pressure signifies a higher pressure compared to Perseverance. The results from MCD data shown in figure 5 (d) tracks in the evolution of the results for the observational data shown in figure 5 (c). For Curiosity there

Table 1. Essential characteristics of seven Martian lander missions performing atmospheric observations. The elevations are based on MOLA data (Smith et al., 2001)

Vehicle	Lat (°N)	Lon (°E)	Elevation (km)	Climate Zone	Operational (years)	Platform Type
Viking lander 1	22	-48	-3.6	North subtropics	1976-82	Stationary
Viking lander 2	48	134	-4.4	North midlatitudes	1976-80	Stationary
Mars Pathfinder	19	-34	-3.7	North subtropics	1997	Stationary
Phoenix	68	-126	-4.1	North polar regions	2008	Stationary
Curiosity	-4.6	137	-4.5	Equatorial regions	2012-	Mobile
InSight	4.5	136	-2.6	Equatorial regions	2020-	Stationary
Perseverance	18	77	-2.6	North subtropics	2021-	Mobile

are two sets of lines in figure 5 (c). These correspond to years 2 and 3 of the mission with year 3 being at a higher elevation which explain the difference in the mean pressure. There are a number of interesting dip or hump-like features over timescales of 100-200 sols in figure 5 (c) and (d) that need explaining.

The dips and humps in the season pressures in figure 5 (c) and (d) are most likely connected to latitude dependant processes that include the orographic, i.e. the large difference in elevation between the northern and southern hemisphere, and the dynamical effects on the pressure cycle (Hourdin et al., 1993). Regarding the orographic effect, during northern hemisphere winter a large mass of cool air is trapped in the low elevation of the northern hemisphere basin. In the winter a low atmospheric scale height traps a large portion of the atmosphere. The result is a higher winter maximum at higher latitudes in the northern hemisphere in winter. For example the heights of the winter and summer pressure peaks for Viking landers 1 is much more symmetric than for Viking lander 2. We will not cover dynamical effect here, which is related to the winds, as it apparently has little influence at the equatorial and middle latitudes considered here. An explanation of the dynamical effect can be found in Hourdin et al. (1993).

The greatest dip seen is for the Viking lander 2 in 5 (d) which is at a latitude of 48°N. This results from the pressure observed by Viking lander 2 increasing more rapidly than the pressure observed by Perseverance most likely due to the orographic effect. For the other landers the, except maybe for Curiosity, the pressure differences in figures 5 (c) and (d) are fairly level indicating the pressures at these landing site increase more or less at the same rate.

A shallow but distinct dip can be seen for Curiosity in figures 5 (c) and (d) over the spring-summer time period. A possible reason for a dip at this time of year

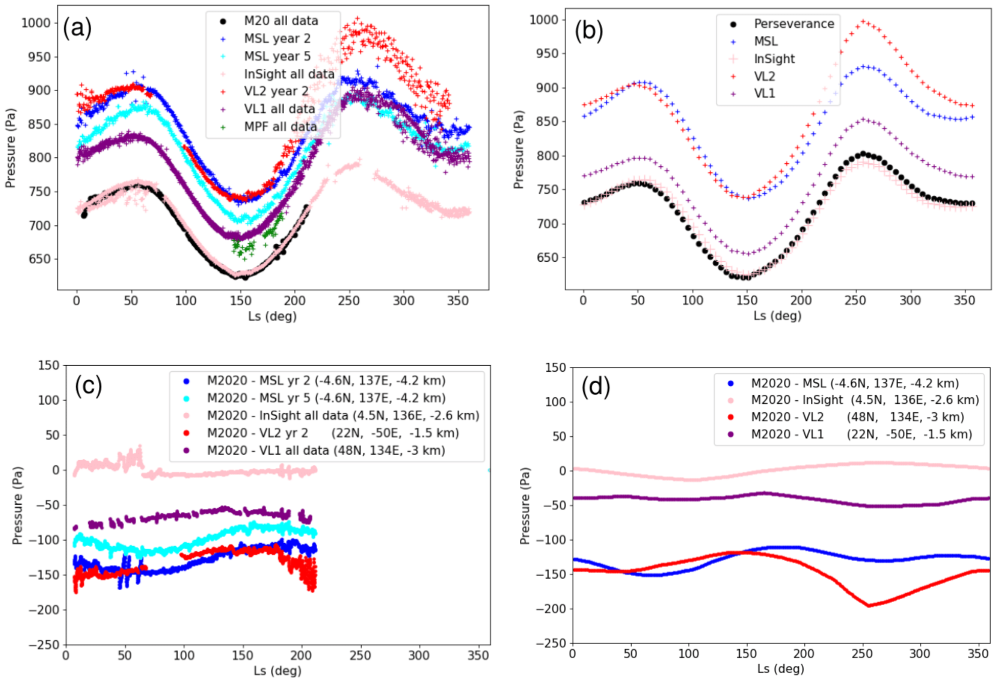

Figure 5. Comparisons of pressure between different lander missions. The top row shows the sol averaged observed pressure data, and the bottom row sol-averaged pressure data by different lander missions subtracted from Perseverance pressures. The left column shows results from the observations while on the right are the same results from the Mars Climate Database.

is that the cold air trapped in the northern hemisphere trapped during the winter is now being released as it is the summer. This lowers the pressure faster at the Perseverance landing site than at the Curiosity landing site, which is located near the equator in the southern hemisphere. This would result a relative increase in the pressure between Curiosity and Perseverance as seen in figure 5 (c) and (d). Both plots for Curiosity exhibit a dip around the summer solstice indicating that the process driving the evolution of the pressure, i.e. the dip, is not related to the change in elevation.

There are shallow dips and and troughs in the data for other landers in figures 5 (c) and (d) but these are less obvious and probably cannot be interpreted with much certainty. For example there appears to be a small dip in the MCD data for InSight in figure 5 (d). This might be expected because InSight is located at a more southerly latitude than Perseverance with InSight being less sensitive to the ejection of summer time air from the northern basin than Perseverance. Interestingly this dip cannot be seen in Figure 5 (c) perhaps suggesting some other process or mechanism is masking the effect in the observations or limits with the model.

5 Diurnal atmospheric pressure and small scale atmospheric phenomena

In situ pressure observations by several landed missions have shown that the Martian atmospheric surface pressure is composed of variations over several time scales and amplitudes. They include, *e.g.*, the overarching seasonal CO2 cycle, regional-scale perturbations caused by planetary waves and thermal tides, including their interactions with topography, hydrostatic adjustment flows, and baroclinic and barotropic disturbances. Small scale eddies and disturbances, e.g. convective vortices are a usual cause of the shortest pressure variations of the order of a few tens of seconds (Harri et al., 2014, e.g.). If the vortices carry an optically distinguishable dust load they are called dust devils.

Thermal tides driven by solar irradiation cause distinct detectable diurnal pressure variations and are especially significant at low latitudes. In the Martian thin atmosphere the thermal tides - and hence the range of diurnal pressure variation - are much larger than in Earth's atmosphere due to the relatively stronger solar forcing at the surface (Zurek, 1982; Kieffer et al., 1992).

At the Jezero crater site measured by Perseverance rover the diurnal atmospheric pressure range seems to be approximately 20 Pa during the first 270 sols of the mission and thereafter during mission sols 270-414 extending to roughly 40 Pa. The wider range of diurnal pressure is likely due to increased amounts of airborne dust measured by Perseverance. Several earlier investigations have found the direct relationship between the amount of airborne dust and the range of diurnal pressure variation as shown by, *e.g.*, Zurek (1981, 1982); Guzewich et al. (2016).

The Perseverance in situ pressure observations show variations ranging from microscale to seasonal scale as has been observed by earlier *in situ* pressure measurements of Viking (Soffen, 1976; Soffen, 1977), Pathfinder (M. P. Golombek et al., 1999), Phoenix (Taylor et al., 2008) and Curiosity missions (Harri et al., 2014; Haberle et al., 2014). The advancing Martian season has a clear signature in the atmospheric pressure as clearly manifested by Figure 6 depicting the diurnal pressure variation by data stacked in steps of 10 sols. It shows the gradual increase of the observed Perseverance pressure levels during the Northern spring until approximately sol 110, then gradual decrease bypassing the Northern midsummer (Ls 90) until sol 320, and thereafter again showing increasing pressure until the last sol (414) of this investigation when the season advances further into the Northern fall. The data of this investigation covers only 60 % of the Martian year, but this kind of seasonal dependence will be seen throughout the Martian year.

When inspecting the structure of diurnal pressure, 2-4 peaks appear in the data on each sol in Figure 6. A clear evolution of the peaks can be seen in the stacked diurnal pressure data. During Northern summer (Figure 6, second row from top) diurnal pressure exhibits two distinct and regular peaks, one in the morning around 6-7 AM and the other one around 8-9 PM LTST. During the Northern spring (Figure 6, top row) and fall (Figure 6, lowest rows) this summertime regular pattern is broken into more like four separate peaks whose amplitudes vary along with advancing season.

It seems that during springtime - at the start of the mission, Perseverance sols 0-150 - smaller peaks are superimposed on the larger peaks. These smaller peaks disappear between about sols 150 and 250 (Northern summertime) and return around sol 300 in early Northern fall. The wintertime has not yet come during the first 414 Perseverance sols. The features in the plots give clues on the behaviour of regional atmospheric dynamics and circulation patterns in the Martian atmosphere (Read & Lewis, 2004, e.g.).

The largely repeatable two-peak shape of the daily surface pressure profile especially during the Northern summertime (Figure 6) is likely due to the strong semi-diurnal thermal tidal component as indicated in Figure 7. Abundant amount of airborne dust is one cause responsible for amplified semi-diurnal tidal component as shown by, e.g., (Zurek, 1981; Newman et al., 2021). Similar two-peak structure was also discovered during Pathfinder mission Schofield et al. (1997).

The harmonic components – principal components - of daily pressure variations sheds light on our understanding on the atmospheric phenomena behind the complex structure of daily pressure cycle. The principal components of the atmospheric diurnal pressure variation can be revealed by decomposing the pressure observations through Fourier transformation. The estimated diurnal, semi-, ter- and quad-diurnal amplitudes are represented by the first four components of the resulting series representation, respectively, as shown in Figure 7 together with the Perseverance optical thickness observations.

The Fourier transformations shown in Figure 7 were calculated using a fast Fourier transform (FFT) scheme. The input data series was created by generating hourly bins of observations from a window of three sols to get at least one observation per hour. In case of multiple observations per hour the bin value was achieved by averaging. The middle sol of the three-sol window was the one that was assigned the calculated amplitudes and phases. When using this procedure it was assumed that the three consecutive sols were sufficiently similar for calculating the principal components. The analysis was performed by sliding the three-sol window over the first 414 sols of Perseverance observations.

The principal components of the Perseverance diurnal pressure variation seem to be smaller than those measured by the Curiosity rover at Gale crater where tidal forcing is stronger due to the location close to the equator and also due to the fact that, at Curiosity's longitude sector, eastward and westward modes are expected to interact constructively (Wilson and Hamilton, 1996; Haberle et al., 2013; Harri et al., 2014).

In the light of the strong semi-diurnal component shown in Figure 7 during the Northern summer (sols 150-250), the prevailing stable 2-peak diurnal pressure cycle may be due to the strong summertime tidal forcing by relatively high amount of regional airborne dust creating a strong and stable semidiurnal component (Figure 7, top panel). This situation resembles that in the terrestrial tropics, where diurnal

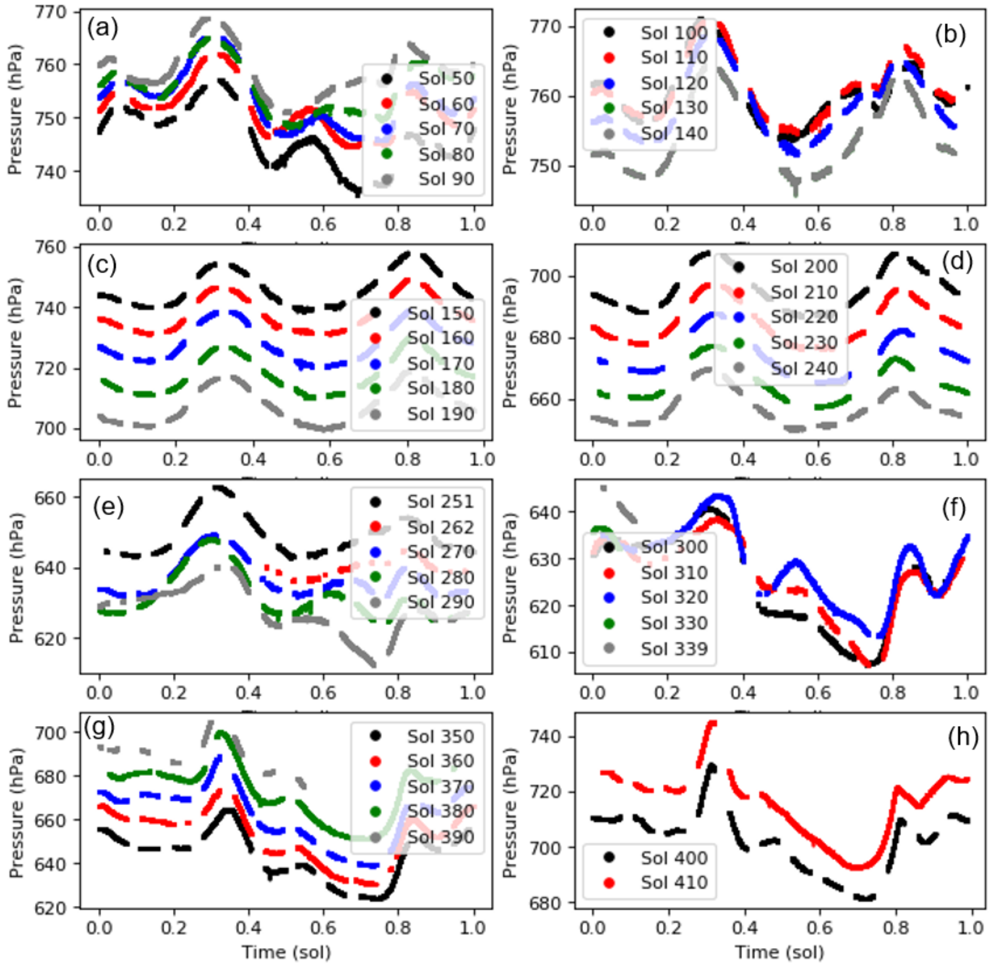

Figure 6. Evolution of diurnal pressure variation in steps of 10 sols covering the first 414 Perseverance sols during the advancing season. Each figure shows data averaged over five sols centered on the sol number shown, except the last on the bottom right (pane h).

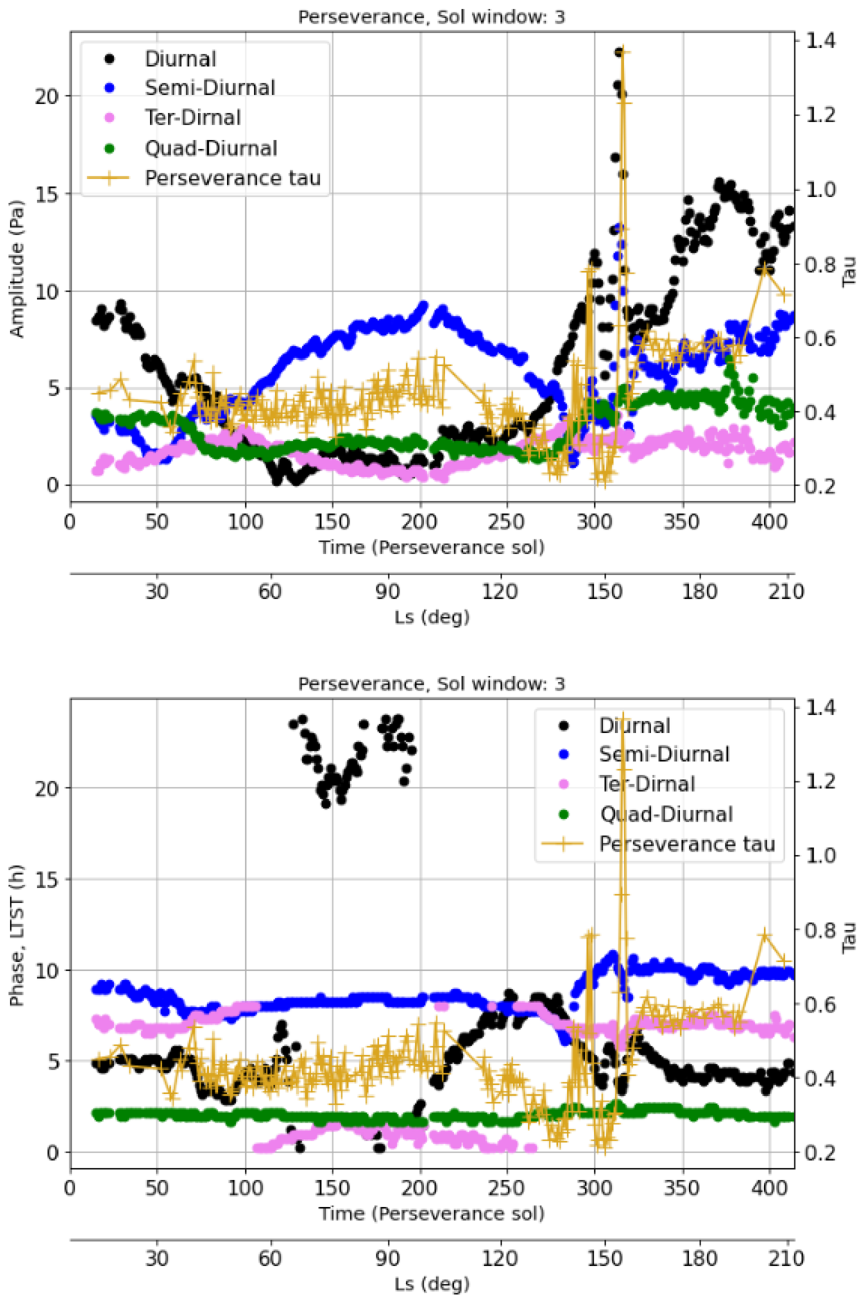

Figure 7. The amplitude and phase of the first four harmonic components of diurnal pressure calculated using FFT for all Perseverance sols. A running averaging window of three sols was used in the calculations. The amplitudes (top pane) and phases (lower pane) are illustrated in different colors (left axis). On the amplitude plot also the optical thickness observed by Perseverance is also shown (right axis).

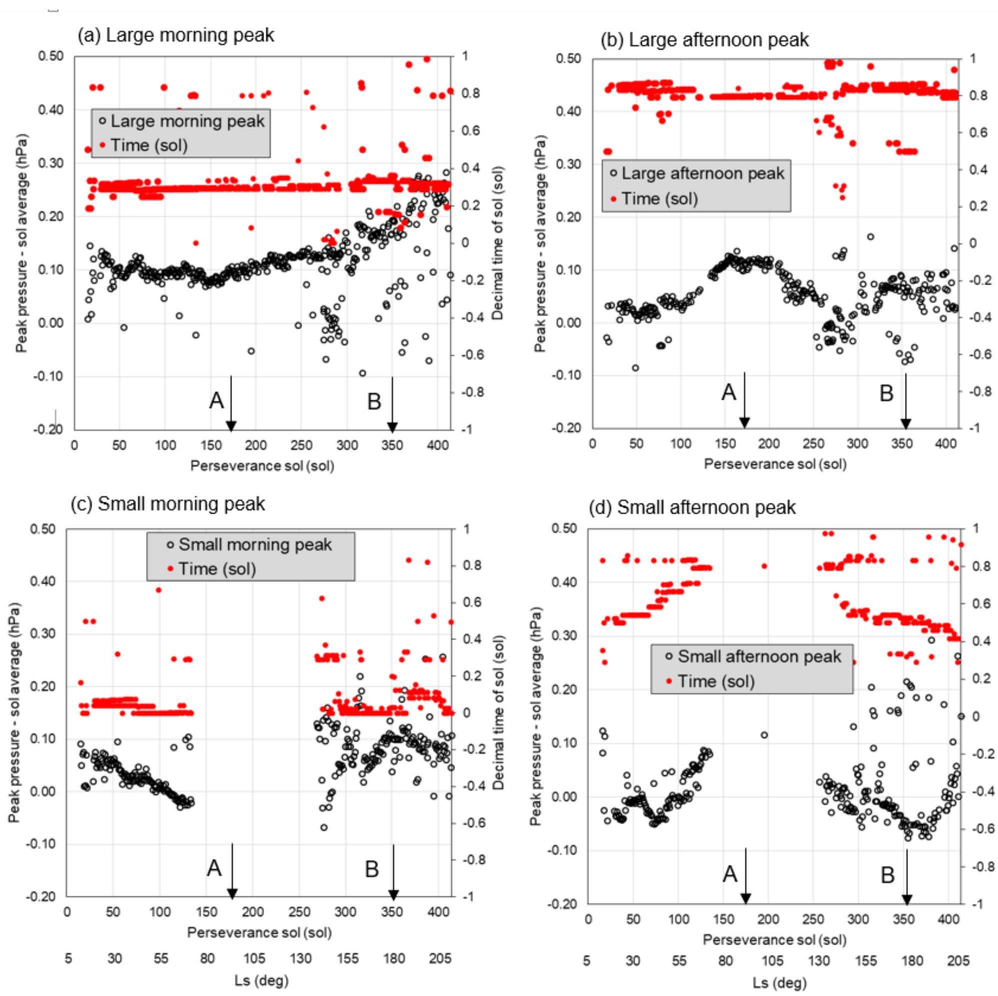

Figure 8. Black circles show the peak pressure minus sol averaged pressure. The time of occurrence of the peaks is also shown in red. The time has an uncertainty on it of plus or minus half an hour. The scatter in the points arises from relatively small fluctuations in flat regions of the data, *e.g.* in the dips between the peaks. The letters 'A' and 'B' point to midsummer (L_s 90° and fall L_s 180°, respectively.

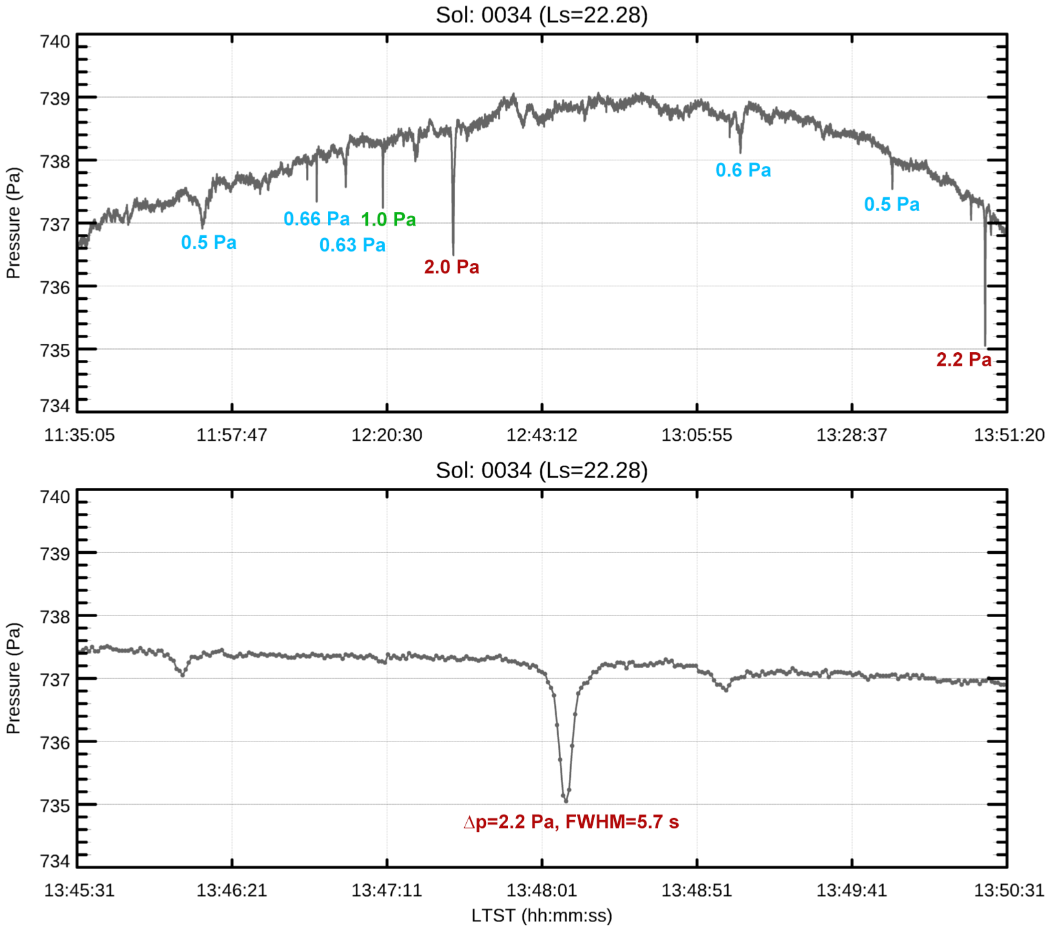

Figure 9. An example of vortex activity detected in pressure data over a 1.5 hour period around noon during the Perceverance mission sol 34. The upper pane displays vortex activity that can be seen as downward spikes in pressure with the depth of some spikes indicated. The lower pane zooms in on the deepest spike (2.2 Pa) to show a more detailed spike structure indicating also the full width at half maximum (FWHM) of the spike.

pressure has two distinct peaks, too – one in the morning and one in the evening. In the terrestrial tropics this is due to high-altitude ozone, whereas in northern late spring and early summer on Mars this may be due to the ever-present airborne dust getting heated by solar irradiation (Read and Lewis, 2001).

The semidiurnal tidal component at Jezero crater seems to be strong during Perseverance's Northern summer. This may be due to the fact that regional atmospheric dust load is relatively high at that time, which would amplify the semidiurnal component - assisted by the strong solar forcing at the Northern summer. Optical depth maps retrieved from the Mars Climate Database, based on data sets generated by Montabone et al. (2015), seem to support our inference. The maps from the MCD suggest that during the summer Perseverance is on the western edge of a patch of elevated optical depth that stretches over several 10s of degrees of longitude to the west. Later on in the year the optical depth at the latitude of Perseverance is more homogeneous.

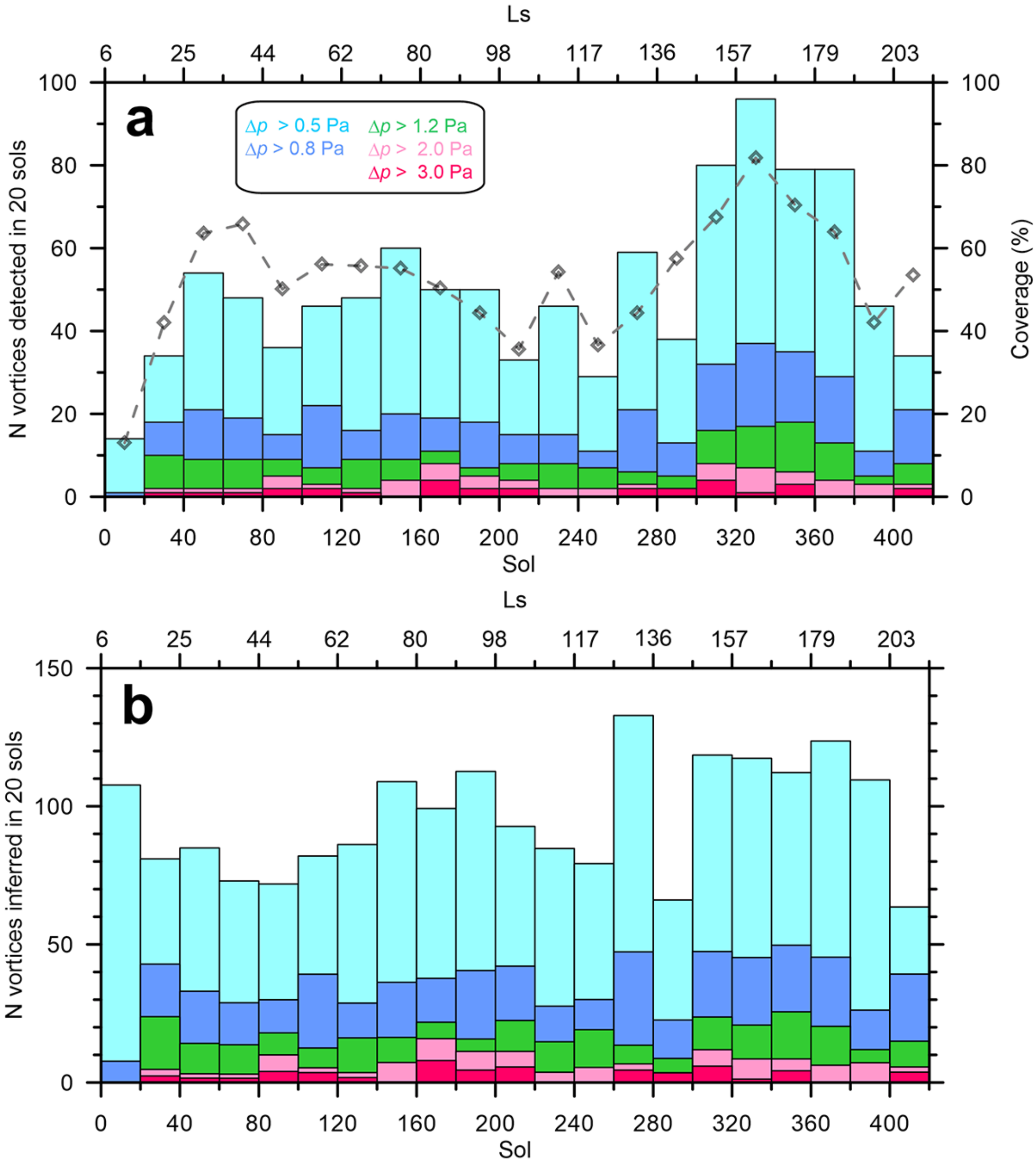

Figure 10. Assessment of the number of vortices by Perceverance through atmospheric pressure drops as a function of sol. (a) Number of vortices actually detected in intervals of 20 sols (left axis). The rhombs show the coverage of MEDA pressure data in each time interval (right axis). (b) Number of vortices that would have been detected if MEDA data would have been measured continuously. In both panes the intensity of the pressure drops is indicated by color coding as explained in the legend.

The seasonal evolution of diurnal pressure and its pattern of variation is shown in Figure 6. We found that during the Northern summertime a fairly stable pattern of two peaks was prevailing in diurnal pressure variation, but that was broken into four peaks during the spring and fall. Now, we can study further the evolution of the daily pressure pattern by analyzing the peaks and their evolution with the advancing season (Figure 8). This is done by subtracting the average pressure of the sol of interest from maximum pressure to get the peak amplitude and also noting the local time of occurrence.

Figure 8 shows the peak pressures relative to the daily-averaged sol pressure and the time that the peaks occur. As can be seen in Figures 6 and 8 there is one large peak both in the morning and in the afternoon that persist in the daily pressure data. These are clearly illustrated in the top row of Figure 8. The time these peaks occur remains steady throughout sols 50 to 400 in the data. Their magnitude varies with the large morning peak increasing after about sol 150. The large afternoon peak reaches a maximum around sol 150.

Figure 6 shows small morning and afternoon peaks prevailing during Northern springtime and fall. They are also depicted in Figure 8, where it can be seen (bottom row) that the small morning peak occurs at the same time each sol but the magnitude decreases until about sol 140 and then the peaks disappear. They reappear around sol 270 but appear to fluctuate in magnitude before settling down to a near constant value around sol 360. In Figure 8 (lower right) the small afternoon peaks appear to increase in magnitude before disappearing around sol 140. They then reappear around sol 260 and decrease in magnitude with the advancing sols.

These interesting morning and afternoon peak variations illustrated by Figures 6 and 8 could be a manifestation of local circulation phenomena causing pressure variation, which is then superposed with the strong semidiurnal pressure mode. During the Northern summer the semi-diurnal thermal tide (as shown by the semi-diurnal pressure variation) is at its strongest, which creates a stable diurnal pressure variation with one distinct large peak in the morning and another one in the afternoon. During the Northern spring and fall the semidiurnal mode of the thermal tide is weaker than in summer. Hence the stable situation is broken resulting in the creation of two additional small peaks, one preceding the large morning peak and another preceding the large afternoon peak.

This kind of pressure peak structure riding on top of the diurnal pressure variation is possibly caused by local effects due to the more complex topography of Jezero crater as compared, *e.g.*, to the topographically more simple and flat region of the Pathfinder and Viking Lander sites (Soffen, 1976; Schofield et al., 1997), where such peaks are not so clearly visible. On the other hand, at the Curiosity rover site additional peaks are also seen in the diurnal pressure variation, which is likely due to the fact that Gale crater is also a topographically complex site (Harri et al., 2014; Haberle et al., 2014). Variations in the thermal tide could also introduce multiple oscillations into the observed surface pressure. Schofield et al. (1997) suggest interference effects between the westward tide and the eastern travelling topographically induced Kelvin mode could produce surface pressure observations with two minima and two maxima per sol.

A highly interesting atmospheric phenomenon regularly observed in pressure data are convective vortices - called dust devils when raising surface dust in the atmosphere (Zurek, 1982; Ferri et al., 2003, e.g.). These rotating small scale atmospheric phenomena are investigated in this journal issue by (Hueso et al., 2023) using Perseverance pressure observations. Vortices appear as pressure drops in MEDA data, some times in bursts of activity as displayed by Figure 9 and 10 based on the investigations by Hueso et al. (2023). These pressure drops are most likely caused by passages of thermal vortices. Some of these events can be identified as dust devils when observing with additional MEDA radiative sensors able to infer the presence of dust, and by other instruments onboard Perseverance such as rover cameras. In the context of the Aeolian environment of Jezero, thermal vortices were discussed by Newman et al. (2022). These studies provide the overall abundance of vortices at Jezero, their daily cycle of activity, which peaks roughly at local noon, with some seasonal variation in the transition from summer to fall, the frequency of vortices that carry dust and are therefore dust devils, and establish the link between vortex activity and the thermal gradient of the near surface atmosphere.

An interesting aspect of vortex activity at Jezero revealed originally by the work of Hueso et al. (2023)) is the nearly constant activity with little seasonal variation during the period of observation of this investigation. This is demonstrated by Figure 10 showing the statistics of detected and estimated amount of vortices during the period of the first 414 Perseverance sols. This allows us to estimate (Figure 10) that about 100 thermal vortices with pressure drops exceeding 0.5 Pa during a 20 sol period are dwelling in the Perseverance neighbourhood throughout the first 414 Perseverance sols. Thus the vortex activity at Jezero seems to be nearly constant through the first 414 Perseverance sols. Apparently solar forcing varying considerably from springtime to fall has not significantly affected the generation of vortices. It is interesting to see whether this pattern will hold through the upcoming Northern wintertime with decreasing thermal forcing.

Martian atmospheric small scale turbulence and dynamics can be investigated using Perseverance observations accompanied by additional Perseverance measurements. These phenomena are studied in an accompanying paper in this journal issue by Sánchez-Lavega et al. (2023).

6 Perseverance diurnal pressure compared with other landing sites and modeling results

Atmospheric diurnal pressure variation is affected by *e.g.* the strength of thermal tide, regional and local geography and amount of airborne dust and hence some local atmospheric phenomena can be partially explained by studying diurnal pressure variation (Zurek, 1982; Zurek et al., 1992b; Haberle et al., 2014; Harri et al., 2014, e.g.). The diurnal pressure amplitude – minimum to maximum range – as a function of solar longitude for both Perseverance and Curiosity rovers is depicted in Figure 11 including the measured optical depth. Additionally results by regional models MWRF (squares) and MRAMS (plus-signs), as well as values by Mars Climate Database (diamonds) are shown. Furthermore, an uncertainty corridor of two standard deviations is drawn on the pressure amplitude by smoothing over a few sols. The standard deviation of the diurnal pressure range is calculated over 10 sols and it is then drawn on both sides of the curve. Thus the width of the uncertainty shown is thus twice the standard deviation.

The diurnal pressure variation exhibits a clear amplitude increase with the increasing amount of the atmospheric dust, which was reported by Curiosity pressure observations (Haberle et al., 2013; Harri et al., 2014). This phenomenon has been discovered also earlier by, *e.g.* Zurek (1978, 1982); Tillman (1988); Kahre and Haberle (2010). Actually, this is considered as a manifestation of how the Martian atmospheric conditions are intertwined with the airborne dust to such extent that atmospheric diurnal pressure observations could even be used to infer the amount of dust afloat *e.g.* (Zurek, 1981; Guzewich et al., 2016).

Figure 11 shows that the observed daily amplitudes in pressure are similar to those predicted by two atmospheric models that cover Jezero crater at km scale

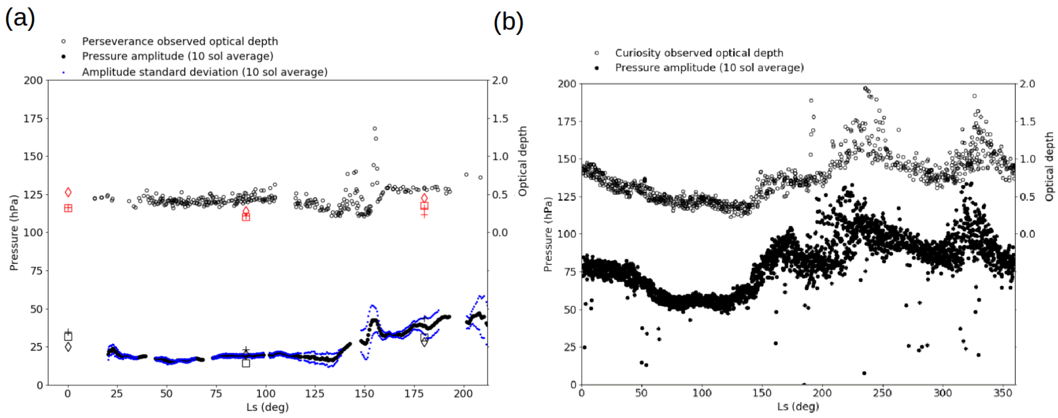

Figure 11. Diurnal pressure amplitude – minimum to maximum range – as a function of solar longitude (black dots, left axis) and the optical depth (small black spheres, right axis). The plots in (a) includes Perseverance pressure (MEDA PS) and optical thickness (M2020 Mastcam-Z) data during the first 414 Perseverance sols and in (b) all Curiosity pressure (REMS-P) and optical thickness (MSL Mastcam) data until Perseverance mission time. The depicted diurnal pressure range is a 10-sol moving average in both plots. The Perseverance plot also includes a 2-sigma belt around the diurnal pressure with the standard deviation (sigma) calculated from the 10 sols for each average point. Additionally results by regional models MWRF (squares) and MRAMS (plus-signs), as well as values by Mars Climate Database (diamonds) are shown.

resolution (MRAMS and MarsWRF). The amplitude predicted by MRAMS is usually slightly higher and MarsWRF slightly lower, for the Ls with data available. The models use TES optical depth zonally averaged over previous non dust storm years (Pla-Garcia et al., 2020) (Newman et al., 2021). As to the MCD values for the location of Perseverance (18°N, 77°E) the optical depth used in these models is similar to those observed by Perseverance. Note that the pressure amplitude in the MCD, which has a resolution of order several hundred km, is also similar to that observed by Perseverance.

It is interesting to compare the average amplitude of diurnal pressure variation – minimum to maximum value – at different locations and for varying Martian altitudes and terrain. The Martian atmospheric pressure has some interannual variation, but it appears to be sufficiently small to the extent that the atmospheric pressure at each landing site seems to be behaving largely in a similar fashion from year to year as shown by, *e.g.*, Tillman (1988); Tillman et al. (1994). This interannual similarity justifies qualitative and also somewhat quantitative comparison of pressure by different landing missions even if they are not observed at the same time, but rather in different Martian years. This applies especially to diurnal pressure variation that is being largely driven by thermal tide, local geography and regional atmospheric flows.

Figure 12 depicts the daily pressure amplitude during the first 414 sols of the Perseverance mission with concurrently observed daily pressure amplitudes of the Insight and Curiosity missions, as well as that of historical Viking Landers, Pathfinder and Phoenix mission data at matching solar longitudes. Basic characteristics of those seven Martian missions are shown in Table 1 including the climate zones and geographical locations (also in Figure 1) of those missions.

It can be readily seen in Figure 12 that the daily pressure amplitude of Perseverance, Viking Lander 1 and Pathfinder are quite similar, which is likely caused by the fact that they are at similar latitudes and experience similar thermal tides. The tides also have a distinct pattern in longitude too, though, due to interference by the large-scale topography although this does not seem to be a factor here. A regional dust storm like in the case of Viking Lander 1 starting on around L_s 200° increases the amplitude. In the case of Pathfinder the amplitude variation increases considerably as a function of the Martian season (Schofield et al., 1997). The diurnal pressure amplitude seems to be highest at the Curiosity and Insight landing areas, which are located close to the equator and hence have the strongest thermal tides. On the other hand, Phoenix observations have the lowest diurnal pressure amplitude as expected due to the weaker thermal tide occurring at such high latitudes.

Basic characteristics of those seven Martian missions are shown in Table 1 including the climate zones and geographical locations (also in Figure 1) of those missions. It is to be noted that similarities on some of those characteristics allow interesting considerations to be made. Insight and Perseverance have a very similar altitude above the Martian geoid, which allows for direct comparison of the sol-averaged pressure data including the pressure variation with advancing Martian season. This is the most direct possibility for comparisons. As to the longitudinal location, Perseverance seems to be relatively isolated from the other landed missions. When inspecting the latitudinal location, Perseverance shares the same climate zone – North subtropics – with the Pathfinder and Viking 1 landers and is similarly able to feel the additional effects of baroclinic disturbances through the mesoscale small pressure variations that these disturbances cause at the surface. The same applies also to the traveling low- and high-pressure systems – typical both on Mars and the Earth - causing pressure variations in a 2–5 sols time range especially in the wintertime subtropics and low midlatitudes (James et al., 1992).

The shape of diurnal pressure variation at different Martian landing sites in four periods evenly separated over the first 414 Perseverance sols are shown in Figure 13. In each case, two sols of data are shown figure 13 (top left) shows clearly that the diurnal pressure amplitude observed by Curiosity in Gale crater is larger by a factor of 2-3 than for Perseverance in Jezero crater. The diurnal pressure amplitude observed by some other landing missions (Figure 13, top right) – Pathfinder, Viking Landers, Insight - is also smaller than what Curiosity has observed. The large amplitude of pressures observed by Curiosity has been shown by using atmospheric models to arise from the influence of a daily cycle of heating on the large slopes of Gale crater, such that warming of air causes mass to flow out of the crater in order to maintain hydrostatic balance along the slopes (Richardson and Newman, 2018). Perseverance observations indicate that the diurnal pressure range at the Jezero crater is smaller by a factor of 2-3, somewhat smaller amplitude than measured by Insight, about the same amplitude than calculated from historical observations of Viking lander 1 and 2 and, however, somewhat larger than diurnal pressure range measured by the Phoenix mission.

In the two lower rows of Figure 13 (panes c-f), approximately two sols for each lander at four solar longitude values marked in panes a-b are shown. Perseverance can be seen to have a similar mean pressure to InSight. This is likely due the similar elevations of around -2.6 km. The diurnal pressure patterns are similar in amplitude but slightly out of phase between Perseverance and InSight, most likely due to the 59° difference in longitude, i.e. the thermal tide will pass over Insight and then over Perseverance four hours later. Also note that the diurnal patterns for Curiosity and InSight, separated by only one degree of longitude, are similar except that Curiosity has a greater diurnal amplitude.

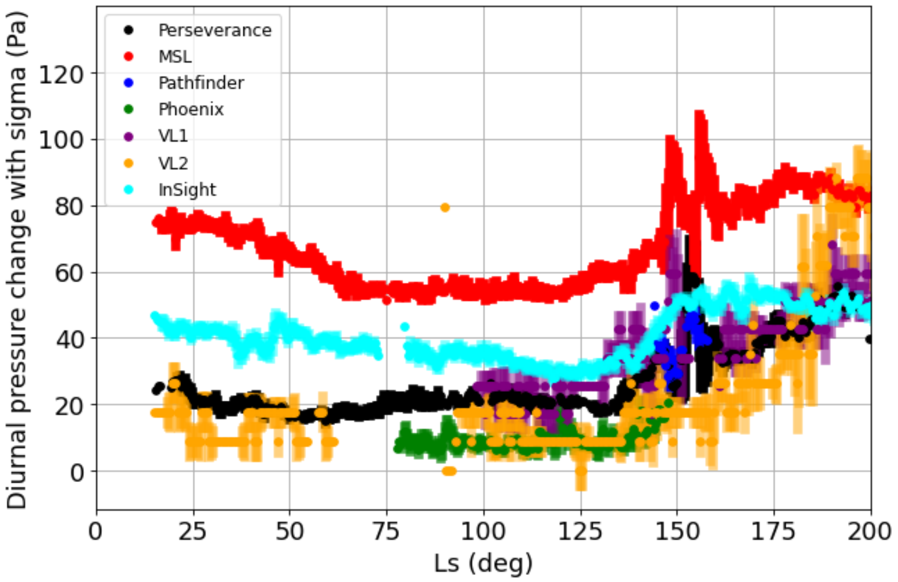

Figure 12. Diurnal pressure amplitude – minimum to maximum value – during the first 414 sols of the Perseverance mission with concurrently observed diurnal pressure amplitude of Insight and Curiosity missions, as well as that of historical Viking Landers, Pathfinder and Phoenix mission data on matching solar longitude range. Each diurnal pressure point is a moving 3-sol central average. The thickness of the curves represent the value of 2 standard deviations calculated over seven sols around each average diurnal pressure point.

At the Viking lander 2 site the daily pressure amplitude approaches similar levels to those observed by Curiosity only in the second half of the year, i.e. in the winter, as can be seen in figure 13 (b). The diurnal pressure amplitudes for the landers at high latitudes, i.e. Phoenix and Viking lander 2, during the northern hemisphere summer are small because of the weak thermal tide (Zhao et al., 2015). Curiosity and InSight latitudes (Table 1) are close to the equator and both have consistent daily pressures amplitudes throughout the year suggesting little variation in the thermal tide conditions at these latitudes.

Regional atmospheric modeling efforts are needed to expand the value of the *in situ* observations. This was done by running MarsWRF and MRAM models (Pla-Garcia et al., 2021) at the Perseverance site on solar longitude values of L_s 270°, 90°, 180° and 270°. Figure 14 illustrates these results together with *in situ* Perseverance observations at L_s 0°, 90°, 180° as well as data points acquired from the Mars Climate Database MCD (LMD-Jussieu, 2021).

MarsWRF and MRAMS simulate Jezero crater at high resolution. MarsWRF is a mesoscale nest embedded inside a global model model and MRAMS is a mesoscale model. Overall, MarsWRF and MRAMS as well as the lower-resolution MCD do fairly well compared to the actual *in situ* pressure observations. MarsWRF seems to reproduce the dip at 1700 better than MRAMS in Figure 14. MarsWRF reproduces the main features quite well except the small peaks at noon in the Northern springtime (L_s 0°, Figure 14a) and fall (L_s 180°, Figure 14c) where it generates a shoulder-like feature instead. The average pressure in Figure 14a for MarsWRF is generally good but in the Northern summertime (L_s 90°, Figure 14b) and fall (Figure 14c) the average pressure is too low. The height of the peaks in Figure 14b

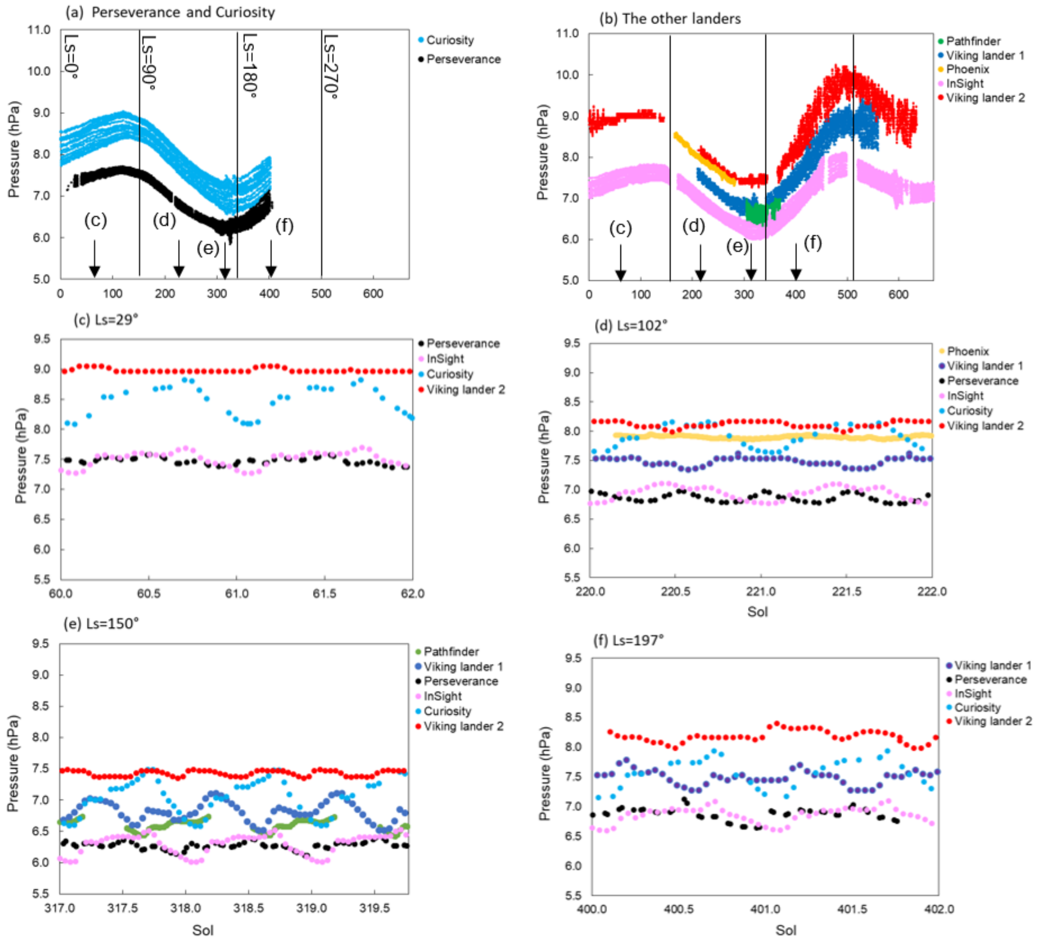

Figure 13. Diurnal pressure range of the Perseverance Rover compared over seasons with the diurnal pressure ranges observed by the Curiosity Rover, Insight Lander, Viking Lander 2 and Pathfinder (top row). Detailed diurnal pressure variation over 2-sol periods on these five surface missions is depicted at four solar longitudes evenly covering the first 414 sols of Perseverance operations. The lander data is plotted against the yearly sol, i.e. midnight on sol 1 corresponds to Ls=0° at the prime meridian, with midnight offset at each landing site depending on their longitude. The 2-sol periods were chosen in (c) to (f) over periods that avoided gaps in the lander data.

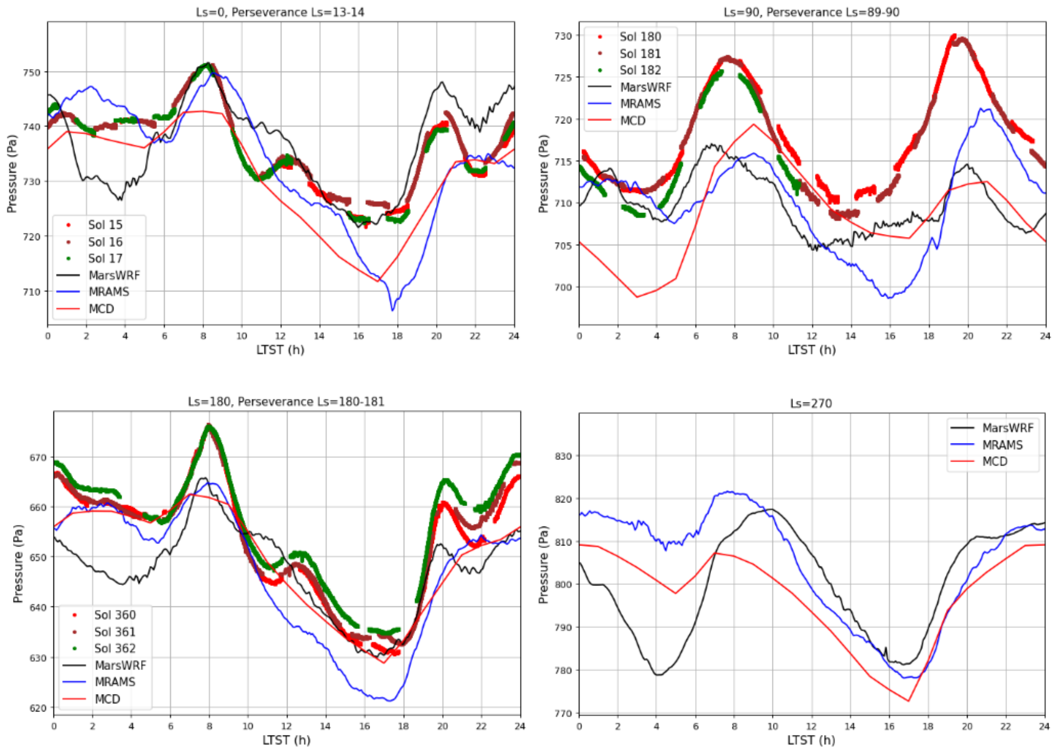

Figure 14. Diurnal pressure variation modeled by atmospheric models that simulate Jezero at km grid spacing MarsWRF, MRAMS and also the same data points from Mars Climate Database at solar longitude L_s 0°, 90°, 180° and 270°, which are depicted in panes a) to d). Around the solar longitude 0, 90 and 180 Perseverance pressure observations from three sols are added (Perseverance has no data as yet at L_s 270°).

are too low in the MarsWRF data. MCD is roughly producing in the average similar results to Mars WRF and MRAMS.

MRAMS matches the average pressure level quite well in Figure 14a if it was not for the big dip at 1700. It is not clear if it reproduces the peaks at 2200 and midnight. The occurrence of the peaks in the MRAMS data seems to be delayed by about 2 hours. Like MarsWRF MRAM does not reproduce the small peak at noon. MRAMS reproduces the height of the two big peaks in Figure 14b but they are on average too low. The timing of the peaks seems to be delayed by about 2 hours in Figure 14b. Overall, it seems to be the case that state-of-the-art regional atmospheric models succeed fairly well in producing diurnal pressure variation at the Jezero crater region. Then, understandably, reproducing through modeling the small peaks in diurnal pressure variation caused largely by the local geography and atmospheric flow conditions proves to be challenging.

The distinct oscillations in the observed surface pressure are expected to be primarily due to the thermal tides and their interactions with the Martian topography, e.g. Wilson and Hamilton (1996). Oscillations in the pressure could also include contributions of the local crater circulations that are especially important for deep craters like Gale crater (Tyler and Barnes, 2015; Wilson, 2017). In addition hydrostatic adjustment has been shown to be important in amplification of the amplitude of the diurnal pressure variation (Richardson and Newman, 2018).

This complex structure in the pressure signal was anticipated by Pla-Garcia et al. (2020). This is demonstrated in a distinct fashion in figure 14. A more comprehensive modeling study is needed, but the Perseverance pressure observations support the initial regional atmospheric modeling results at the Perseverance site made with the Mars WRF and MRAMS models as well as the data provided by MCD.

Jezero crater does not seem to have a similarly strong amplification from hydrostatic adjustment as is the case at the Gale crater based on the observations by the Curiosity rover (Harri et al., 2014; Newman et al., 2021). A plausible reason for this is the fact that compared to the Gale crater, the Jezero crater is shallow and wide resulting in relatively weaker amplification effect on the diurnal pressure variation amplitude. In addition the thermal tide at the Gale crater is stronger at most times of year than at Jezero crater because it is closer to the subsolar point for most of the year.

Combining the atmospheric regional modeling with *in situ* pressure observations proves to be highly useful – it adds the value of the observations by expanding their effect beyond the actual point of observation and sheds more light on the physical and meteorological processes behind the Martian atmospheric phenomena. The physics and implementation of the models themselves can also be modified to better address the actual atmosphere.

7 Summary and discussion

The Mars2020 Perseverance Rover landed successfully onto the Martian surface on the Jezero Crater floor (18°N, 77°E) at the Martian solar longitude L_s 5° in February 2021. Since then it has produced highly valuable environmental measurements with a versatile scientific payload including a suite of environmental sensors MEDA (Mars Environmental Dynamics Analyzer). One of the MEDA sensor systems is MEDA PS pressure device weighing 40 grams.

The Martian atmospheric pressure observations by MEDA PS have proved to be of excellent quality fulfilling expectations with the estimated overall uncertainty being equal or better than 3.5 Pa and the resolution about 0.13 Pa. The system resources required by the whole MEDA PS package are dimensions being 62×50×17 mm, mass 40g and power consumption less than 15 mW.

This paper presents initial results of the first 414 sols of Martian atmospheric surface pressure observations by the MEDA PS device whose performance was found to fulfill the specification. Observations controlled by the Perseverance resources allocation schedule cover approximately 50 – 70 % of the Perseverance operational time.

The atmospheric pressure measurement device (MEDA PS) is based on the silicon-micro-machined pressure sensor head (Barocap®) and transducer technology developed by Vaisala Inc. The Barocap® version used by MEDA PS is optimized for the Martian near-surface atmospheric pressure. The transducer electronics and required electromagnetic shielding and mechanical support structures were developed by Finnish Meteorological Institute (FMI).

The MEDA PS pressure device is making measurements continuously with 1 Hz frequency in average for every other hour according to the operational schedule by the Persevereance Rover. That enables us to generate data sets with averaged pressure measurements approximately at 1-hour intervals, as well as data sets with pressure observations at 1 second intervals for one or a few hours in a row for short time scale studies. In this work we use data sets with 1-hour intervals. The 1-hour data sets are not complete but they do have some gaps due to scheduling of Perseverance and MEDA operations. However, the available data coverage allows good characterisation of both the diurnal and seasonal variations in the pressure.

The seasonal-to-annual time scales the CO2 condensation-sublimation cycle of the Martian atmosphere is nicely demonstrated at the Jezero crater site by the Perseverance Rover measurements.The observed sol-averaged atmospheric pressure during the 414 first Perseverance sols from the landing time at early Northern springtime to Northern fall follow an anticipated pattern of total pressure variation in the course of the advancing season. The data has the first maximum in late spring roughly on the Perseverance sol 110 and minimum on sol 310, whereas by the Perseverance sol 414 corresponding to approximately L_s 212° the atmospheric pressure is climbing higher than the first maximum toward the seasonal maximum. When comparing Perseverance with concurrent observations by the Curiosity Rover and the Insight lander as well as with the historical Viking Landers data, we can see distinct differences with the amplitude of the seasonal pressure variation that are due to different surface elevations.

When comparing pressure observations of the seven Martian landing missions on different locations on Mars the first part of seasonal atmospheric pressure cycle measured by Perseverance seems to follow the seasonal increase and decrease in the atmospheric pressure as expected. The visible bias between the landers' pressure observations is largely due to different landing elevations. Detailed investigation reveals that during L_s $0 - 170°$ the Perseverance pressure looks to be decreasing somewhat more slowly than the pressure measured by the historical Viking landers. However, Insight exhibits similar kind of slow pressure decrease and hence this could be due to a regional occurrence possibly related with the regional topography or variability in large scale atmospheric flows.

The observed diurnal pressure amplitude is ranging roughly within 2 -5 % of the sol-averaged pressure with the absolute amplitude (10 – 35 hPa) not having a direct relationship with the sol-averaged pressure. The optical thickness varying with the amount of airborne dust seems to affect considerably the diurnal pressure amplitude. The increase of optical thickness from 0.5 to 0.8 around sols 130-160 seems to raise the diurnal pressure amplitude from approximately 20 hPa to 35 hPa. Regional atmospheric models seem to give roughly similar results on the average diurnal pressure amplitude, when Perseverance -like airborne dust conditions are assumed.

It appears to be evident that the range of diurnal atmospheric pressure varies considerably with location on Mars. The Perseverance diurnal pressure variation seem to be smaller than those measured by the Curiosity rover at Gale crater where tidal forcing is stronger due to the location close to the equator and also due to the fact that at Curiosity's longitude sector eastward and westward modes are expected to interact constructively. Comparison with pressure observations at other Martian sites it looks that also regional and local geography also play a role in the range of observed diurnal pressure variation.

When inspecting the structure of diurnal pressure, 2-4 small peaks appear in the data on each sol (Figure 6). A clear evolution of the peaks can be seen in the stacked diurnal pressure data. During Northern summer (Figure 6, second row from top) diurnal pressure exhibits two distinct and regular peaks, one in the morning around 6-7 AM and the other one around 8-9 PM LTST. During the Northern spring (Figure 6, top row) and fall (Figure 6, lowest rows) this summertime regular pattern is broken into more like four separate peaks whose amplitudes vary along with advancing season.

During Northern springtime - at the start of the mission, Perseverance sols 0-150 - it appears that smaller peaks are superimposed on the larger peaks. These smaller peaks disappear between about sols 150 and 250 (Northern summertime) and return around sol 300 in early fall. The wintertime has not yet come during the first 414 Perseverance sols. The features in the plots give clues on the behaviour of regional atmospheric dynamics and circulation patterns in the Martian atmosphere

The daily surface pressure profile seems to exhibit a largely repeatable two-peak shape during the Northern summertime (Figure 6). This is probably mostly due to the strong semi-diurnal thermal tidal component, which seems to be the case as illustrated in Figure 7.

MEDA PS observations allow us to estimate that about 100 thermal vortices with ¿ 0.5 Pa pressure drops during a 20 sol period throughout the first 414 Perseverance sols. Based on this analysis, the vortex activity at Jezero crater in the vicinity of Perseverance seems to be nearly constant with little seasonal variation. Apparently solar forcing varying considerably from springtime to fall has not affected the frequency of occurrence of thermal vortices. It is interesting to see whether this pattern will hold through the upcoming Northern wintertime.

Through *in situ* pressure observations and regional atmospheric modeling results a distinct local circulation pattern including nighttime katabatic and daytime upslope flows over the boundary of the Jezero crater was discovered. This circulation amplifies the diurnal pressure variation.

For comparison, the Gale crater diurnal pressure amplitude measured by the Curiosity Rover is much larger (50 to 120 hPa) than at the Jezero crater. This may be due to the fact that Gale is smaller and deeper than Jezero resulting in a stronger diurnal pressure cycle due to hydrostatic adjustment. On the plateaus with more gentle local circulation the diurnal pressure variation based on Viking Lander observations is weaker than at the Gale crater and about the same as given by Perseverance observations. On the other hand Insight diurnal pressure is higher than that of Perseverance during Northern springtime and summer but assumes roughly the same level during fall. Apparently the behavior of local diurnal pressure is affected by a mixture of solar forcing on the surface, airborne dust, regional geography and atmospheric wave activity.

The observed diurnal pressure variation seems to have a significant seasonal dependence. During Northern summer diurnal pressure displays two distinct and regular peaks, one in the morning around 6-7 AM and the other one around 8-9 PM LTST. This regular pattern is likely caused by the interaction of strong thermal tide and the seasonally varying airborne dust causing an amplified semi-diurnal component. During the Northern fall and spring this summertime regular pattern is broken into four separate peaks whose amplitudes vary along with advancing season.

The seasonal form of the diurnal pressure variation was investigated through regional atmospheric modeling by Mars WRF and MRAMS limited area models using the modeling results described in Pla-Garcia et al. (2020). The modeling results were compared with actual MEDA PS observations at solar longitude values L_s 0°, 90° and 180°, as well as with the MCD data. In the summertime (midsummer L_s 90°) the modeling results match very well with the shape and two-peak pattern of diurnal pressure cycle, but they underestimate the average pressure level. These modeling results showed the importance of the boundary fields for the regional models in getting pressure levels correct. Also the complexity of the diurnal pressure signal especially during the springtime and fall was revealed.

Overall, the modeling data seems to fit surprisingly well with the Perseverance pressure observations. Mars WRF and MRAMS have higher resolution than the relatively coarse MCD and hence these models pick up the local daily pressure variation better than MCD. But even the MCD seems to work surprisingly well, which is an excellent indication of the capabilities of current Martian atmospheric modeling tools. The modelling data indicates that they are correctly modelling the large-scale forcing of the main components of the daily pressure curves.

These modeling efforts underlined the clear need to investigate more in detail the diurnal pressure cycle as a superposition of the thermal tide, regional and local crater circulations and of various barotropic and baroclinic wave forms with seasonal dependence. These differences between the models and the observations inform us about the needs and areas to focus on in improving atmospheric models.

8 Open Research

The observational data used for this work is available in Planetary Data System (PDS) at the web site https://pds.nasa.gov/. MEDA instrument data is available in the PDS Atmospheres node in https://doi.org/10.17189/1522849 (Rodriguez-Manfredi & de la Torre Juarez, 2021).

Acknowledgments

Ari-Matti Harri, Mark Paton, Maria Hieta and Jouni Polkko are thankful for the Finnish Academy grant number 310509. Agustín Sánchez-Lavega and Ricardo Hueso were supported by Grant PID2019-109467GB-I00 funded by MCIN/AEI/10.13039/501100011033/ and by Grupos Gobierno Vasco IT1742-22.

References

Barnes, J. R., Pollack, J. B., Haberle, R. M., Leovy, C. B., Zurek, R. W., Lee, H., & Schaeffer, J. (1993). Mars atmospheric dynamics as simulated by the NASA Ames General Circulation Model, 2, transient baroclinic eddies. *J. Geophys. Res.*, *98*, 3125–3148.

Basu, S., Richardson, M. I., & Wilson, R. J. (2004, November). Simulation of the Martian dust cycle with the GFDL Mars GCM. *Journal of Geophysical Research (Planets)*, *109*(E11), E11006. doi: 10.1029/2004JE002243

Battalio, J. M., & Lora, J. M. (2021, August). Annular modes of variability in the atmospheres of Mars and Titan. *Nature Astronomy*, *5*, 1139-1147. doi: 10.1038/s41550-021-01447-4

Ferri, F., Smith, P. H., Lemmon, M., & Rennó, N. O. (2003, December). Dust devils as observed by Mars Pathfinder. *Journal of Geophysical Research (Planets)*, *108*(E12), 5133. doi: 10.1029/2000JE001421

Forget, F., Hourdin, F., Fournier, R., Hourdin, C., Talagrand, O., Collins, M., ... Huot, J.-P. (1999, October). Improved general circulation models of the Martian atmosphere from the surface to above 80 km. *J. Geophys. Res.*, *104*, 24155-24176. doi: 10.1029/1999JE001025

Golombek, M., Williams, N., Warner, N. H., Parker, T., Williams, M. G., Daubar, I., ... Sklyanskiy, E. (2020, October). Location and Setting of the Mars InSight Lander, Instruments, and Landing Site. *Earth and Space Science*, *7*(10), e01248. doi: 10.1029/2020EA001248

Golombek, M. P., Bridges, N. T., Moore, H. J., Murchie, S. L., Murphy, J. R., Parker, T. J., ... Wilson, G. R. (1999, April). Overview of the Mars Pathfinder Mission: Launch through landing, surface operations, data sets, and science results. *J. Geophys. Res.*, *104*(E4), 8523-8554. doi: 10.1029/98JE02554

Gómez-Elvira, J., Armiens, C., Castañer, L., Domínguez, M., Genzer, M., Gómez, F., ... Martín-Torres, J. (2012, September). REMS: The Environmental Sensor Suite for the Mars Science Laboratory Rover. *Space Sci. Rev.*, *170*, 583-640. doi: 10.1007/s11214-012-9921-1

Guo, X., Lawson, W. G., Richardson, M. I., & Toigo, A. (2009, July). Fitting the Viking lander surface pressure cycle with a Mars General Circulation Model. *Journal of Geophysical Research (Planets)*, *114*(E7), E07006. doi: 10.1029/2008JE003302

Guzewich, S. D., Newman, C. E., de la Torre Juárez, M., Wilson, R. J., Lemmon, M., Smith, M. D., ... Harri, A. M. (2016, April). Atmospheric tides in Gale Crater, Mars. *Icarus*, *268*, 37-49. doi: 10.1016/j.icarus.2015.12.028

Haberle, Houben, H. C., Hertenstein, R., & Herdtle, T. (1993, June). A boundary-layer model for Mars - Comparison with Viking lander and entry data. *J. Atmos. Sci.*, *50*, 1544-1559. doi: 10.1175/1520-0469(1993)050⟨1544:ABLMFM⟩2.0.CO;2

Haberle, R. M., Gómez-Elvira, J., de la Torre Juárez, M., Harri, A.-M., Hollingsworth, J. L., Kahanpää, H., ... Teams, R. S. (2014). Preliminary interpretation of the rems pressure data from the first 100 sols of the msl mission. *Journal of Geophysical Research: Planets*, *119*(3), 440-453. Retrieved from `https://agupubs.onlinelibrary.wiley.com/doi/abs/10.1002/2013JE004488` doi: https://doi.org/10.1002/2013JE004488

Harri, A. M., Genzer, M., Kemppinen, O., Kahanpää, H., Gomez-Elvira, J., Rodriguez-Manfredi, J. A., ... REMS/MSL Science Team (2014, January). Pressure observations by the Curiosity rover: Initial results. *Journal of Geophysical Research (Planets)*, *119*(1), 82-92. doi: 10.1002/2013JE004423

Hess, S. L., Ryan, J. A., Tillman, J. E., Henry, R. M., & Leovy, C. B. (1980, March). The annual cycle of pressure on Mars measured by Viking landers 1 and 2. *Geophys. Res. Lett.*, *7*, 197-200. doi: 10.1029/GL007i003p00197

Hourdin, F., Le van, P., Forget, F., & Talagrand, O. (1993, November). Meteorological Variability and the Annual Surface Pressure Cycle on Mars. *Journal of Atmospheric Sciences*, *50*(21), 3625-3640. doi: 10.1175/1520-0469(1993)050⟨3625:MVATAS⟩2.0.CO;2

Hueso, R., Newman, C. E., del Río-Gaztelurrutia, T., Munguira, A., Sánchez-Lavega, A., Toledo, D., ... Lepinette-Malvite, A. (2023). Convective vortices and dust devils detected and characterized by mars 2020. *Journal of Geophysical Research: Planets*, *128*(2), e2022JE007516. Retrieved from `https://agupubs.onlinelibrary.wiley.com/doi/abs/10.1029/2022JE007516` (e2022JE007516 2022JE007516) doi: https://doi.org/10.1029/2022JE007516

James, P. B., Kieffer, H. H., & Paige, D. A. (1992). The seasonal cycle of carbon dioxide on Mars. In H. H. Kieffer, B. M. Jakosky, C. W. Snyder, & M. S. Matthews (Eds.), *Mars* (p. 934-968). University of Arizona Press.

Kahre, M. A., & Haberle, R. M. (2010, June). Mars CO_2 cycle: Effects of airborne dust and polar cap ice emissivity. *Icarus*, *207*, 648-653.

Kieffer, H. H., Chase, S. C., Miner, E. D., Munch, G., & Neugebauer, G. (1973). Preliminary report on infrared radiometric measurements from the Mariner 9 spacecraft. *J. Geophys. Res.*, *78*, 4291–4312.

Kieffer, H. H., Jakosky, B. M., Snyder, C. W., & Matthews, M. S. (Eds.). (1992). *Mars*. University of Arizona Press.

Kieffer, H. H., Martin, T. Z., Peterfreund, A. R., Jakosky, B. M., Miner, E. D., & Palluconi, F. D. (1977). Thermal and albedo mapping of Mars during the Viking primary mission. *J. Geophys. Res.*, *82*, 4249–4291.

Kliore, A., Cain, D. L., Fjeldbo, G., Seidel, B. L., Sykes, M. J., & Woiceshyn, P. M. (1973, March). Some Recent Results of Mariner 9 Occultation Measurements of Mars. In *Bulletin of the american astronomical society* (Vol. 5, p. 298).

Kliore, A., Cain, D. L., Levy, G. S., Eshleman, V. R., Fjeldbo, G., & Drake, F. D. (1965, September). Occultation Experiment: Results of the First Direct Measurement of Mars's Atmosphere and Ionosphere. *Science*, *149*(3689), 1243-1248. doi: 10.1126/science.149.3689.1243

Kliore, A., Fjeldbo, G., Seidel, B. L., & Rasool, S. I. (1969, December). Mariners 6 and 7: Radio Occultation Measurements of the Atmosphere of Mars. *Science*, *166*(3911), 1393-1397. doi: 10.1126/science.166.3911.1393

Lee, C., Lawson, W. G., Richardson, M. I., Anderson, J. L., Collins, N., Hoar, T., & Mischna, M. (2011, November). Demonstration of ensemble data assimilation for Mars using DART, MarsWRF, and radiance observations from MGS TES. *Journal of Geophysical Research (Planets)*, *116*(E11), E11011. doi: 10.1029/2011JE003815

Lemmon, M. T., Smith, M. D., Viudez-Moreiras, D., de la Torre-Juarez, M., Vicente-Retortillo, A., Munguira, A., ... Apestigue, V. (2022). Dust, sand, and winds within an active martian storm in jezero crater. *Geophysical Research Letters*, *49*(17), e2022GL100126. Retrieved from `https://agupubs.onlinelibrary.wiley.com/doi/abs/10.1029/2022GL100126` (e2022GL100126 2022GL100126) doi: https://doi.org/10.1029/2022GL100126

Leovy, C. B., & Mintz, Y. (1969). Numerical simulation of the atmospheric circulation and climate of Mars. *J. Geophys. Res.*, *26*, 1167–1190.

LMD-Jussieu. (2021). *Mcd - mars climate database.* Retrieved from `http://www-mars.lmd.jussieu.fr/` (Accessed = 2022-8-26)

Montabone, L., Forget, F., Millour, E., Wilson, R. J., Lewis, S. R., Cantor, B., ... Wolff, M. J. (2015). Eight-year climatology of dust optical depth on mars. *Icarus*, *251*, 65-95. (Dynamic Mars) doi: https://doi.org/10.1016/j.icarus.2014.12.034

Montabone, L., Marsh, K., Lewis, S. R., Read, P. L., Smith, M. D., Holmes, J., ... Pamment, A. (2014). The mars analysis correction data assimilation (macda) dataset v1.0. *Geoscience Data Journal*, *1*(2), 129-139. Retrieved from

https://rmets.onlinelibrary.wiley.com/doi/abs/10.1002/gdj3.13 doi: https://doi.org/10.1002/gdj3.13
Newman, C., Bertrand, T., Battalio, J., Day, M., De La Torre Juárez, M., Elrod, M. K., ... Zorzano, M.-P. (2021, May). Toward More Realistic Simulation and Prediction of Dust Storms on Mars. In *Bulletin of the american astronomical society* (Vol. 53, p. 278). doi: 10.3847/25c2cfeb.726b0b65
Newman, C., Juárez, M., Pla-García, J., Wilson, R., Lewis, S., Neary, L., ... Rodriguez-Manfredi, J. (2021, 02). Multi-model meteorological and aeolian predictions for mars 2020 and the jezero crater region. *Space Science Reviews*, *217*. doi: 10.1007/s11214-020-00788-2
Newman, C. E., Gómez-Elvira, J., Marin, M., Navarro, S., Torres, J., Richardson, M. I., ... Bridges, N. T. (2017, July). Winds measured by the Rover Environmental Monitoring Station (REMS) during the Mars Science Laboratory (MSL) rover's Bagnold Dunes Campaign and comparison with numerical modeling using MarsWRF. *Icarus*, *291*, 203-231. doi: 10.1016/j.icarus.2016.12.016
Newman, C. E., Hueso, R., Lemmon, M. T., Munguira, A., Álvaro Vicente-Retortillo, Apestigue, V., ... Guzewich, S. D. (2022). The dynamic atmospheric and aeolian environment of jezero crater, mars. *Science Advances*, *8*(21), eabn3783. Retrieved from https://www.science.org/doi/abs/10.1126/sciadv.abn3783 doi: 10.1126/sciadv.abn3783
Newman, C. E., Lee, C., Mischna, M. A., Richardson, M. I., & Shirley, J. H. (2019, January). An initial assessment of the impact of postulated orbit-spin coupling on Mars dust storm variability in fully interactive dust simulations. *Icarus*, *317*, 649-668. doi: 10.1016/j.icarus.2018.07.023
Paige, D. A., & Ingersoll, A. P. (1985, June). Annual Heat Balance of Martian Polar Caps: Viking Observations. *Science*, *228*(4704), 1160-1168. doi: 10.1126/science.228.4704.1160
Pollack, J. B., Haberle, R. M., Schaeffer, J., & Lee, H. (1990). Simulations of the general circulation of the Martian atmosphere 1. polar processes. *J. Geophys. Res.*, *95*, 1447–1473.
Pollack, J. B., Leovy, C. B., Greiman, P. W., & Mintz, Y. (1981). A Martian general circulation experiment with large topography. *J. Atmos. Sci.*, *38*, 3–29.
Rafkin, S. C. R., Pla-Garcia, J., Kahre, M., Gomez-Elvira, J., Hamilton, V. E., Marín, M., ... Vasavada, A. (2016, December). The meteorology of Gale Crater as determined from Rover Environmental Monitoring Station observations and numerical modeling. Part II: Interpretation. *Icarus*, *280*, 114-138. doi: 10.1016/j.icarus.2016.01.031
Read, P., & Lewis, S. (2004). *The martian climate revisited - atmosphere and environment of a desert planet.* Springer.
Richardson, M. I., & Newman, C. E. (2018, December). On the relationship between surface pressure, terrain elevation, and air temperature. Part I: The large diurnal surface pressure range at Gale Crater, Mars and its origin due to lateral hydrostatic adjustment. *Planet. Space Sci.*, *164*, 132-157. doi: 10.1016/j.pss.2018.07.003
Richardson, M. I., Toigo, A. D., & Newman, C. E. (2007). PlanetWRF: A general purpose, local to global numerical model for planetary atmospheric and climate dynamics. *J. Geophys. Res.*, *112*, 9001. doi: 10.1029/2006JE002825
Rodriguez-Manfredi, J. A., de la Torre Juárez, M., Alonso, A., Apéstigue, V., Arruego, I., Atienza, T., ... MEDA Team (2021, April). The Mars Environmental Dynamics Analyzer, MEDA. A Suite of Environmental Sensors for the Mars 2020 Mission. *Space Sci. Rev.*, *217*(3), 48. doi: 10.1007/s11214-021-00816-9
Rodriguez-Manfredi, J. A., & de la Torre Juarez, M. (2021). *Mars 2020 meda bundle dataset.* (NASA. Retrievable from https://doi.org/10.17189/1522849)

Rogberg, P., Read, P. L., Lewis, S. R., & Montabone, L. (2010, August). Assessing atmospheric predictability on Mars using numerical weather prediction and data assimilation. *Quarterly Journal of the Royal Meteorological Society*, *136*(651), 1614-1635. doi: 10.1002/qj.677

Savijärvi, H., & Kauhanen, J. (2008, April). Surface and boundary-layer modelling for the mars exploration rover sites. *Quarterly J. Royal Met. Soc.*, *134*, 635-641. doi: 10.1002/qj.232

Savijärvi, H., & Määttänen, A. (2010, August). Boundary-layer simulations for the Mars Phoenix lander site. *Quarterly J. Royal Met. Soc.*, *136*, 1497-1505. doi: 10.1002/qj.650

Schofield, J. T., Barnes, J. R., Crisp, D., Haberle, R. M., Larsen, S., Magalhaes, J. A., ... Wilson, G. (1997, December). The Mars Pathfinder Atmospheric Structure Investigation/Meteorology. *Science*, *278*, 1752. doi: 10.1126/science.278.5344.1752

Smith, D. E., Zuber, M. T., Frey, H. V., Garvin, J. B., Head, J. W., Muhleman, D. O., ... Sun, X. (2001, October). Mars Orbiter Laser Altimeter: Experiment summary after the first year of global mapping of Mars. *J. Geophys. Res.*, *106*(E10), 23689-23722. doi: 10.1029/2000JE001364

Snyder, C. W., & Moroz, V. I. (1992). Spacecraft exploration of Mars. In H. H. Kieffer, B. M. Jakosky, C. W. Snyder, & M. S. Matthews (Eds.), *Mars* (p. 71-119). University of Arizona Press.

Soffen, G. A. (1976, December). Scientific results of the Viking missions. *Science*, *194*, 1274-1276. doi: 10.1126/science.194.4271.1274

Soffen, G. A. (1977, September). The viking project. *J. Geophys. Res.*, *82*, 3959-3970. doi: 10.1029/JS082i028p03959

Sánchez-Lavega, A., del Rio-Gaztelurrutia, T., Hueso, R., Juárez, M. d. l. T., Martínez, G. M., Harri, A.-M., ... Mäkinen, T. (2023). Mars 2020 perseverance rover studies of the martian atmosphere over jezero from pressure measurements. *Journal of Geophysical Research: Planets*, *128*(1), e2022JE007480. Retrieved from `https://agupubs.onlinelibrary.wiley.com/doi/abs/10.1029/2022JE007480` (e2022JE007480 2022JE007480) doi: https://doi.org/10.1029/2022JE007480

Taylor, P. A., Catling, D. C., Daly, M., Dickinson, C. S., Gunnlaugsson, H. P., Harri, A.-M., & Lange, C. F. (2008, July). Temperature, pressure, and wind instrumentation in the Phoenix meteorological package. *J. Geophys. Res.*, *113*, 0. doi: 10.1029/2007JE003015

Tillman, J. E. (1988, August). Mars global atmospheric oscillations - Annually synchronized, transient normal-mode oscillations and the triggering of global dust storms. *J. Geophys. Res.*, *93*, 9433-9451. doi: 10.1029/JD093iD08p09433

Tillman, J. E., Henry, R. M., & Hess, S. L. (1979, June). Frontal systems during passage of the Martian north polar HOOD over the Viking Lander 2 site prior to the first 1977 dust storm. *J. Geophys. Res.*, *84*, 2947-2955. doi: 10.1029/JB084iB06p02947

Tillman, J. E., Johnson, N. C., Guttorp, P., & Percival, D. B. (1994). Erratum: "The Martian annual atmospheric pressure cycle: Years without great dust storms" [J. Geophys. Res., 98(E6), 10,963-10,971 (1993]. *J. Geophys. Res.*, *99*, 3813-3814. doi: 10.1029/94JE00232

Toigo, A. D., & Richardson, M. I. (2003, November). Meteorology of proposed Mars Exploration Rover landing sites. *Journal of Geophysical Research (Planets)*, *108*(E12), 8092. doi: 10.1029/2003JE002064

Wilson, R. J., & Hamilton, K. (1996, May). Comprehensive model simulation of thermal tides in the Martian atmosphere. *Journal of Atmospheric Sciences*, *53*(9), 1290-1326. doi: 10.1175/1520-0469(1996)053⟨1290:CMSOTT⟩2.0.CO;2

Young, L. D. G. (1969, November). Interpretation of High-Resolution Spectra of Mars. I. CO_2 Abundance and Surface Pressure Derived from the Curve of

Growth. *icarus*, *11*(3), 386-389. doi: 10.1016/0019-1035(69)90070-0
Zurek, R. W. (1978, August). Solar heating of the Martian dusty atmosphere. *Icarus*, *35*, 196-208. doi: 10.1016/0019-1035(78)90005-2
Zurek, R. W. (1981, January). Inference of dust opacities for the 1977 Martian great dust storms from Viking Lander 1 pressure data. *Icarus*, *45*, 202-215. doi: 10.1016/0019-1035(81)90014-2
Zurek, R. W. (1982, June). Martian great dust storms - an update. *Icarus*, *50*, 288-310. doi: 10.1016/0019-1035(82)90127-0
Zurek, R. W. (1992). Comparative aspects of the climate of Mars: an introduction to the current atmosphere. In H. H. Kieffer, B. M. Jakosky, C. W. Snyder, & M. S. Matthews (Eds.), *Mars* (p. 799-817). University of Arizona Press.
Zurek, R. W., Barnes, J. R., Haberle, R. M., Pollack, J. B., Tillman, J. E., & Leovy, C. B. (1992a). Dynamics of the atmosphere of Mars. In H. H. Kieffer, B. M. Jakosky, C. W. Snyder, & M. S. Matthews (Eds.), *Mars* (p. 835-934). University of Arizona Press.
Zurek, R. W., Barnes, J. R., Haberle, R. M., Pollack, J. B., Tillman, J. E., & Leovy, C. B. (1992b). Dynamics of the atmosphere of Mars. In H. H. Kieffer, B. M. Jakosky, C. W. Snyder, & M. S. Matthews (Eds.), *Mars* (p. 835–934). University of Arizona Press.

Perseverance MEDA Atmospheric Pressure Observations - Initial Results

Ari-Matti Harri[1*], Mark Paton[1], Maria Hieta[1], Jouni Polkko[1], Claire Newman[2], Jorge Pla-Garcia[3], Joonas Leino[1], Terhi Mäkinen[1], Janne Kauhanen[1], Iina Jaakonaho[1], Agustin Sánchez-Lavega[4], Ricardo Hueso[4], Maria Genzer[1], Ralph Lorenz[5], Mark Lemmon[6], Alvaro Vicente-Retortillo[3], Leslie K. Tamppari[7], Daniel Viudez-Moreiras[3], Manuel de la Torre-Juarez[7], Hannu Savijärvi[1], Javier A. Rodríguez-Manfredi[3], German Martinez[8]

[1]Finnish Meteorological Institute, Helsinki, Finland
[2]Aeolis Research, Chandler, AZ, USA
[3]Centro de Astrobiología (INTA-CSIC), Madrid, Spain
[4]UPV/EHU, Bilbao, Spain
[5]Johns Hopkins Applied Physics Laboratory, Laurel, MD, USA
[6]Space Science Institute, College Station, TX, USA
[7]Jet Propulsion Laboratory/California Institute of Technology, Pasadena, CA, USA
[8]Lunar and Planetary Institute, Houston, TX, USA

Key Points:

- The atmospheric pressure observations by Perseverance Rover have proved to be of excellent quality fulfilling expectations
- Jezero crater pressure exhibits significant differences to other Martian areas likely due to varying regional geography and solar forcing
- Overall, the diurnal and seasonal atmospheric pressure cycles at Jezero Crater follow an anticipated pattern of pressure variation

*P.O. Box 503, 00101 Helsiki, Finland

Corresponding author: Ari-Matti Harri, `Ari-Matti.Harri@fmi.fi`

Abstract

The Mars2020 Perseverance Rover landed successfully on the Martian surface on the Jezero Crater floor (18.44°N, 77.45°E) at Martian solar longitude, L_s, ∼5 in February 2021. Since then it has produced highly valuable environmental measurements with a versatile scientific payload including the MEDA (Mars Environmental Dynamics Analyzer) suite of environmental sensors. One of the MEDA systems is the PS pressure sensor system which weighs 40 grams and has an estimated absolute accuracy of better than 3.5 Pa and a resolution of 0.13 Pa. We present initial results from the first 414 sols of Martian atmospheric surface pressure observations by the PS whose performance was found to meet its specifications. Observed sol-averaged atmospheric pressures follow an anticipated pattern of pressure variation in the course of the advancing season and are consistent with data from other landing missions. The observed diurnal pressure amplitude varies by ∼2-5 % of the sol-averaged pressure, with absolute amplitude 10-35 Pa in an approximately direct relationship with airborne dust. During a regional dust storm, which began at L_s 135° the diurnal pressure amplitude roughly doubles. The diurnal pressure variations were found to be remarkably sensitive to the seasonal evolution of the atmosphere. In particular analysis of the diurnal pressure signature revealed diagnostic information likely related to the regional scale structure of the atmosphere. Comparison of Perseverance pressure observations to data from other landers reveals the global scale seasonal behaviour of Mars' atmosphere.

Plain Language Summary

The Mars2020 Perseverance Rover successfully arrived at Mars in February 2021. It landed during an early Martian spring afternoon in a crater north of Mars' equator called Jezero crater. The rover is equipped with meteorological instruments that have so far produced extensive and valuable data for understanding the Martian atmosphere. One of the meteorological instruments is an accurate and precise pressure sensor. The pressure sensor has revealed large changes in the pressure over the seasons that are related to large changes in the actual mass of the Martian atmosphere. This is in line with seasonal pressure changes measured during previous Mars missions and can be explained as the freezing of the atmosphere onto the Martian poles and its subsequent thaw. On a shorter time scale the pressure sensor revealed complex pressure changes over a Martian day. These variations are thought to be related to atmospheric dust whose ubiquitous nature is known to have a strong influence on the Martian climate. As the seasons progressed the daily pressure variations morphed to exhibit different patterns likely related to the large-scale regional changes in the atmosphere. Comparison of Perseverance pressure observations to other landers revealed the global nature of the atmosphere.

1 Introduction

The Mars2020 Perseverance Rover landed successfully on the Martian surface on the Jezero Crater floor (18.44°N, 77.45°E) at the Martian solar longitude, $L_s, 5°$ in February 2021. Since then, it has produced highly valuable environmental measurements with a versatile scientific payload including the MEDA (Mars Environmental Dynamics Analyzer) suite of environmental sensors (?, ?). One of the MEDA sensor systems is the pressure sensor (PS) whose observations and initial results utilizing the data acquired during the first 414 sols of the mission ($L_s 5 - 212°$) will be addressed in this manuscript.

Martian atmospheric investigations through spacecraft observations began in the early to middle 1960s as reported by, *e.g.*, ? (?, ?) and later by ? (?, ?, ?, ?, ?).

Surface pressure of the atmosphere was firstly estimated using remote sensing methods, both ground based by *e.g.* (?, ?) and from spacecraft starting from Mariner as reported by, *e.g*, (?, ?). The Viking landers in 1974-77 provided the first time series of *in situ* atmospheric observations that turned out to be a treasure trove of data covering multiple Martian years (?, ?, ?, ?, ?). Thereafter Mars Pathfinder (?, ?, ?), the Phoenix lander (?, ?, ?), the Mars Science Laboratory aka Curiosity Rover (?, ?), the InSight lander (?, ?) and the Perseverance Rover (?, ?) have continued *in situ* investigations of the Martian atmosphere including accurate atmospheric pressure observations.

During the years of *in situ* and remote observations, Martian atmospheric observations have been accompanied and supplemented by increasingly sophisticated and varied modeling efforts in a range of spatial and temporal scales already since late 1960s (?, ?, ?, ?, ?, ?, ?, ?, ?, ?, ?, ?). Pressure observations from surface stations have prompted investigations of the CO2 cycle and its connection to the poles, ice and dust e.g. ? (?, ?). The characacterisation of pressure changes due to large scale circulations (?, ?, ?) and local meteorology (?, ?, ?) have been predicted and characterised using computer models.

Data assimilation using orbital data is an important activity to enable realistic predictions using atmospheric models and verifying the physics (?, ?, ?, ?). Better understanding of the behaviour of the Martian atmosphere can help develop better predictions e.g. ? (?). A network of surface pressure stations could could be key to characterising fast evolving weather systems and dust lifting events (?, ?). Our current understanding of the Martian atmosphere and its processes is still understandably far less detailed than our understanding of our own terrestrial atmosphere, but the Martian atmospheric phenomena are presently clearly much better understood than those of any other solar system atmospheres.

Some of the earlier Martian landing vehicles have operated at similar latitudes or elevations to Perseverance, resulting in similarities in terms of climate zone or annual mean atmospheric pressure. Figure 1 shows the locations of Martian landing vehicles with Martian topography, giving a clear idea of the differences in the altitude and type of terrain of the landing sites. In terms of longitude, however, Perseverance seems to be relatively isolated, which has implications when comparing to data from other landed missions. Perseverance observations also have particular significance because they mean that for the first time, we have four *in situ* sets of meteorological observations being carried out at the same time at different locations on the Martian surface (including observations by MSL, InSight, Perseverance, and also China's Zhurong rover, data from which are not currently publicly available). We will present several interesting initial discoveries based on these facts, in addition to the independent Perseverance pressure observations.

In addition to this article there are two companion articles in this journal utilizing the pressure data focusing on atmospheric dynamics (?, ?) and small-scale thermal vortices (?, ?).

2 Brief MEDA PS device specification and performance

Instrument description. The Perseverance pressure measurement device (MEDA PS) is based on the silicon-micro-machined pressure sensor head (Barocap®) and transducer technology developed by Vaisala Inc. The Barocap® version used by MEDA PS is optimized for the Martian near-surface atmospheric pressure. Changing ambient pressure is changing the sensor head capacitance by varying the distance of the sensor head capacitor plates. Besides being pressure dependent, the Barocap® capacitance is also sensitive to temperature, and thus accurate temper-

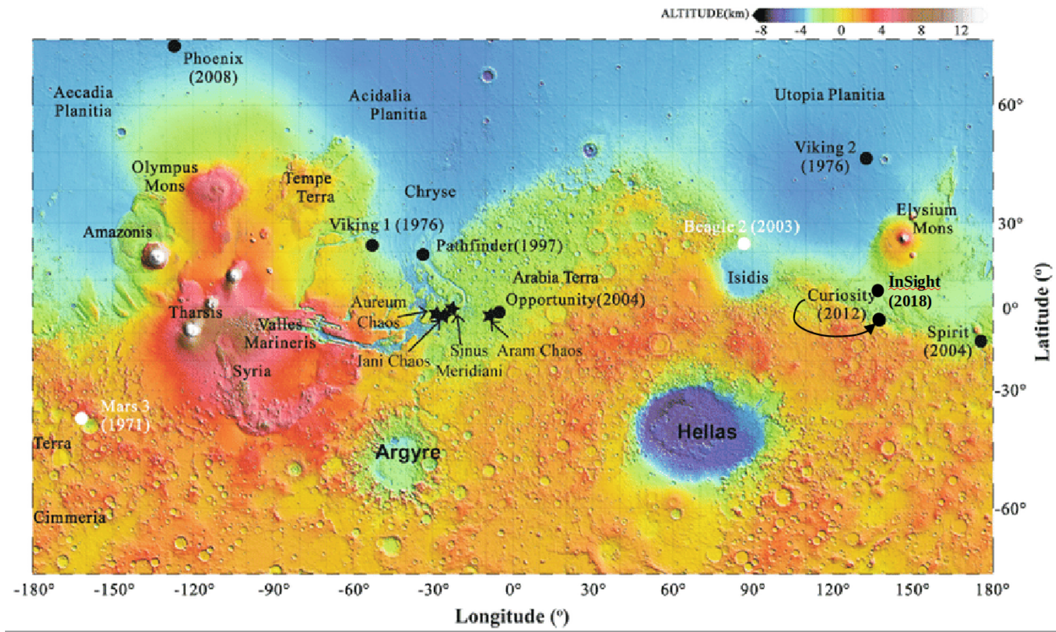

Figure 1. Landing sites of the seven spacecraft having provided *in situ* atmospheric data depicted on a topographic map of Mars (NASA JPL, 2021).

ature measurements close to the sensor head are necessary. The supporting housekeeping temperature measurements are provided by Vaisala's Thermocap® sensor heads.

MEDA PS consists of two transducers, each having its controlling ASIC (application specific integrated circuit) and 8 channels containing the Barocap sensor heads, Thermocap sensor heads and constant reference capacitors. Two types of Barocap sensors are used: the NGM type with high stability and relatively long warm-up time and the less stable but faster RSP2M type as a backup. Hence, the primary sensor for scientific investigations is the NGM type Barocap on transducer 1 channel 8 and the secondary sensor the RSP2M Barocap on transducer 1 channel 6. We provide a calibrated pressure reading for both sensor heads in the DER and CAL type data products in the PDS archive (?, ?) that are optimal for most investigations.

Calibration and performance. MEDA PS has been calibrated at the Finnish Meteorological Institute (FMI) laboratories over the expected operational pressure and temperature ranges. The calibration has been performed in stable temperatures from -45°C to +55°C and stable pressure points ranging from 0 hPa to 14 hPa, which extend well beyond the pressure and temperature ranges prevailing within the electronics compartment housing the MEDA PS on Mars itself. Calibration measurements were also performed in changing pressure and temperature conditions. The Barocap sensors are known to have small changes in the temperature dependence or sensor offset when introduced to a new electrical and thermal environment, and thus calibration checks were performed at all stages after the sensor-level calibration. The calibration checks were performed after integration to the MEDA electronics compartment (MEDA ICU), during the final rover-level thermal vacuum test, during the interplanetary cruise and soon after landing on Mars. The RSP2M Barocaps are also periodically cross-checked against the primary Barocap for possible drift compensation.

fig-2-MEDA-PS-sensorhead-and.package.png

Figure 2. MEDA PS device within its Faraday cage made out of thin conductive foil (ltop eft pane) and the instrument with its pressure sensor heads and part of the electronics visible without the Faraday cover (top right pane). The structure of the silicon micromachined sensor head is shown on the lower row.

The estimated MEDA PS uncertainty based on the sensor- and rover-level measurements was analyzed to be better than 3.5 Pa. This includes the effects of the short-term repeatability, environmental effects and the pressure reference accuracy. The resolution of the primary Barocap, restricted mostly by the electronics noise, is 0.13 Pa in nominal measurement mode, and 0.1 Pa in high-resolution mode, as determined in sensor-level measurements. According to the test data, the time response of MEDA PS is equal to or less than 1 s, having almost no effect on the measurements at the nominal sampling rate of 1 Hz. The effect of the warm-up time of the NGM Barocaps has been removed by the calibration.

The system resources required by the whole MEDA PS package are dimensions 62×50×17 mm, mass 43 g and power consumption less than 15 mW. The MEDA PS detailed specification available before the launch of the Perseverance Rover is described in detail by (?, ?). The MEDA PS is located inside the MEDA Instrument Control Unit (ICU) in the rover body, with a filter-protected tube connecting it to the outside environment and conveying ambient pressure to be measured. The MEDA PS device is depicted in Figure 2 illustratating the pressure sensor head and its encapsulation of the full pressure device in a Faraday cage giving shielding against electromagnetic interference.

During the first 414 Martian sols of Perseverance operations MEDA PS has been functioning as expected. The temperature dependence of the Barocap sensors was checked and corrected at the beginning of the operations against the primary Barocap, which is known to be very stable based on the test data. In the first drift offset check performed after 150 sols, the drift of the secondary Barocap was less than 0.3 Pa and slightly larger for the other RSP2M Barocaps.

3 MEDA PS observation strategy and pressure data coverage

MEDA has been designed for flexible operations that are being conducted according to the scheduling by the Perseverance rover. MEDA measures for five minutes at the top of each hour in local mean solar time (LMST) in every mission sol, other than during exceptional circumstances. In addition, on average, MEDA is operating continuously for every other hour. That enables us to generate data sets with averaged pressure measurements approximately at 1-hour intervals, as well as data sets with pressure observations at 1 second intervals for a period of one hour or a few hours in a row for *e.g.* turbulence-related studies. There are also periods, when MEDA is only able to measure for five minutes per hour (or sometimes fifteen or twenty minutes per hour) or is doing no measurements at all for a few hours, due to Perseverance resource allocation reasons.

In the present investigations we use data sets with 1-hour intervals. The 1-hour data sets are not complete but they do have gaps due to scheduling of Perseverance and MEDA operations. Figure 3 illustrates how well the observed data sets cover each Perseverance sol. in the average about 50-70 % of the 24 hour of a sol throughout the season with some periods having 100 % coverage and few sols have no pressure data at all. The gaps in the 1-hour data set take place more or less randomly around the 24 hour Martian sol. The data coverage of this level allows good characterisation of both the diurnal and seasonal variations in the pressure.

4 Changes in Jezero crater atmospheric pressure with seasonal cycle

The condensation and sublimation of CO2 in the polar regions during winter and spring causes planetwide seasonal variations in the surface pressure, which were first detected by the Viking landers as reported by, *e.g.*, ? (?, ?). The seasonal CO2

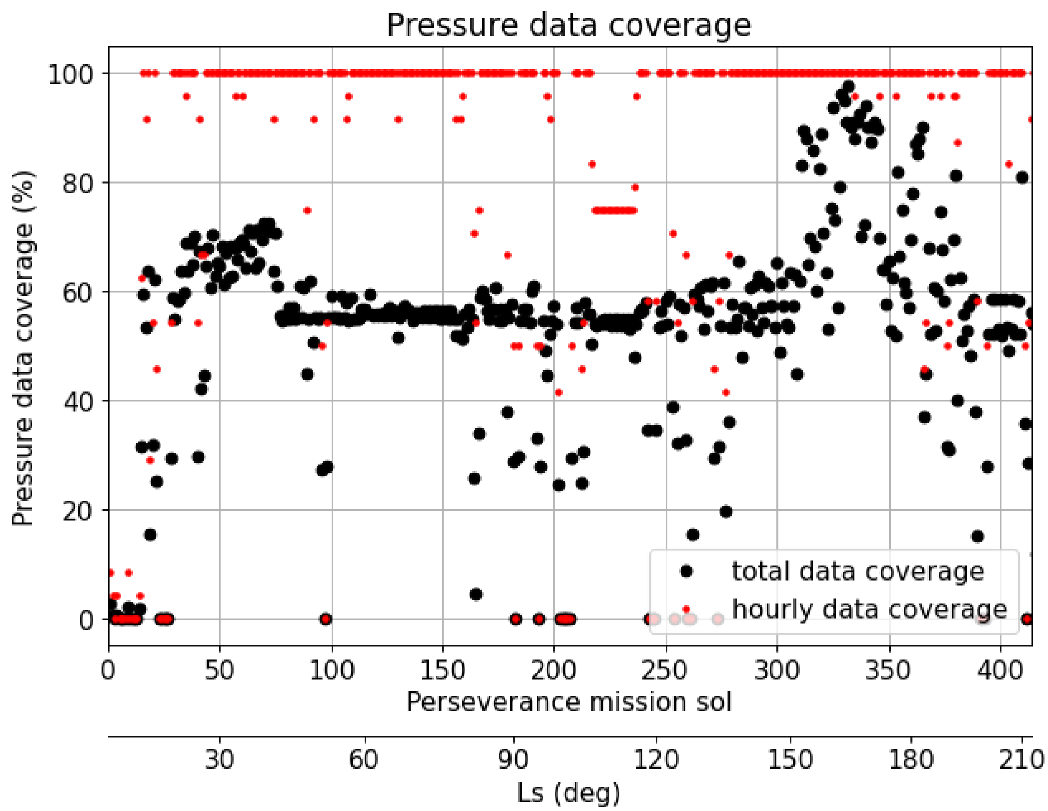

Figure 3. The coverage of atmospheric pressure observations made by the MEDA PS instrument. The black dots depict the overall percentage of pressure readings once per second in a sol, red dots the percentage of the pressure readings available at 1-hour intervals.

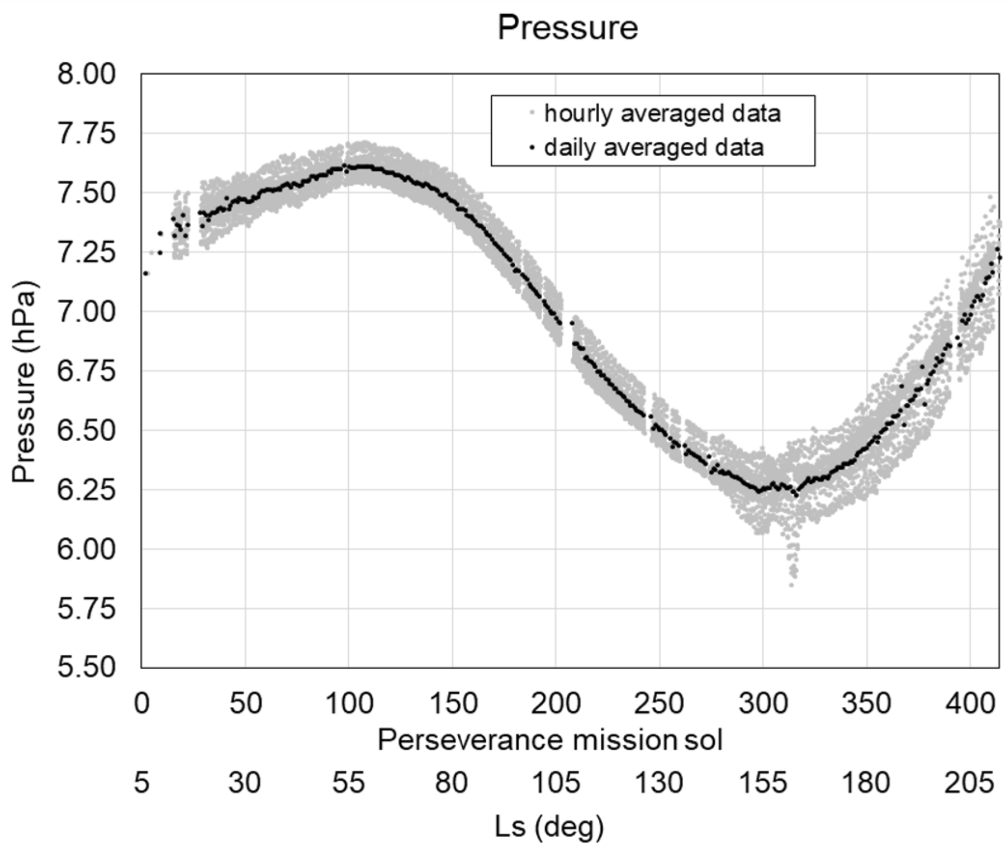

Figure 4. The sol averaged pressure data and the diurnal pressure amplitude (approximate total peak-to-peak range based on observations once per hour) for Perseverance during the period of the first 414 sols corresponding to approximately solar longitude range of L_s $5 - 212°$.

cycle, which is largely controlled by the polar heat balance (?, ?, e.g.,), can clearly be seen in the seasonal variation of daily average surface pressure.

This is nicely demonstrated at the Jezero crater site by the Perseverance Rover measurements. The daily averaged atmospheric surface pressure during the first 414 sols of the Perseverance mission is depicted in Figure 4. The figure also includes the range of diurnal pressure variation plotted on both sides of the average pressure line with a gray color. Hence the gray area illustrates the approximate total range of diurnal pressure variation around the average pressure of a sol. The minimum pressure peak at around Ls 153 shown in Figure 4 was likely caused by a regional dust storm (?, ?).

In seasonal-to-annual time scales the CO2 condensation-sublimation cycle at the polar regions gives rise to a seasonal pressure variation on the order of as much as 30 % of the local surface pressure (?, ?, ?, e.g.,). The observed sol-averaged atmospheric pressure during the 414 first Perseverance sols, from the landing time at early Northern springtime to Northern fall, follows an anticipated pattern of total pressure variation in the course of the advancing season. The data has the first maximum in late spring roughly on Perseverance sol 110 and a minimum on sol 310, whereas by the Perseverance sol 414 (corresponding to approximately L_s 212°) the atmospheric pressure is climbing higher than the first maximum toward the annual maximum. When comparing Perseverance with concurrent observations by the

Table 1. Essential characteristics of seven Martian lander missions performing atmospheric observations. The elevations are based on MOLA data (?, ?)

Vehicle	Lat (°N)	Lon (°E)	Elevation (km)	Climate Zone	Operational (years)	Platform Type
Viking lander 1	22	-48	-3.6	North subtropics	1976-82	Stationary
Viking lander 2	48	134	-4.4	North midlatitudes	1976-80	Stationary
Mars Pathfinder	19	-34	-3.7	North subtropics	1997	Stationary
Phoenix	68	-126	-4.1	North polar regions	2008	Stationary
Curiosity	-4.6	137	-4.5	Equatorial regions	2012-	Mobile
InSight	4.5	136	-2.6	Equatorial regions	2020-	Stationary
Perseverance	18	77	-2.6	North subtropics	2021-	Mobile

Curiosity Rover and the Insight lander as well as with the historical Viking Landers data, we can see distinct differences in the amplitude of the seasonal pressure variations that are due to different surface elevations.

The sol-averaged MEDA PS atmospheric pressure data together with the hourly-averaged pressure depicted in Figure 4 is nicely showing the evolution of the atmospheric pressure over first 414 Perseverance sols at the Jezero crater site. In the beginning of the data set the pressure is going down during the Northern spring and summer seasons and turning to an increasing leg during the late summer. The diurnal amplitude, shown approximately by the gray area in Figure 4, shows a clear increase during periods with increased amounts of airborne dust starting approximately from Perseverance sol 270 and staying high until sol 414 (when our investigation period ends). There seems to be a direct relationship between the range of diurnal pressure variation and the amount of airborne dust as has been earlier discovered by, *e.g.*, ? (?, ?, ?).

The seasonal dependence of the Martian atmospheric pressure drives the atmosphere to the extent that about one third of the mass of the Martian atmosphere is deposited on the polar caps during Northern and Southern winters and evaporated back to the atmosphere during summertime. This results in the characteristic atmospheric pressure pattern having two local maxima and minima during a Martian year, with the maxima occurring approximately at solar longitudes L_s 60° and L_s 260°. This pattern can clearly be seen in Figure 5, which compares the sol-averaged pressure of Perseverance with Curiosity Rover, Insight Lander, Viking Landers and the Pathfinder mission. Table 1 gives the basic characteristics of each mission.

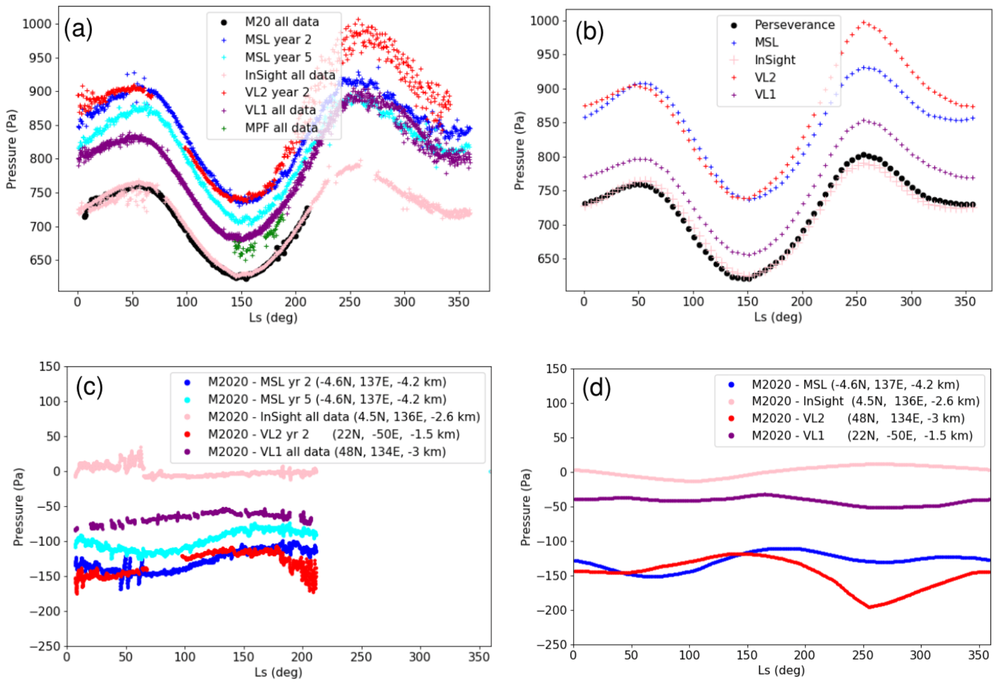

Figure 5. Comparisons of pressure between different lander missions. The top row shows the sol averaged observed pressure data, and the bottom row sol-averaged pressure data by different lander missions subtracted from Perseverance pressures. The left column shows results from the observations while on the right are the same results from the Mars Climate Database.

Investigations of the seasonal pressure cycle together with observations from other Martian landing missions enhance our understanding of the CO2 cycle, the annual heat balance of the polar caps and the global scale atmospheric circulation of Mars (?, ?, ?). Major drivers behind the seasonal variation are solar radiation and surface and subsurface thermal properties (Wood and Paige, 1992). Atmospheric dust loading and regional circulation will influence short scale variations (?, ?, ?). The annually averaged atmospheric pressure is largely depending on the elevation of the site and hence the atmospheric pressures are differing between observation sites (?, ?, ?).

In order to investigate the relative evolution of the pressure cycle at different latitudes figures 5 (c) and 5 (d) show the differences in pressure between the Perseverance landing site and the other four landers, excluding Pathfinder. In figures 5 (c) and (d) a more negative pressure signifies a higher pressure compared to Perseverance. The results from MCD data shown in figure 5 (d) tracks in the evolution of the results for the observational data shown in figure 5 (c). For Curiosity there are two sets of lines in figure 5 (c). These correspond to years 2 and 3 of the mission with year 3 being at a higher elevation which explain the difference in the mean pressure. There are a number of interesting dip or hump-like features over timescales of 100-200 sols in figure 5 (c) and (d) that need explaining.

The dips and humps in the season pressures in figure 5 (c) and (d) are most likely connected to latitude dependant processes that include the orographic, i.e.

the large difference in elevation between the northern and southern hemisphere, and the dynamical effects on the pressure cycle (?, ?). Regarding the orographic effect, during northern hemisphere winter a large mass of cool air is trapped in the low elevation of the northern hemisphere basin. In the winter a low atmospheric scale height traps a large portion of the atmosphere. The result is a higher winter maximum at higher latitudes in the northern hemisphere in winter. For example the heights of the winter and summer pressure peaks for Viking landers 1 is much more symmetric than for Viking lander 2. We will not cover dynamical effect here, which is related to the winds, as it apparently has little influence at the equatorial and middle latitudes considered here. An explanation of the dynamical effect can be found in ? (?).

The greatest dip seen is for the Viking lander 2 in 5 (d) which is at a latitude of 48°N. This results from the pressure observed by Viking lander 2 increasing more rapidly than the pressure observed by Perseverance most likely due to the orographic effect. For the other landers the, except maybe for Curiosity, the pressure differences in figures 5 (c) and (d) are fairly level indicating the pressures at these landing site increase more or less at the same rate.

A shallow but distinct dip can be seen for Curiosity in figures 5 (c) and (d) over the spring-summer time period. A possible reason for a dip at this time of year is that the cold air trapped in the northern hemisphere trapped during the winter is now being released as it is the summer. This lowers the pressure faster at the Perseverance landing site than at the Curiosity landing site, which is located near the equator in the southern hemisphere. This would result a relative increase in the pressure between Curiosity and Perseverance as seen in figure 5 (c) and (d). Both plots for Curiosity exhibit a dip around the summer solstice indicating that the process driving the evolution of the pressure, i.e. the dip, is not related to the change in elevation.

There are shallow dips and and troughs in the data for other landers in figures 5 (c) and (d) but these are less obvious and probably cannot be interpreted with much certainty. For example there appears to be a small dip in the MCD data for InSight in figure 5 (d). This might be expected because InSight is located at a more southerly latitude than Perseverance with InSight being less sensitive to the ejection of summer time air from the northern basin than Perseverance. Interestingly this dip cannot be seen in Figure 5 (c) perhaps suggesting some other process or mechanism is masking the effect in the observations or limits with the model.

5 Diurnal atmospheric pressure and small scale atmospheric phenomena

In situ pressure observations by several landed missions have shown that the Martian atmospheric surface pressure is composed of variations over several time scales and amplitudes. They include, *e.g.*, the overarching seasonal CO2 cycle, regional-scale perturbations caused by planetary waves and thermal tides, including their interactions with topography, hydrostatic adjustment flows, and baroclinic and barotropic disturbances. Small scale eddies and disturbances, e.g. convective vortices are a usual cause of the shortest pressure variations of the order of a few tens of seconds (?, ?, e.g.). If the vortices carry an optically distinguishable dust load they are called dust devils.

Thermal tides driven by solar irradiation cause distinct detectable diurnal pressure variations and are especially significant at low latitudes. In the Martian thin atmosphere the thermal tides - and hence the range of diurnal pressure variation

- are much larger than in Earth's atmosphere due to the relatively stronger solar forcing at the surface (?, ?, ?).

At the Jezero crater site measured by Perseverance rover the diurnal atmospheric pressure range seems to be approximately 20 Pa during the first 270 sols of the mission and thereafter during mission sols 270-414 extending to roughly 40 Pa. The wider range of diurnal pressure is likely due to increased amounts of airborne dust measured by Perseverance. Several earlier investigations have found the direct relationship between the amount of airborne dust and the range of diurnal pressure variation as shown by, *e.g.*, ? (?, ?, ?).

The Perseverance in situ pressure observations show variations ranging from microscale to seasonal scale as has been observed by earlier *in situ* pressure measurements of Viking (?, ?, ?), Pathfinder (?, ?), Phoenix (?, ?) and Curiosity missions (?, ?, ?). The advancing Martian season has a clear signature in the atmospheric pressure as clearly manifested by Figure 6 depicting the diurnal pressure variation by data stacked in steps of 10 sols. It shows the gradual increase of the observed Perseverance pressure levels during the Northern spring until approximately sol 110, then gradual decrease bypassing the Northern midsummer (Ls 90) until sol 320, and thereafter again showing increasing pressure until the last sol (414) of this investigation when the season advances further into the Northern fall. The data of this investigation covers only 60 % of the Martian year, but this kind of seasonal dependence will be seen throughout the Martian year.

When inspecting the structure of diurnal pressure, 2-4 peaks appear in the data on each sol in Figure 6. A clear evolution of the peaks can be seen in the stacked diurnal pressure data. During Northern summer (Figure 6, second row from top) diurnal pressure exhibits two distinct and regular peaks, one in the morning around 6-7 AM and the other one around 8-9 PM LTST. During the Northern spring (Figure 6, top row) and fall (Figure 6, lowest rows) this summertime regular pattern is broken into more like four separate peaks whose amplitudes vary along with advancing season.

It seems that during springtime - at the start of the mission, Perseverance sols 0-150 - smaller peaks are superimposed on the larger peaks. These smaller peaks disappear between about sols 150 and 250 (Northern summertime) and return around sol 300 in early Northern fall. The wintertime has not yet come during the first 414 Perseverance sols. The features in the plots give clues on the behaviour of regional atmospheric dynamics and circulation patterns in the Martian atmosphere (?, ?, e.g.).

The largely repeatable two-peak shape of the daily surface pressure profile especially during the Northern summertime (Figure 6) is likely due to the strong semi-diurnal thermal tidal component as indicated in Figure 7. Abundant amount of airborne dust is one cause responsible for amplified semi-diurnal tidal component as shown by, e.g., (?, ?, ?). Similar two-peak structure was also discovered during Pathfinder mission ? (?).

The harmonic components – principal components - of daily pressure variations sheds light on our understanding on the atmospheric phenomena behind the complex structure of daily pressure cycle. The principal components of the atmospheric diurnal pressure variation can be revealed by decomposing the pressure observations through Fourier transformation. The estimated diurnal, semi-, ter- and quad-diurnal amplitudes are represented by the first four components of the resulting series representation, respectively, as shown in Figure 7 together with the Perseverance optical thickness observations.

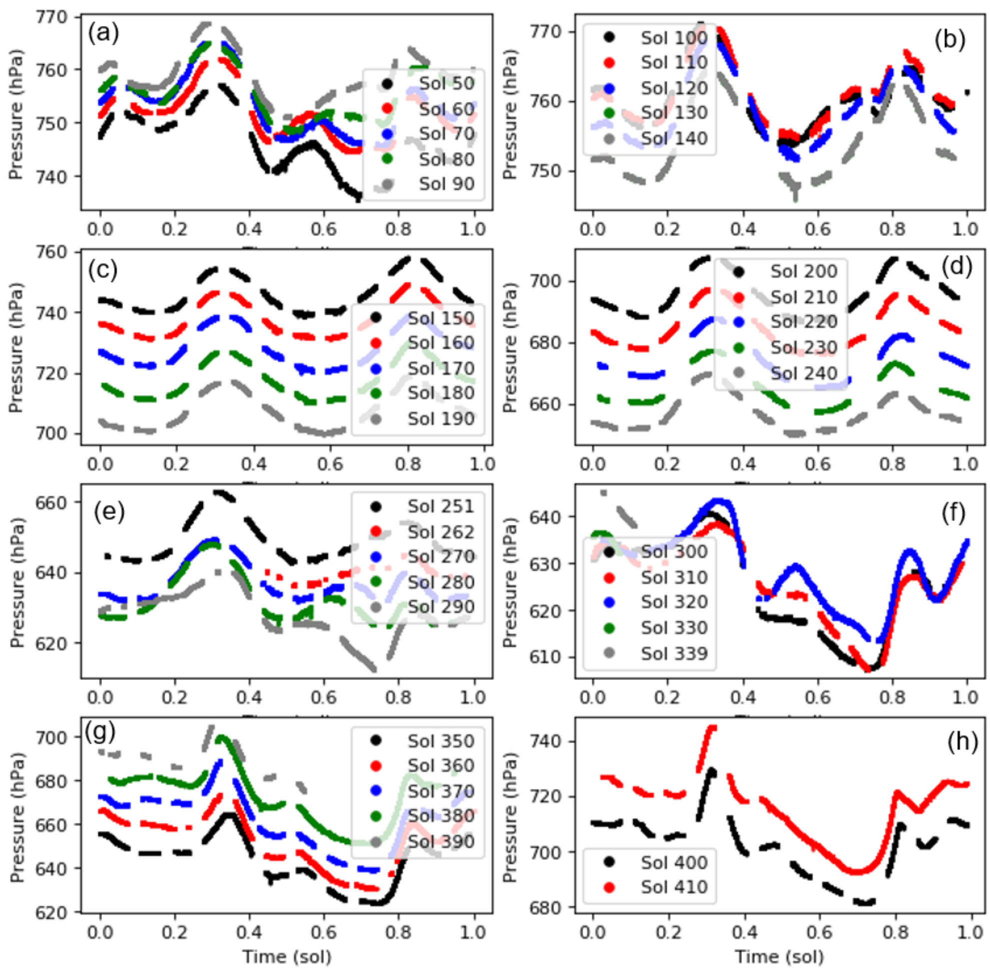

Figure 6. Evolution of diurnal pressure variation in steps of 10 sols covering the first 414 Perseverance sols during the advancing season. Each figure shows data averaged over five sols centered on the sol number shown, except the last on the bottom right (pane h).

figs/fig-7-P-Diurnal-FFT-Amp-Phase.png

Figure 7. The amplitude and phase of the first four harmonic components of diurnal pressure calculated using FFT for all Perseverance sols. A running averaging window of three sols was used in the calculations. The amplitudes (top pane) and phases (lower pane) are illustrated in different colors (left axis). On the amplitude plot also the optical thickness observed by Perseverance is also shown (right axis).

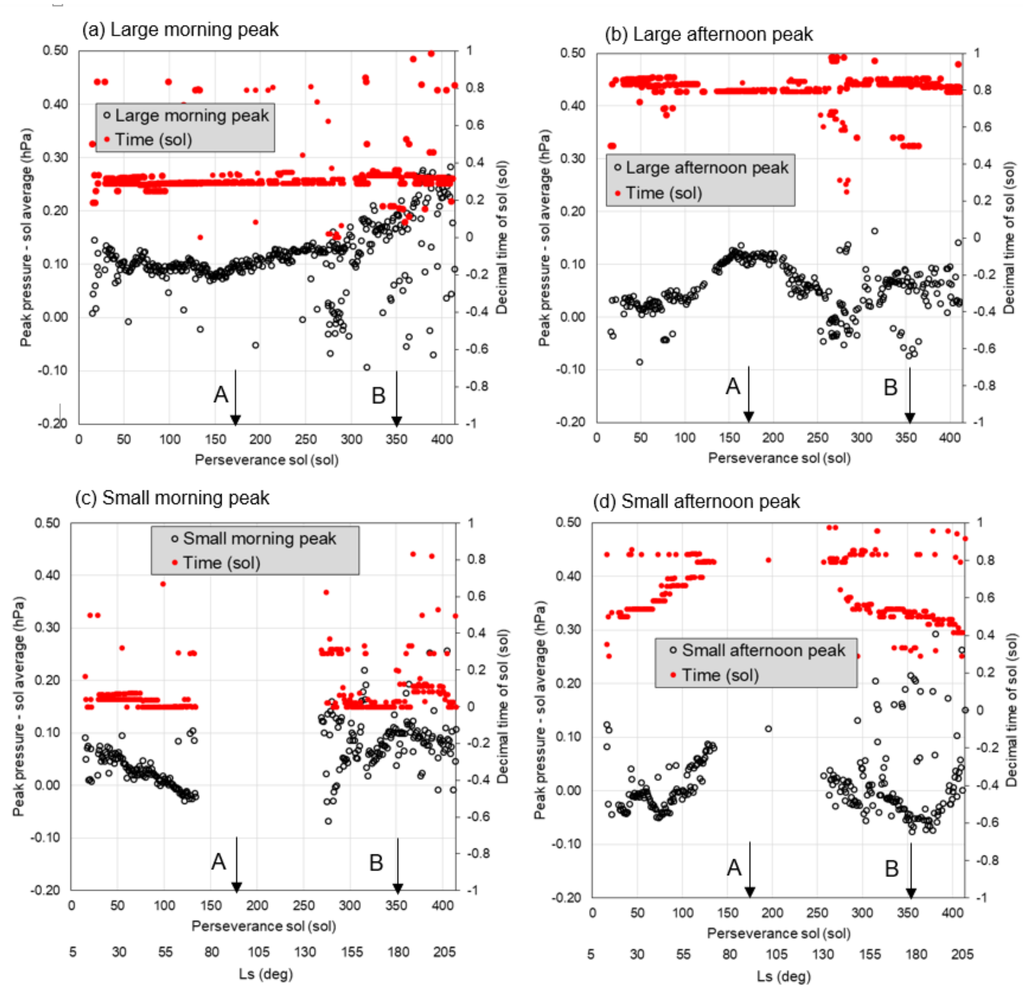

Figure 8. Black circles show the peak pressure minus sol averaged pressure. The time of occurrence of the peaks is also shown in red. The time has an uncertainty on it of plus or minus half an hour. The scatter in the points arises from relatively small fluctuations in flat regions of the data, *e.g.* in the dips between the peaks. The letters 'A' and 'B' point to midsummer (L_s 90° and fall L_s 180°, respectively.

The Fourier transformations shown in Figure 7 were calculated using a fast Fourier transform (FFT) scheme. The input data series was created by generating hourly bins of observations from a window of three sols to get at least one observation per hour. In case of multiple observations per hour the bin value was achieved by averaging. The middle sol of the three-sol window was the one that was assigned the calculated amplitudes and phases. When using this procedure it was assumed that the three consecutive sols were sufficiently similar for calculating the principal components. The analysis was performed by sliding the three-sol window over the first 414 sols of Perseverance observations.

The principal components of the Perseverance diurnal pressure variation seem to be smaller than those measured by the Curiosity rover at Gale crater where tidal forcing is stronger due to the location close to the equator and also due to the fact that, at Curiosity's longitude sector, eastward and westward modes are expected to interact constructively (Wilson and Hamilton, 1996; Haberle et al., 2013; Harri et al., 2014).

In the light of the strong semi-diurnal component shown in Figure 7 during the Northern summer (sols 150-250), the prevailing stable 2-peak diurnal pressure cycle may be due to the strong summertime tidal forcing by relatively high amount of regional airborne dust creating a strong and stable semidiurnal component (Figure 7, top panel). This situation resembles that in the terrestrial tropics, where diurnal pressure has two distinct peaks, too – one in the morning and one in the evening. In the terrestrial tropics this is due to high-altitude ozone, whereas in northern late spring and early summer on Mars this may be due to the ever-present airborne dust getting heated by solar irradiation (Read and Lewis, 2001).

The semidiurnal tidal component at Jezero crater seems to be strong during Perseverance's Northern summer. This may be due to the fact that regional atmospheric dust load is relatively high at that time, which would amplify the semidiurnal component - assisted by the strong solar forcing at the Northern summer. Optical depth maps retrieved from the Mars Climate Database, based on data sets generated by ? (?), seem to support our inference. The maps from the MCD suggest that during the summer Perseverance is on the western edge of a patch of elevated optical depth that stretches over several 10s of degrees of longitude to the west. Later on in the year the optical depth at the latitude of Perseverance is more homogeneous.

The seasonal evolution of diurnal pressure and its pattern of variation is shown in Figure 6. We found that during the Northern summertime a fairly stable pattern of two peaks was prevailing in diurnal pressure variation, but that was broken into four peaks during the spring and fall. Now, we can study further the evolution of the daily pressure pattern by analyzing the peaks and their evolution with the advancing season (Figure 8). This is done by subtracting the average pressure of the sol of interest from maximum pressure to get the peak amplitude and also noting the local time of occurrence.

Figure 8 shows the peak pressures relative to the daily-averaged sol pressure and the time that the peaks occur. As can be seen in Figures 6 and 8 there is one large peak both in the morning and in the afternoon that persist in the daily pressure data. These are clearly illustrated in the top row of Figure 8. The time these peaks occur remains steady throughout sols 50 to 400 in the data. Their magnitude varies with the large morning peak increasing after about sol 150. The large afternoon peak reaches a maximum around sol 150.

Figure 6 shows small morning and afternoon peaks prevailing during Northern springtime and fall. They are also depicted in Figure 8, where it can be seen

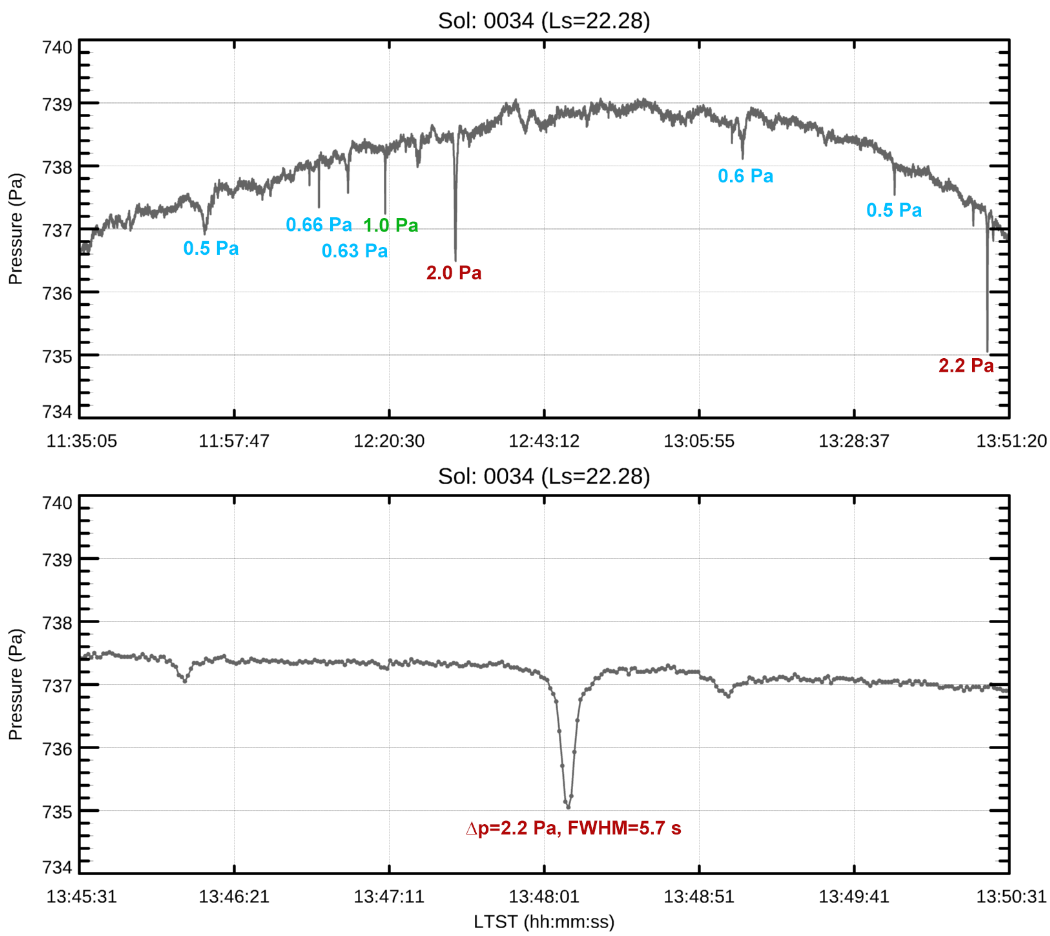

Figure 9. An example of vortex activity detected in pressure data over a 1.5 hour period around noon during the Perceverance mission sol 34. The upper pane displays vortex activity that can be seen as downward spikes in pressure with the depth of some spikes indicated. The lower pane zooms in on the deepest spike (2.2 Pa) to show a more detailed spike structure indicating also the full width at half maximum (FWHM) of the spike.

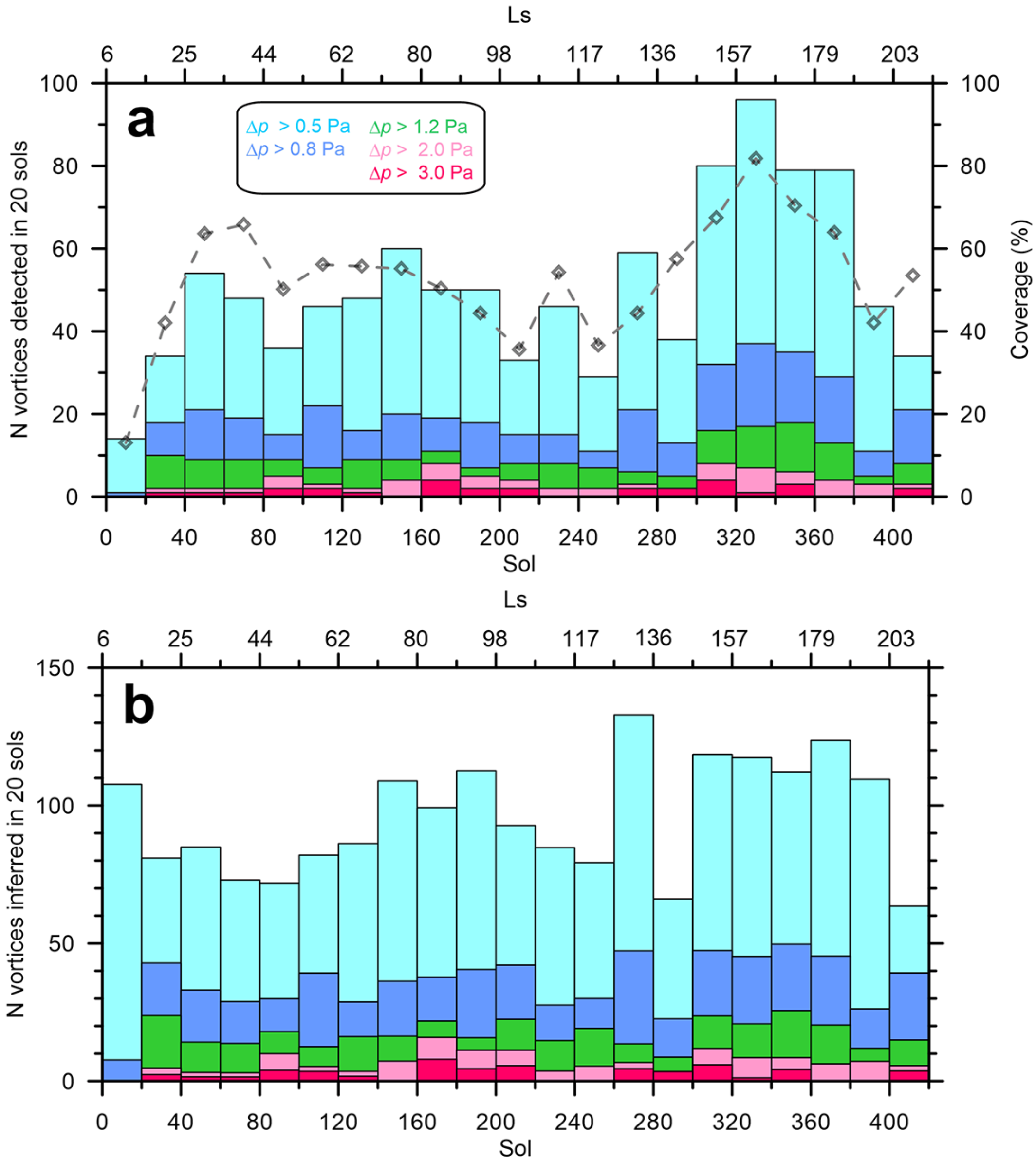

Figure 10. Assessment of the number of vortices by Perceverance through atmospheric pressure drops as a function of sol. (a) Number of vortices actually detected in intervals of 20 sols (left axis). The rhombs show the coverage of MEDA pressure data in each time interval (right axis). (b) Number of vortices that would have been detected if MEDA data would have been measured continuously. In both panes the intensity of the pressure drops is indicated by color coding as explained in the legend.

(bottom row) that the small morning peak occurs at the same time each sol but the magnitude decreases until about sol 140 and then the peaks disappear. They reappear around sol 270 but appear to fluctuate in magnitude before settling down to a near constant value around sol 360. In Figure 8 (lower right) the small afternoon peaks appear to increase in magnitude before disappearing around sol 140. They then reappear around sol 260 and decrease in magnitude with the advancing sols.

These interesting morning and afternoon peak variations illustrated by Figures 6 and 8 could be a manifestation of local circulation phenomena causing pressure variation, which is then superposed with the strong semidiurnal pressure mode. During the Northern summer the semi-diurnal thermal tide (as shown by the semi-diurnal pressure variation) is at its strongest, which creates a stable diurnal pressure variation with one distinct large peak in the morning and another one in the afternoon. During the Northern spring and fall the semidiurnal mode of the thermal tide is weaker than in summer. Hence the stable situation is broken resulting in the creation of two additional small peaks, one preceding the large morning peak and another preceding the large afternoon peak.

This kind of pressure peak structure riding on top of the diurnal pressure variation is possibly caused by local effects due to the more complex topography of Jezero crater as compared, *e.g.*, to the topographically more simple and flat region of the Pathfinder and Viking Lander sites (?, ?, ?), where such peaks are not so clearly visible. On the other hand, at the Curiosity rover site additional peaks are also seen in the diurnal pressure variation, which is likely due to the fact that Gale crater is also a topographically complex site (?, ?, ?). Variations in the thermal tide could also introduce multiple oscillations into the observed surface pressure. ? (?) suggest interference effects between the westward tide and the eastern travelling topographically induced Kelvin mode could produce surface pressure observations with two minima and two maxima per sol.

A highly interesting atmospheric phenomenon regularly observed in pressure data are convective vortices - called dust devils when raising surface dust in the atmosphere (?, ?, ?, e.g.). These rotating small scale atmospheric phenomena are investigated in this journal issue by (?, ?) using Perseverance pressure observations. Vortices appear as pressure drops in MEDA data, some times in bursts of activity as displayed by Figure 9 and 10 based on the investigations by ? (?). These pressure drops are most likely caused by passages of thermal vortices. Some of these events can be identified as dust devils when observing with additional MEDA radiative sensors able to infer the presence of dust, and by other instruments onboard Perseverance such as rover cameras. In the context of the Aeolian environment of Jezero, thermal vortices were discussed by ? (?). These studies provide the overall abundance of vortices at Jezero, their daily cycle of activity, which peaks roughly at local noon, with some seasonal variation in the transition from summer to fall, the frequency of vortices that carry dust and are therefore dust devils, and establish the link between vortex activity and the thermal gradient of the near surface atmosphere.

An interesting aspect of vortex activity at Jezero revealed originally by the work of ? (?)) is the nearly constant activity with little seasonal variation during the period of observation of this investigation. This is demonstrated by Figure 10 showing the statistics of detected and estimated amount of vortices during the period of the first 414 Perseverance sols. This allows us to estimate (Figure 10) that about 100 thermal vortices with pressure drops exceeding 0.5 Pa during a 20 sol period are dwelling in the Perseverance neighbourhood throughout the first 414 Perseverance sols. Thus the vortex activity at Jezero seems to be nearly constant through the first 414 Perseverance sols. Apparently solar forcing varying considerably from springtime to fall has not significantly affected the generation of vortices. It is interesting to see whether this pattern will hold through the upcoming Northern wintertime with decreasing thermal forcing.

Martian atmospheric small scale turbulence and dynamics can be investigated using Perseverance observations accompanied by additional Perseverance measurements. These phenomena are studied in an accompanying paper in this journal issue by ? (?).

6 Perseverance diurnal pressure compared with other landing sites and modeling results

Atmospheric diurnal pressure variation is affected by *e.g.* the strength of thermal tide, regional and local geography and amount of airborne dust and hence some local atmospheric phenomena can be partially explained by studying diurnal pressure variation (?, ?, ?, ?, ?, e.g.). The diurnal pressure amplitude – minimum to maximum range – as a function of solar longitude for both Perseverance and Curiosity rovers is depicted in Figure 11 including the measured optical depth. Additionally results by regional models MWRF (squares) and MRAMS (plus-signs), as well as values by Mars Climate Database (diamonds) are shown. Furthermore, an uncertainty corridor of two standard deviations is drawn on the pressure amplitude by smoothing over a few sols. The standard deviation of the diurnal pressure range is calculated over 10 sols and it is then drawn on both sides of the curve. Thus the width of the uncertainty shown is thus twice the standard deviation.

The diurnal pressure variation exhibits a clear amplitude increase with the increasing amount of the atmospheric dust, which was reported by Curiosity pressure observations (Haberle et al., 2013; Harri et al., 2014). This phenomenon has been discovered also earlier by, *e.g.* ? (?, ?, ?, ?). Actually, this is considered as a manifestation of how the Martian atmospheric conditions are intertwined with the airborne dust to such extent that atmospheric diurnal pressure observations could even be used to infer the amount of dust afloat *e.g.* (?, ?, ?).

Figure 11 shows that the observed daily amplitudes in pressure are similar to those predicted by two atmospheric models that cover Jezero crater at km scale resolution (MRAMS and MarsWRF). The amplitude predicted by MRAMS is usually slightly higher and MarsWRF slightly lower, for the Ls with data available. The models use TES optical depth zonally averaged over previous non dust storm years (Pla-Garcia et al., 2020) (?, ?). As to the MCD values for the location of Perseverance (18°N, 77°E) the optical depth used in these models is similar to those observed by Perseverance. Note that the pressure amplitude in the MCD, which has a resolution of order several hundred km, is also similar to that observed by Perseverance.

It is interesting to compare the average amplitude of diurnal pressure variation – minimum to maximum value – at different locations and for varying Martian altitudes and terrain. The Martian atmospheric pressure has some interannual variation, but it appears to be sufficiently small to the extent that the atmospheric pressure at each landing site seems to be behaving largely in a similar fashion from year to year as shown by, *e.g.*, ? (?, ?). This interannual similarity justifies qualitative and also somewhat quantitative comparison of pressure by different landing missions even if they are not observed at the same time, but rather in different Martian years. This applies especially to diurnal pressure variation that is being largely driven by thermal tide, local geography and regional atmospheric flows.

Figure 12 depicts the daily pressure amplitude during the first 414 sols of the Perseverance mission with concurrently observed daily pressure amplitudes of the Insight and Curiosity missions, as well as that of historical Viking Landers, Pathfinder and Phoenix mission data at matching solar longitudes. Basic characteristics of

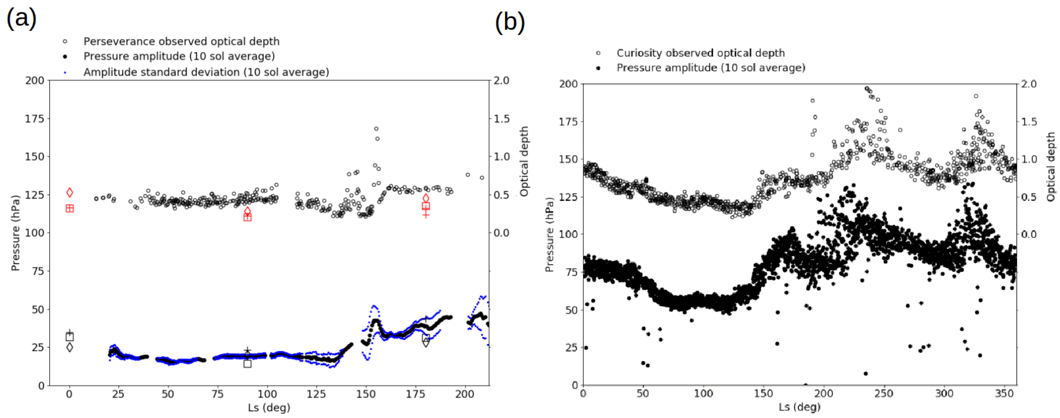

Figure 11. Diurnal pressure amplitude – minimum to maximum range – as a function of solar longitude (black dots, left axis) and the optical depth (small black spheres, right axis). The plots in (a) includes Perseverance pressure (MEDA PS) and optical thickness (M2020 Mastcam-Z) data during the first 414 Perseverance sols and in (b) all Curiosity pressure (REMS-P) and optical thickness (MSL Mastcam) data until Perseverance mission time. The depicted diurnal pressure range is a 10-sol moving average in both plots. The Perseverance plot also includes a 2-sigma belt around the diurnal pressure with the standard deviation (sigma) calculated from the 10 sols for each average point. Additionally results by regional models MWRF (squares) and MRAMS (plus-signs), as well as values by Mars Climate Database (diamonds) are shown.

those seven Martian missions are shown in Table 1 including the climate zones and geographical locations (also in Figure 1) of those missions.

It can be readily seen in Figure 12 that the daily pressure amplitude of Perseverance, Viking Lander 1 and Pathfinder are quite similar, which is likely caused by the fact that they are at similar latitudes and experience similar thermal tides. The tides also have a distinct pattern in longitude too, though, due to interference by the large-scale topography although this does not seem to be a factor here. A regional dust storm like in the case of Viking Lander 1 starting on around L_s 200° increases the amplitude. In the case of Pathfinder the amplitude variation increases considerably as a function of the Martian season (?, ?). The diurnal pressure amplitude seems to be highest at the Curiosity and Insight landing areas, which are located close to the equator and hence have the strongest thermal tides. On the other hand, Phoenix observations have the lowest diurnal pressure amplitude as expected due to the weaker thermal tide occurring at such high latitudes.

Basic characteristics of those seven Martian missions are shown in Table 1 including the climate zones and geographical locations (also in Figure 1) of those missions. It is to be noted that similarities on some of those characteristics allow interesting considerations to be made. Insight and Perseverance have a very similar altitude above the Martian geoid, which allows for direct comparison of the sol-averaged pressure data including the pressure variation with advancing Martian season. This is the most direct possibility for comparisons. As to the longitudinal location, Perseverance seems to be relatively isolated from the other landed missions. When inspecting the latitudinal location, Perseverance shares the same climate zone – North subtropics – with the Pathfinder and Viking 1 landers and is similarly able to feel the additional effects of baroclinic disturbances through the mesoscale small pressure variations that these disturbances cause at the surface. The same applies

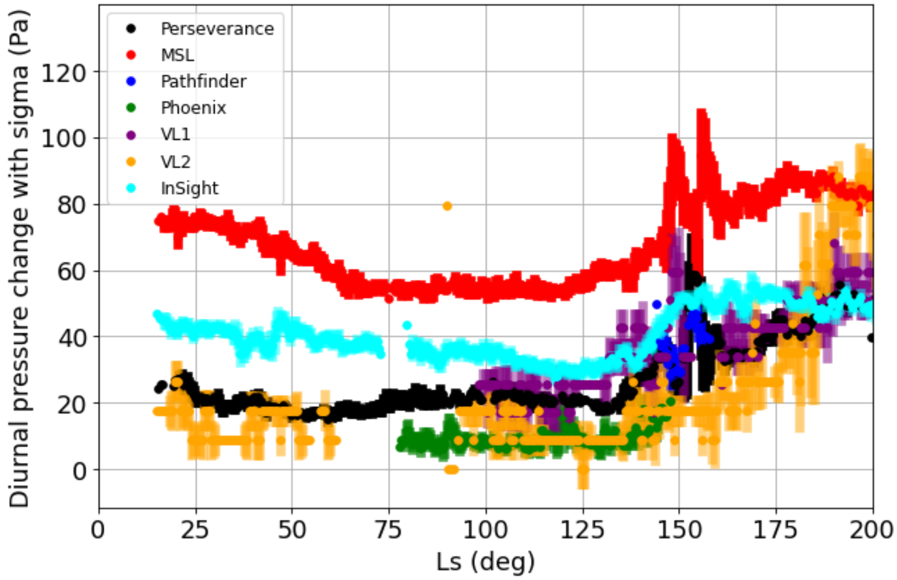

Figure 12. Diurnal pressure amplitude – minimum to maximum value – during the first 414 sols of the Perseverance mission with concurrently observed diurnal pressure amplitude of Insight and Curiosity missions, as well as that of historical Viking Landers, Pathfinder and Phoenix mission data on matching solar longitude range. Each diurnal pressure point is a moving 3-sol central average. The thickness of the curves represent the value of 2 standard deviations calculated over seven sols around each average diurnal pressure point.

also to the traveling low- and high-pressure systems – typical both on Mars and the Earth - causing pressure variations in a 2–5 sols time range especially in the wintertime subtropics and low midlatitudes (?, ?).

The shape of diurnal pressure variation at different Martian landing sites in four periods evenly separated over the first 414 Perseverance sols are shown in Figure 13. In each case, two sols of data are shown figure 13 (top left) shows clearly that the diurnal pressure amplitude observed by Curiosity in Gale crater is larger by a factor of 2-3 than for Perseverance in Jezero crater. The diurnal pressure amplitude observed by some other landing missions (Figure 13, top right) – Pathfinder, Viking Landers, Insight - is also smaller than what Curiosity has observed. The large amplitude of pressures observed by Curiosity has been shown by using atmospheric models to arise from the influence of a daily cycle of heating on the large slopes of Gale crater, such that warming of air causes mass to flow out of the crater in order to maintain hydrostatic balance along the slopes (Richardson and Newman, 2018). Perseverance observations indicate that the diurnal pressure range at the Jezero crater is smaller by a factor of 2-3, somewhat smaller amplitude than measured by Insight, about the same amplitude than calculated from historical observations of Viking lander 1 and 2 and, however, somewhat larger than diurnal pressure range measured by the Phoenix mission.

In the two lower rows of Figure 13 (panes c-f), approximately two sols for each lander at four solar longitude values marked in panes a-b are shown. Perseverance can be seen to have a similar mean pressure to InSight. This is likely due the similar elevations of around -2.6 km. The diurnal pressure patterns are similar in amplitude but slightly out of phase between Perseverance and InSight, most likely due to the 59° difference in longitude, i.e. the thermal tide will pass over Insight and then over

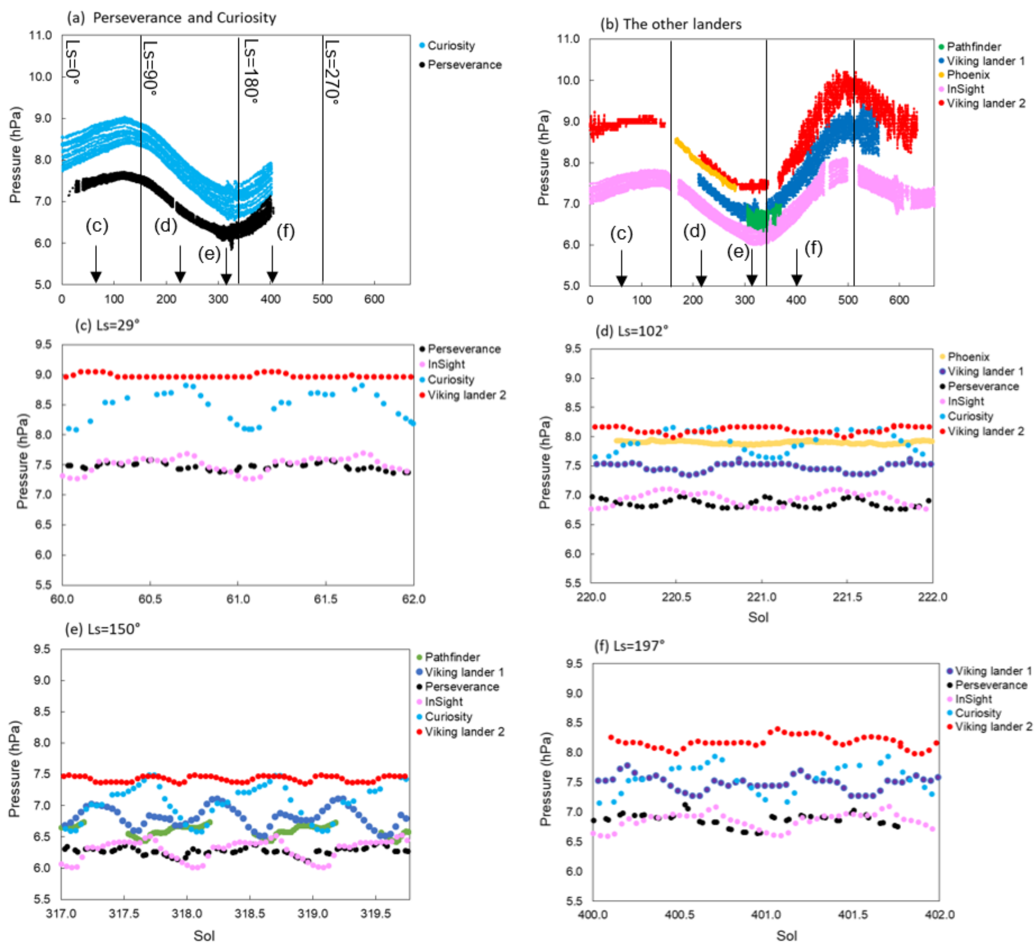

Figure 13. Diurnal pressure range of the Perseverance Rover compared over seasons with the diurnal pressure ranges observed by the Curiosity Rover, Insight Lander, Viking Lander 2 and Pathfinder (top row). Detailed diurnal pressure variation over 2-sol periods on these five surface missions is depicted at four solar longitudes evenly covering the first 414 sols of Perseverance operations. The lander data is plotted against the yearly sol, i.e. midnight on sol 1 corresponds to Ls=0° at the prime meridian, with midnight offset at each landing site depending on their longitude. The 2-sol periods were chosen in (c) to (f) over periods that avoided gaps in the lander data.

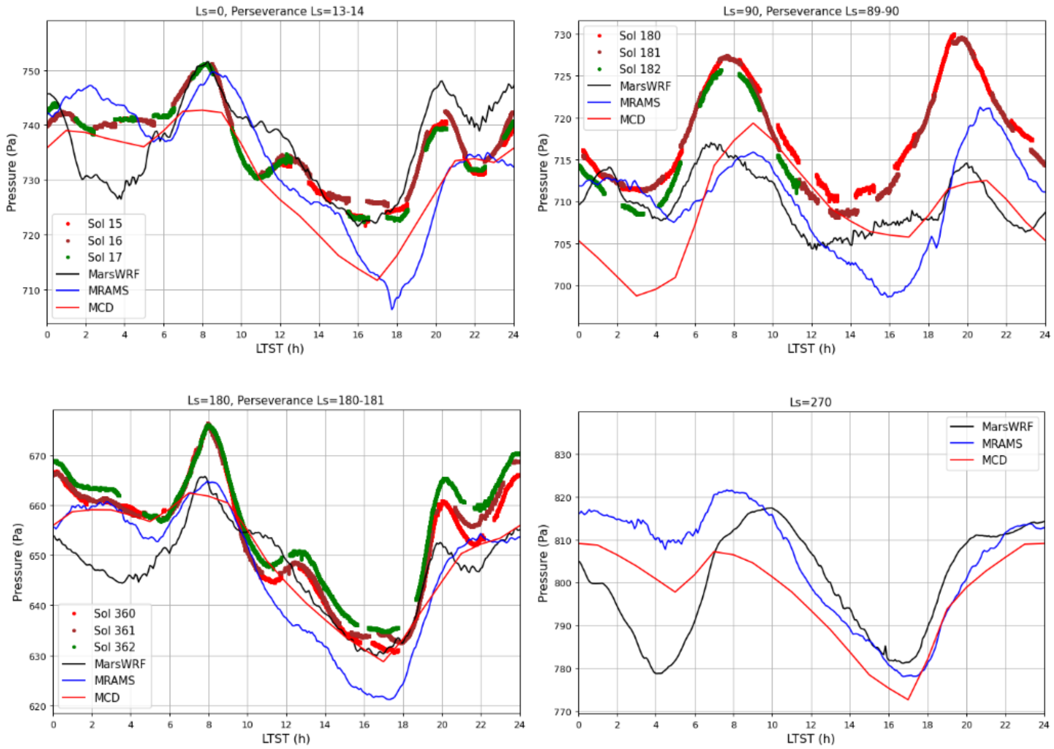

Figure 14. Diurnal pressure variation modeled by atmospheric models that simulate Jezero at km grid spacing MarsWRF, MRAMS and also the same data points from Mars Climate Database at solar longitude L_s 0°, 90°, 180° and 270°, which are depicted in panes a) to d). Around the solar longitude 0, 90 and 180 Perseverance pressure observations from three sols are added (Perseverance has no data as yet at L_s 270°).

Perseverance four hours later. Also note that the diurnal patterns for Curiosity and InSight, separated by only one degree of longitude, are similar except that Curiosity has a greater diurnal amplitude.

At the Viking lander 2 site the daily pressure amplitude approaches similar levels to those observed by Curiosity only in the second half of the year, i.e. in the winter, as can be seen in figure 13 (b). The diurnal pressure amplitudes for the landers at high latitudes, i.e. Phoenix and Viking lander 2, during the northern hemisphere summer are small because of the weak thermal tide (Zhao et al., 2015). Curiosity and InSight latitudes (Table 1) are close to the equator and both have consistent daily pressures amplitudes throughout the year suggesting little variation in the thermal tide conditions at these latitudes.

Regional atmospheric modeling efforts are needed to expand the value of the *in situ* observations. This was done by running MarsWRF and MRAM models (Pla-Garcia et al., 2021) at the Perseverance site on solar longitude values of L_s 270°, 90°, 180° and 270°. Figure 14 illustrates these results together with *in situ* Perseverance observations at L_s 0°, 90°, 180° as well as data points acquired from the Mars Climate Database MCD (?, ?).

MarsWRF and MRAMS simulate Jezero crater at high resolution. MarsWRF is a mesoscale nest embedded inside a global model model and MRAMS is a mesoscale model. Overall, MarsWRF and MRAMS as well as the lower-resolution MCD do fairly well compared to the actual *in situ* pressure observations. MarsWRF seems to reproduce the dip at 1700 better than MRAMS in Figure 14. MarsWRF reproduces the main features quite well except the small peaks at noon in the Northern springtime (L_s 0°, Figure 14a) and fall (L_s 180°, Figure 14c) where it generates a shoulder-like feature instead. The average pressure in Figure 14a for MarsWRF is generally good but in the Northern summertime (L_s 90°, Figure 14b) and fall (Figure 14c) the average pressure is too low. The height of the peaks in Figure 14b are too low in the MarsWRF data. MCD is roughly producing in the average similar results to Mars WRF and MRAMS.

MRAMS matches the average pressure level quite well in Figure 14a if it was not for the big dip at 1700. It is not clear if it reproduces the peaks at 2200 and midnight. The occurrence of the peaks in the MRAMS data seems to be delayed by about 2 hours. Like MarsWRF MRAM does not reproduce the small peak at noon. MRAMS reproduces the height of the two big peaks in Figure 14b but they are on average too low. The timing of the peaks seems to be delayed by about 2 hours in Figure 14b. Overall, it seems to be the case that state-of-the-art regional atmospheric models succeed fairly well in producing diurnal pressure variation at the Jezero crater region. Then, understandably, reproducing through modeling the small peaks in diurnal pressure variation caused largely by the local geography and atmospheric flow conditions proves to be challenging.

The distinct oscillations in the observed surface pressure are expected to be primarily due to the thermal tides and their interactions with the Martian topography, e.g. Wilson and Hamilton (1996). Oscillations in the pressure could also include contributions of the local crater circulations that are especially important for deep craters like Gale crater (Tyler and Barnes, 2015; Wilson, 2017). In addition hydrostatic adjustment has been shown to be important in amplification of the amplitude of the diurnal pressure variation (Richardson and Newman, 2018).

This complex structure in the pressure signal was anticipated by Pla-Garcia et al. (2020). This is demonstrated in a distinct fashion in figure 14. A more comprehensive modeling study is needed, but the Perseverance pressure observations support the initial regional atmospheric modeling results at the Perseverance site made with the Mars WRF and MRAMS models as well as the data provided by MCD.

Jezero crater does not seem to have a similarly strong amplification from hydrostatic adjustment as is the case at the Gale crater based on the observations by the Curiosity rover (Harri et al., 2014; Newman et al., 2021). A plausible reason for this is the fact that compared to the Gale crater, the Jezero crater is shallow and wide resulting in relatively weaker amplification effect on the diurnal pressure variation amplitude. In addition the thermal tide at the Gale crater is stronger at most times of year than at Jezero crater because it is closer to the subsolar point for most of the year.

Combining the atmospheric regional modeling with *in situ* pressure observations proves to be highly useful – it adds the value of the observations by expanding their effect beyond the actual point of observation and sheds more light on the physical and meteorological processes behind the Martian atmospheric phenomena. The physics and implementation of the models themselves can also be modified to better address the actual atmosphere.

7 Summary and discussion

The Mars2020 Perseverance Rover landed successfully onto the Martian surface on the Jezero Crater floor (18°N, 77°E) at the Martian solar longitude L_s 5° in February 2021. Since then it has produced highly valuable environmental measurements with a versatile scientific payload including a suite of environmental sensors MEDA (Mars Environmental Dynamics Analyzer). One of the MEDA sensor systems is MEDA PS pressure device weighing 40 grams.

The Martian atmospheric pressure observations by MEDA PS have proved to be of excellent quality fulfilling expectations with the estimated overall uncertainty being equal or better than 3.5 Pa and the resolution about 0.13 Pa. The system resources required by the whole MEDA PS package are dimensions being $62\times50\times17$ mm, mass 40g and power consumption less than 15 mW.

This paper presents initial results of the first 414 sols of Martian atmospheric surface pressure observations by the MEDA PS device whose performance was found to fulfill the specification. Observations controlled by the Perseverance resources allocation schedule cover approximately 50 – 70 % of the Perseverance operational time.

The atmospheric pressure measurement device (MEDA PS) is based on the silicon-micro-machined pressure sensor head (Barocap®) and transducer technology developed by Vaisala Inc. The Barocap® version used by MEDA PS is optimized for the Martian near-surface atmospheric pressure. The transducer electronics and required electromagnetic shielding and mechanical support structures were developed by Finnish Meteorological Institute (FMI).

The MEDA PS pressure device is making measurements continuously with 1 Hz frequency in average for every other hour according to the operational schedule by the Persevereance Rover. That enables us to generate data sets with averaged pressure measurements approximately at 1-hour intervals, as well as data sets with pressure observations at 1 second intervals for one or a few hours in a row for short time scale studies. In this work we use data sets with 1-hour intervals. The 1-hour data sets are not complete but they do have some gaps due to scheduling of Perseverance and MEDA operations. However, the available data coverage allows good characterisation of both the diurnal and seasonal variations in the pressure.

The seasonal-to-annual time scales the CO2 condensation-sublimation cycle of the Martian atmosphere is nicely demonstrated at the Jezero crater site by the Perseverance Rover measurements.The observed sol-averaged atmospheric pressure during the 414 first Perseverance sols from the landing time at early Northern springtime to Northern fall follow an anticipated pattern of total pressure variation in the course of the advancing season. The data has the first maximum in late spring roughly on the Perseverance sol 110 and minimum on sol 310, whereas by the Perseverance sol 414 corresponding to approximately L_s 212° the atmospheric pressure is climbing higher than the first maximum toward the seasonal maximum. When comparing Perseverance with concurrent observations by the Curiosity Rover and the Insight lander as well as with the historical Viking Landers data, we can see distinct differences with the amplitude of the seasonal pressure variation that are due to different surface elevations.

When comparing pressure observations of the seven Martian landing missions on different locations on Mars the first part of seasonal atmospheric pressure cycle measured by Perseverance seems to follow the seasonal increase and decrease in the atmospheric pressure as expected. The visible bias between the landers' pressure observations is largely due to different landing elevations. Detailed investigation reveals that during L_s 0 – 170° the Perseverance pressure looks to be decreasing somewhat more slowly than the pressure measured by the historical Viking landers. However, Insight exhibits similar kind of slow pressure decrease and hence this could be due to a regional occurrence possibly related with the regional topography or variability in large scale atmospheric flows.

The observed diurnal pressure amplitude is ranging roughly within 2 -5 % of the sol-averaged pressure with the absolute amplitude (10 – 35 hPa) not having a direct relationship with the sol-averaged pressure. The optical thickness varying with the amount of airborne dust seems to affect considerably the diurnal pressure amplitude. The increase of optical thickness from 0.5 to 0.8 around sols 130-160 seems to raise the diurnal pressure amplitude from approximately 20 hPa to 35 hPa. Regional atmospheric models seem to give roughly similar results on the average diurnal pressure amplitude, when Perseverance -like airborne dust conditions are assumed.

It appears to be evident that the range of diurnal atmospheric pressure varies considerably with location on Mars. The Perseverance diurnal pressure variation seem to be smaller than those measured by the Curiosity rover at Gale crater where tidal forcing is stronger due to the location close to the equator and also due to the fact that at Curiosity's longitude sector eastward and westward modes are expected to interact constructively. Comparison with pressure observations at other Martian sites it looks that also regional and local geography also play a role in the range of observed diurnal pressure variation.

When inspecting the structure of diurnal pressure, 2-4 small peaks appear in the data on each sol (Figure 6). A clear evolution of the peaks can be seen in the stacked diurnal pressure data. During Northern summer (Figure 6, second row from top) diurnal pressure exhibits two distinct and regular peaks, one in the morning around 6-7 AM and the other one around 8-9 PM LTST. During the Northern spring (Figure 6, top row) and fall (Figure 6, lowest rows) this summertime regular pattern is broken into more like four separate peaks whose amplitudes vary along with advancing season.

During Northern springtime - at the start of the mission, Perseverance sols 0-150 - it appears that smaller peaks are superimposed on the larger peaks. These smaller peaks disappear between about sols 150 and 250 (Northern summertime) and return around sol 300 in early fall. The wintertime has not yet come during the first 414 Perseverance sols. The features in the plots give clues on the behaviour of regional atmospheric dynamics and circulation patterns in the Martian atmosphere

The daily surface pressure profile seems to exhibit a largely repeatable two-peak shape during the Northern summertime (Figure 6). This is probably mostly due to the strong semi-diurnal thermal tidal component, which seems to be the case as illustrated in Figure 7.

MEDA PS observations allow us to estimate that about 100 thermal vortices with ¿ 0.5 Pa pressure drops during a 20 sol period throughout the first 414 Perseverance sols. Based on this analysis, the vortex activity at Jezero crater in the vicinity of Perseverance seems to be nearly constant with little seasonal variation. Apparently solar forcing varying considerably from springtime to fall has not affected the frequency of occurrence of thermal vortices. It is interesting to see whether this pattern will hold through the upcoming Northern wintertime.

Through *in situ* pressure observations and regional atmospheric modeling results a distinct local circulation pattern including nighttime katabatic and daytime upslope flows over the boundary of the Jezero crater was discovered. This circulation amplifies the diurnal pressure variation.

For comparison, the Gale crater diurnal pressure amplitude measured by the Curiosity Rover is much larger (50 to 120 hPa) than at the Jezero crater. This may be due to the fact that Gale is smaller and deeper than Jezero resulting in a stronger diurnal pressure cycle due to hydrostatic adjustment. On the plateaus with more gentle local circulation the diurnal pressure variation based on Viking Lander observations is weaker than at the Gale crater and about the same as given by Perseverance observations. On the other hand Insight diurnal pressure is higher than that of Perseverance during Northern springtime and summer but assumes roughly the same level during fall. Apparently the behavior of local diurnal pressure is affected by a mixture of solar forcing on the surface, airborne dust, regional geography and atmospheric wave activity.

The observed diurnal pressure variation seems to have a significant seasonal dependence. During Northern summer diurnal pressure displays two distinct and regular peaks, one in the morning around 6-7 AM and the other one around 8-9 PM LTST. This regular pattern is likely caused by the interaction of strong thermal tide and the seasonally varying airborne dust causing an amplified semi-diurnal component. During the Northern fall and spring this summertime regular pattern is broken into four separate peaks whose amplitudes vary along with advancing season.

The seasonal form of the diurnal pressure variation was investigated through regional atmospheric modeling by Mars WRF and MRAMS limited area models using the modeling results described in Pla-Garcia et al. (2020). The modeling results were compared with actual MEDA PS observations at solar longitude values L_s 0°, 90° and 180°, as well as with the MCD data. In the summertime (midsummer L_s 90°) the modeling results match very well with the shape and two-peak pattern of diurnal pressure cycle, but they underestimate the average pressure level. These modeling results showed the importance of the boundary fields for the regional models in getting pressure levels correct. Also the complexity of the diurnal pressure signal especially during the springtime and fall was revealed.

Overall, the modeling data seems to fit surprisingly well with the Perseverance pressure observations. Mars WRF and MRAMS have higher resolution than the relatively coarse MCD and hence these models pick up the local daily pressure variation better than MCD. But even the MCD seems to work surprisingly well, which is an excellent indication of the capabilities of current Martian atmospheric modeling tools. The modelling data indicates that they are correctly modelling the large-scale forcing of the main components of the daily pressure curves.

These modeling efforts underlined the clear need to investigate more in detail the diurnal pressure cycle as a superposition of the thermal tide, regional and local crater circulations and of various barotropic and baroclinic wave forms with seasonal dependence. These differences between the models and the observations inform us about the needs and areas to focus on in improving atmospheric models.

8 Open Research

The observational data used for this work is available in Planetary Data System (PDS) at the web site https://pds.nasa.gov/. MEDA instrument data is available in the PDS Atmospheres node in https://doi.org/10.17189/1522849 (?, ?).

Acknowledgments
Ari-Matti Harri, Mark Paton, Maria Hieta and Jouni Polkko are thankful for the Finnish Academy grant number 310509. Agustín Sánchez-Lavega and Ricardo Hueso were supported by Grant PID2019-109467GB-I00 funded by MCIN/AEI/10.13039/501100011033/ and by Grupos Gobierno Vasco IT1742-22.

Figure 1.

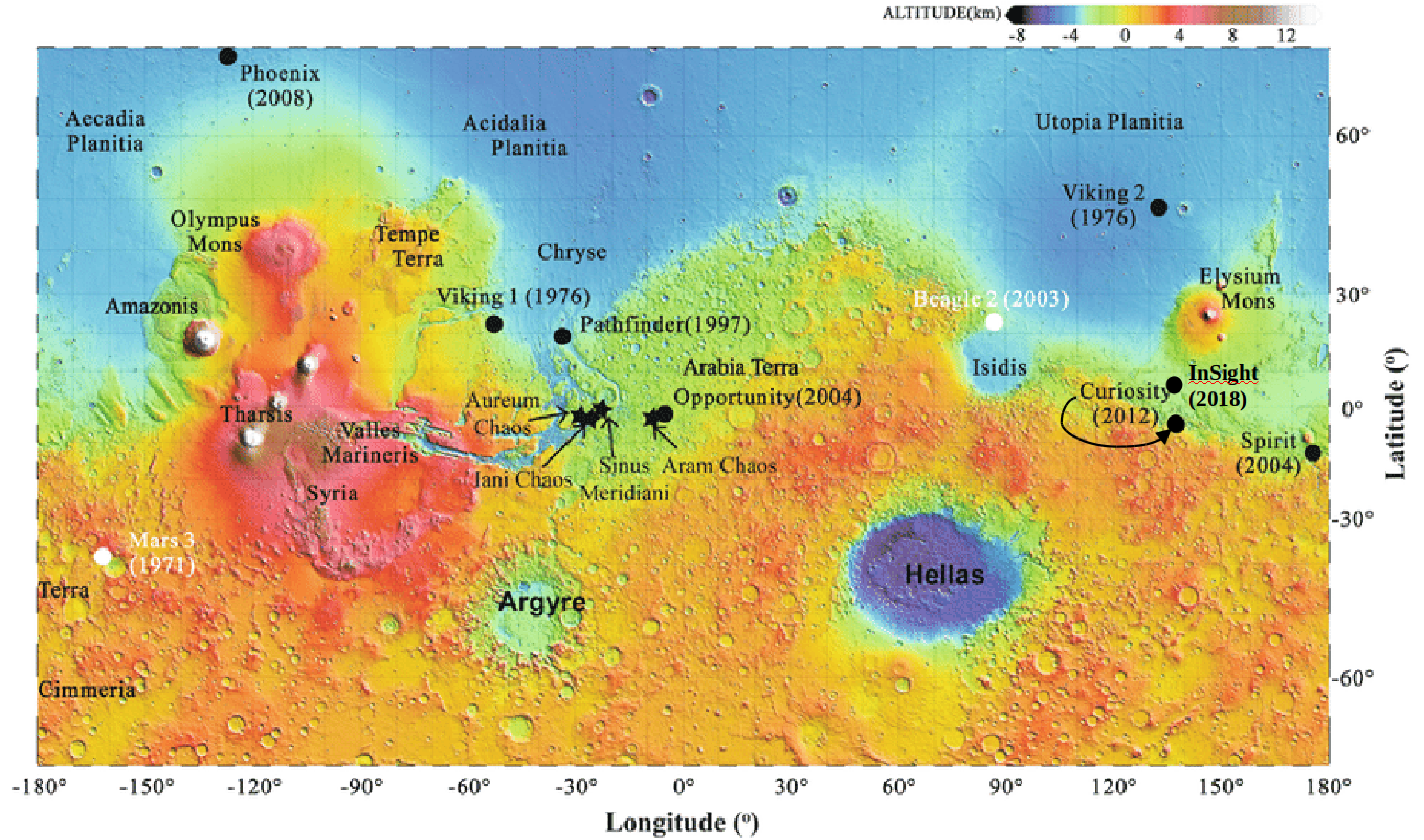

ALTITUDE(km)
-8
-4
0
4
8
12
Phoenix (2008)
Aecadia Planitia
Acidalia Planitia
Utopia Planitia
60°
Viking 2 (1976)
Olympus Mons
Tempe Terra
Chryse
Elysium Mons
Amazonis
Viking 1 (1976)
Beagle 2 (2003)
30°
Pathfinder(1997)
Isidis
Arabia Terra
InSight (2018)
Curiosity (2012)
Opportunity(2004)
Tharsis
Aureum Chaos
Valles Marineris
0°
Spirit (2004)
Sinus Meridiani
Aram Chaos
Jani Chaos
Syria
-30°
Mars 3 (1971)
Hellas
Terra
Argyre
Cimmeria
-60°
-180°
-150°
-120°
-90°
-60°
-30°
0°
30°
60°
90°
120°
150°
180°
Longitude (°)
Latitude (°)

Figure 2.

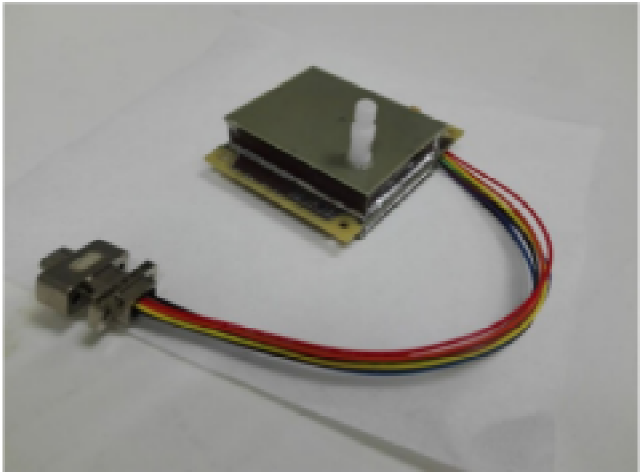

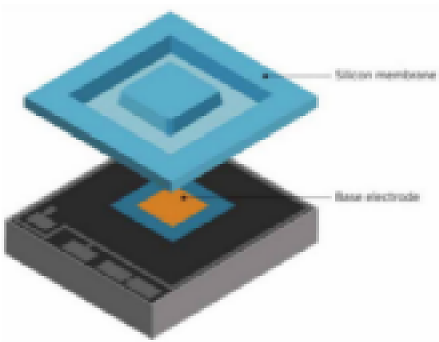

BAROCAP sensor

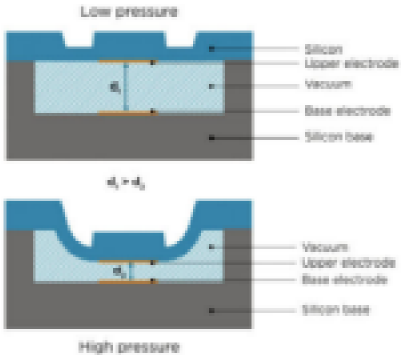

Cross-section of the BAROCAP sensor

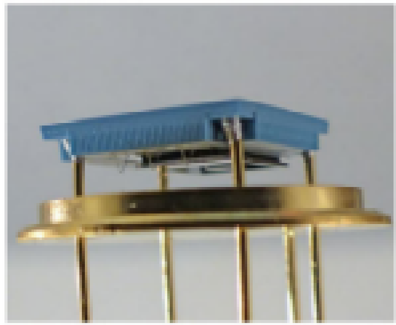

Figure 3.

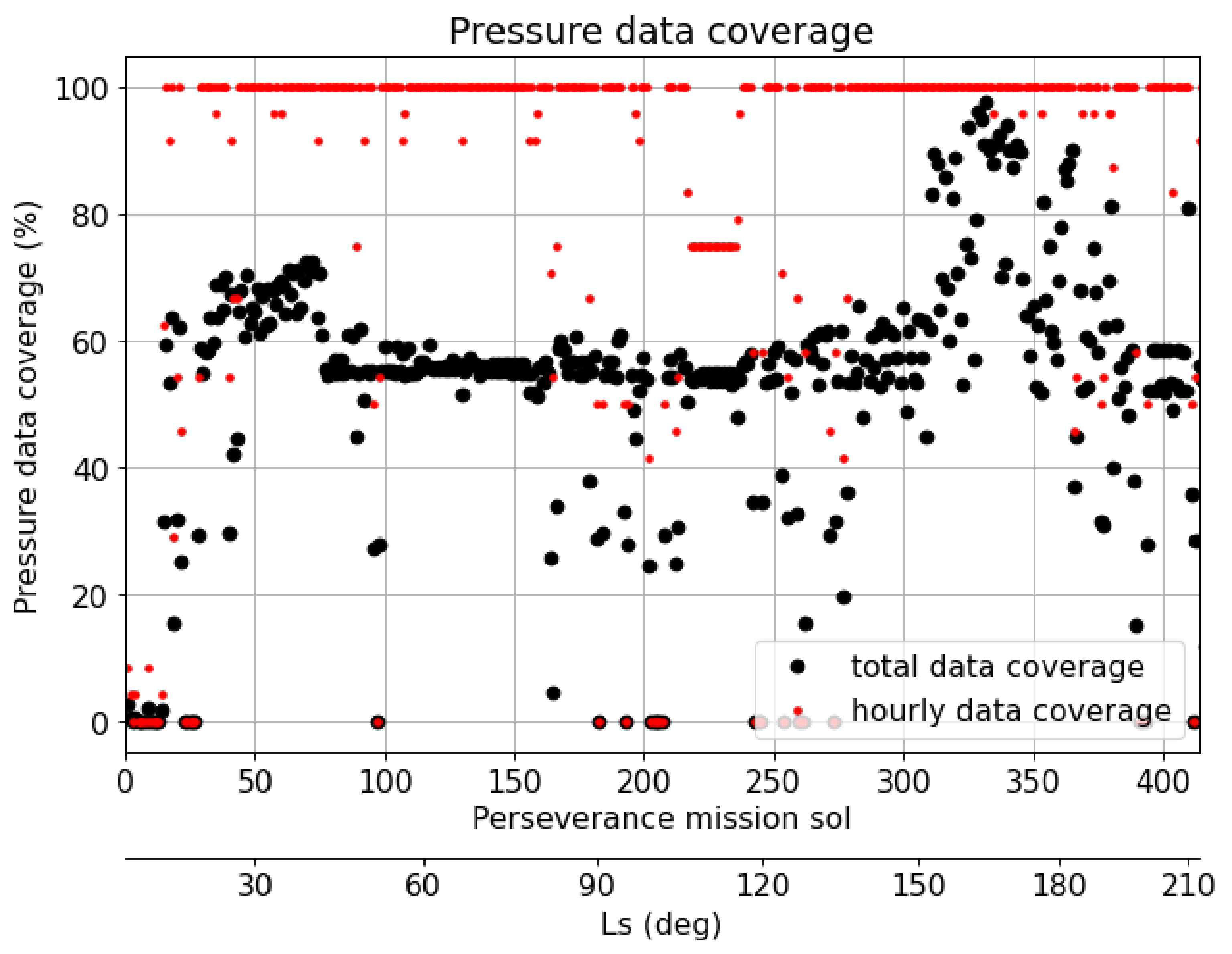
Pressure data coverage
Pressure data coverage (%)
100
80
60
40
20
0
0
50
100
150
200
250
300
350
400
Perseverance mission sol
30
60
90
120
150
180
210
Ls (deg)
total data coverage
hourly data coverage

Figure 4.

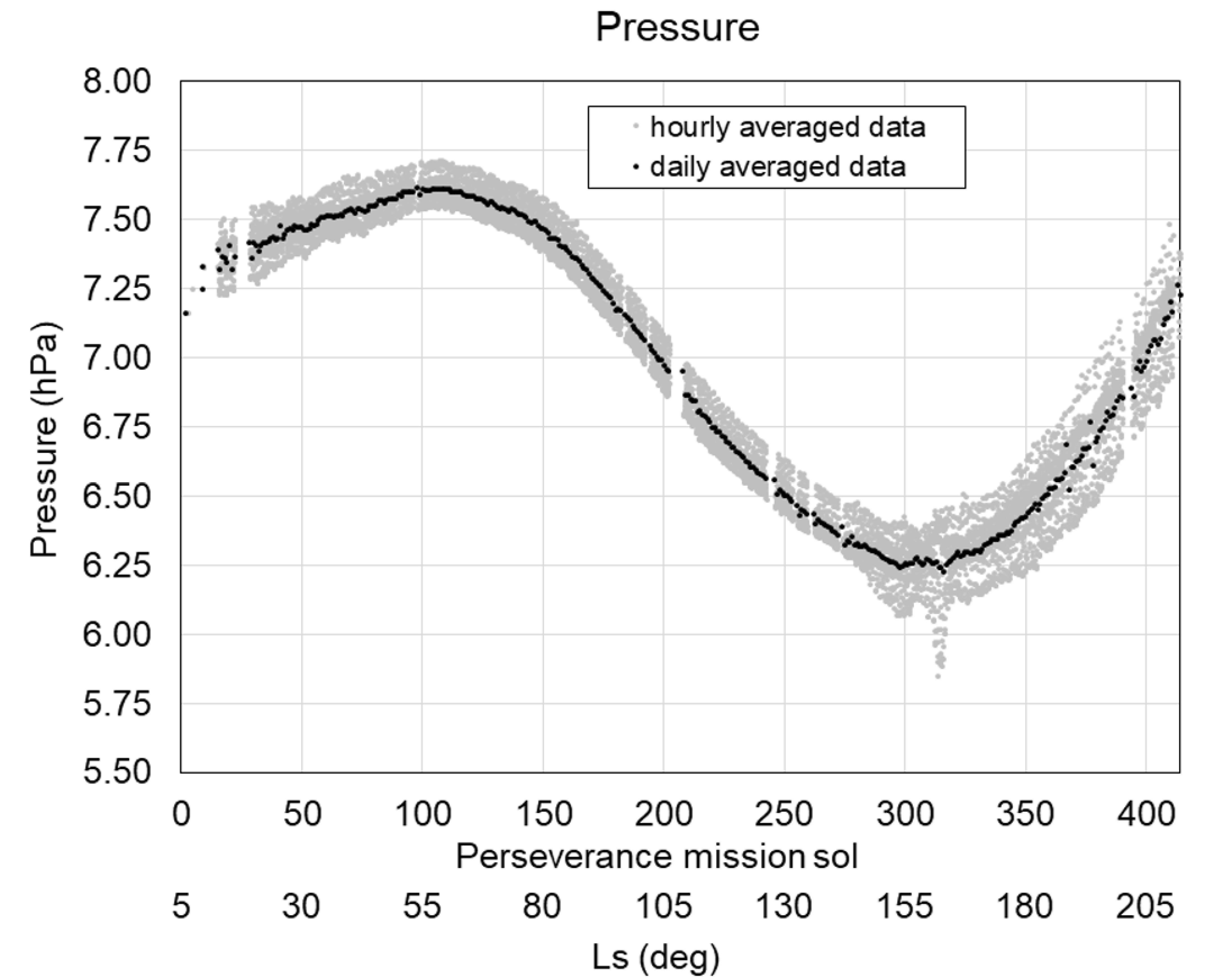

Pressure
hourly averaged data
daily averaged data
Pressure (hPa)
8.00
7.75
7.50
7.25
7.00
6.75
6.50
6.25
6.00
5.75
5.50
0
50
100
150
200
250
300
350
400
Perseverance mission sol
5
30
55
80
105
130
155
180
205
Ls (deg)

Figure 5.

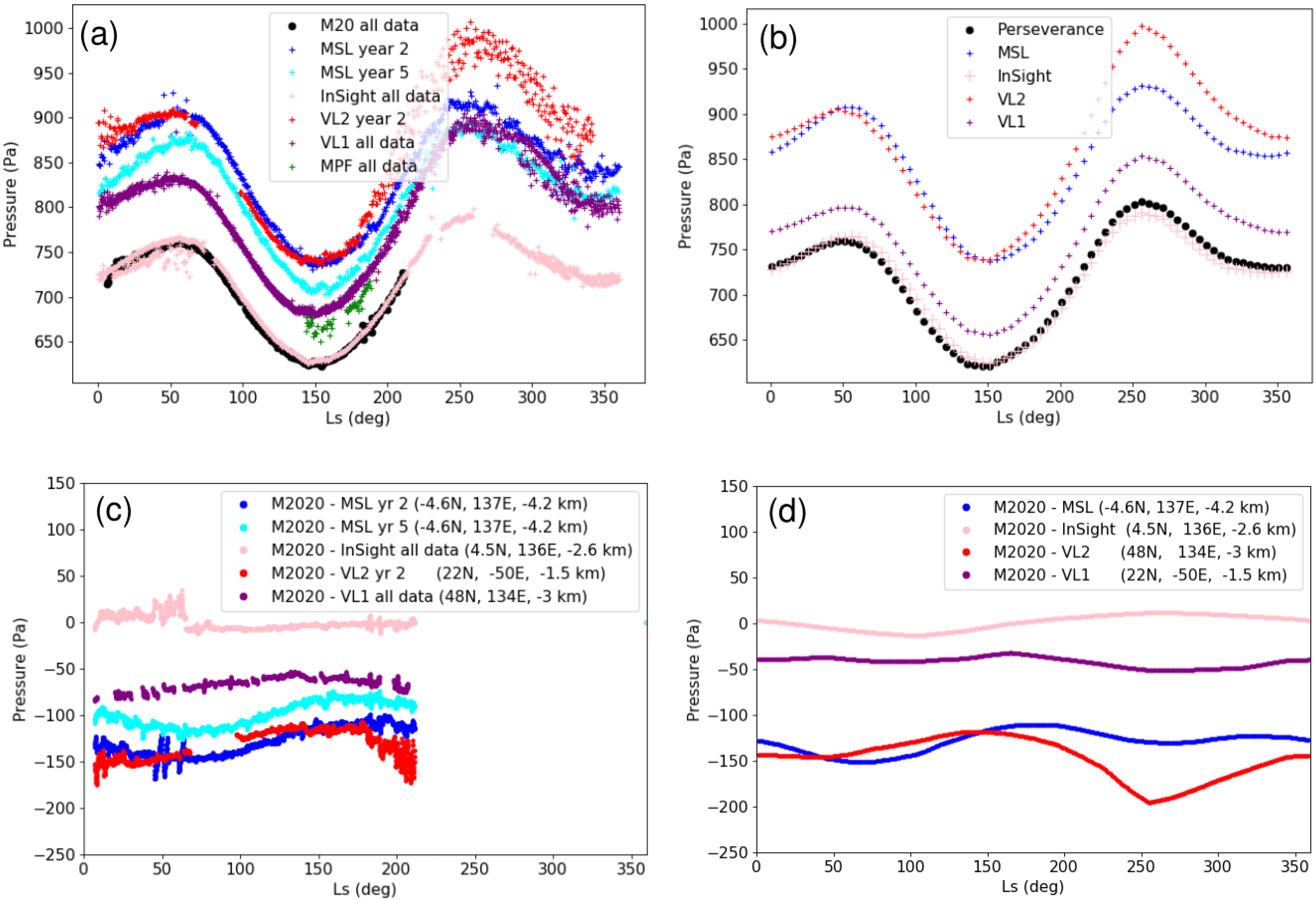

(a)
M20 all data
MSL year 2
MSL year 5
InSight all data
VL2 year 2
VL1 all data
MPF all data
Pressure (Pa)
Ls (deg)
(b)
Perseverance
MSL
InSight
VL2
VL1
Pressure (Pa)
Ls (deg)
(c)
M2020 - MSL yr 2 (-4.6N, 137E, -4.2 km)
M2020 - MSL yr 5 (-4.6N, 137E, -4.2 km)
M2020 - InSight all data (4.5N, 136E, -2.6 km)
M2020 - VL2 yr 2 (22N, -50E, -1.5 km)
M2020 - VL1 all data (48N, 134E, -3 km)
Pressure (Pa)
Ls (deg)
(d)
M2020 - MSL (-4.6N, 137E, -4.2 km)
M2020 - InSight (4.5N, 136E, -2.6 km)
M2020 - VL2 (48N, 134E, -3 km)
M2020 - VL1 (22N, -50E, -1.5 km)
Pressure (Pa)
Ls (deg)

Figure 6.

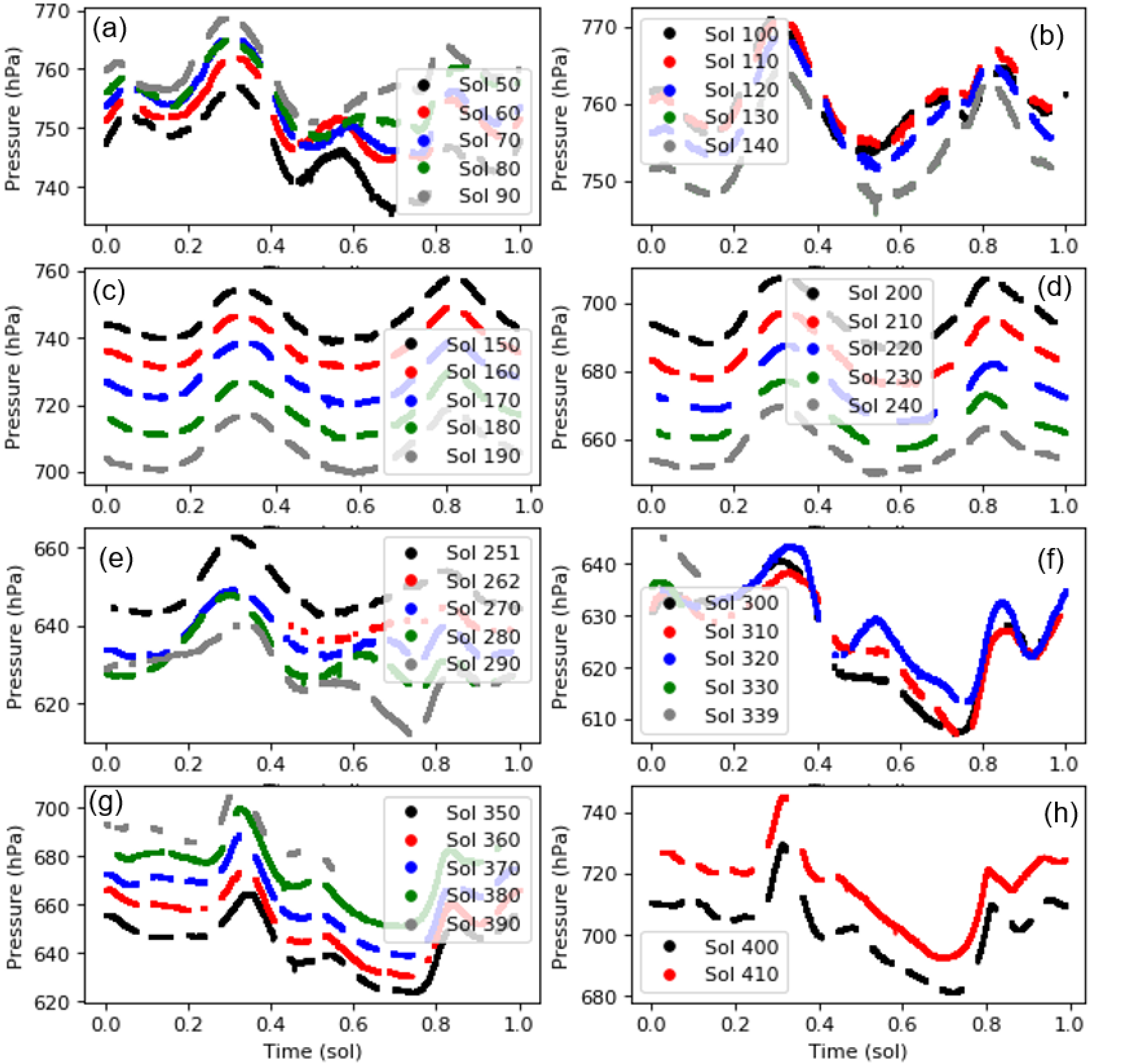

(a)
Sol 50
Sol 60
Sol 70
Sol 80
Sol 90
(b)
Sol 100
Sol 110
Sol 120
Sol 130
Sol 140
(c)
Sol 150
Sol 160
Sol 170
Sol 180
Sol 190
(d)
Sol 200
Sol 210
Sol 220
Sol 230
Sol 240
(e)
Sol 251
Sol 262
Sol 270
Sol 280
Sol 290
(f)
Sol 300
Sol 310
Sol 320
Sol 330
Sol 339
(g)
Sol 350
Sol 360
Sol 370
Sol 380
Sol 390
(h)
Sol 400
Sol 410
Pressure (hPa)
Time (sol)

Figure 7.

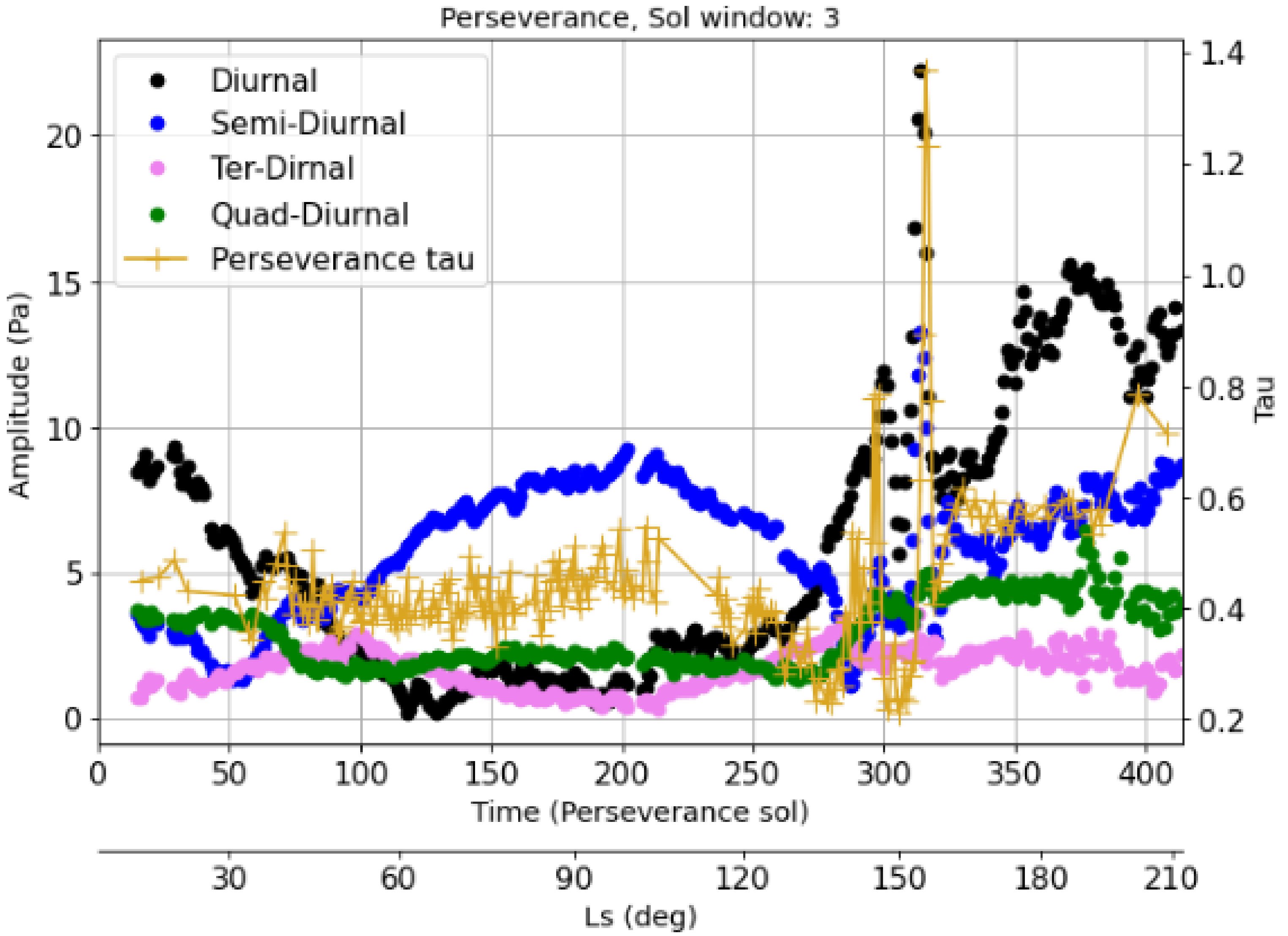
Perseverance, Sol window: 3
Diurnal
Semi-Diurnal
Ter-Dirnal
Quad-Diurnal
Perseverance tau
Amplitude (Pa)
Tau
Time (Perseverance sol)
Ls (deg)

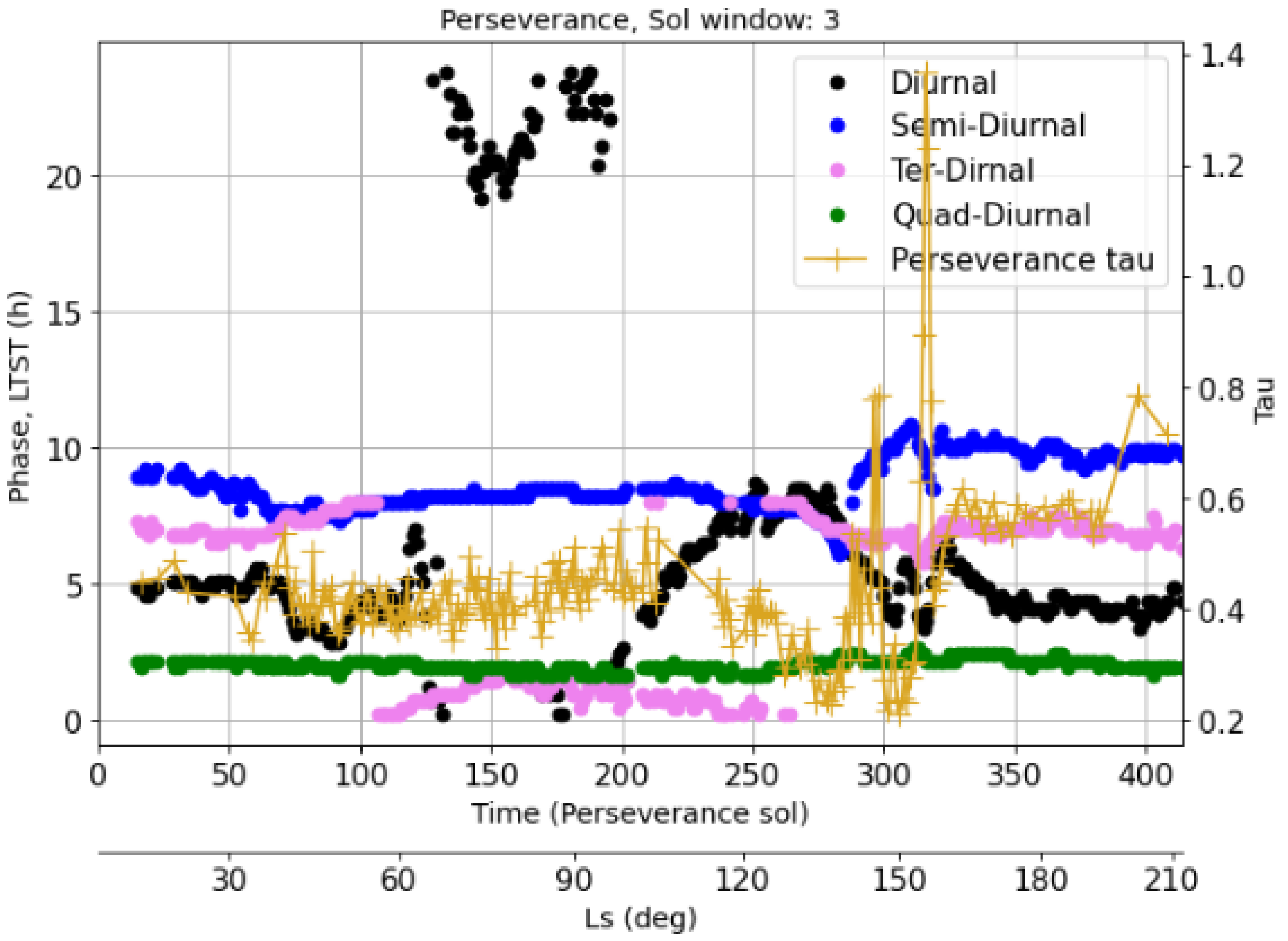
Perseverance, Sol window: 3
Diurnal
Semi-Diurnal
Ter-Dirnal
Quad-Diurnal
Perseverance tau
Phase, LTST (h)
Tau
Time (Perseverance sol)
Ls (deg)

Figure 8.

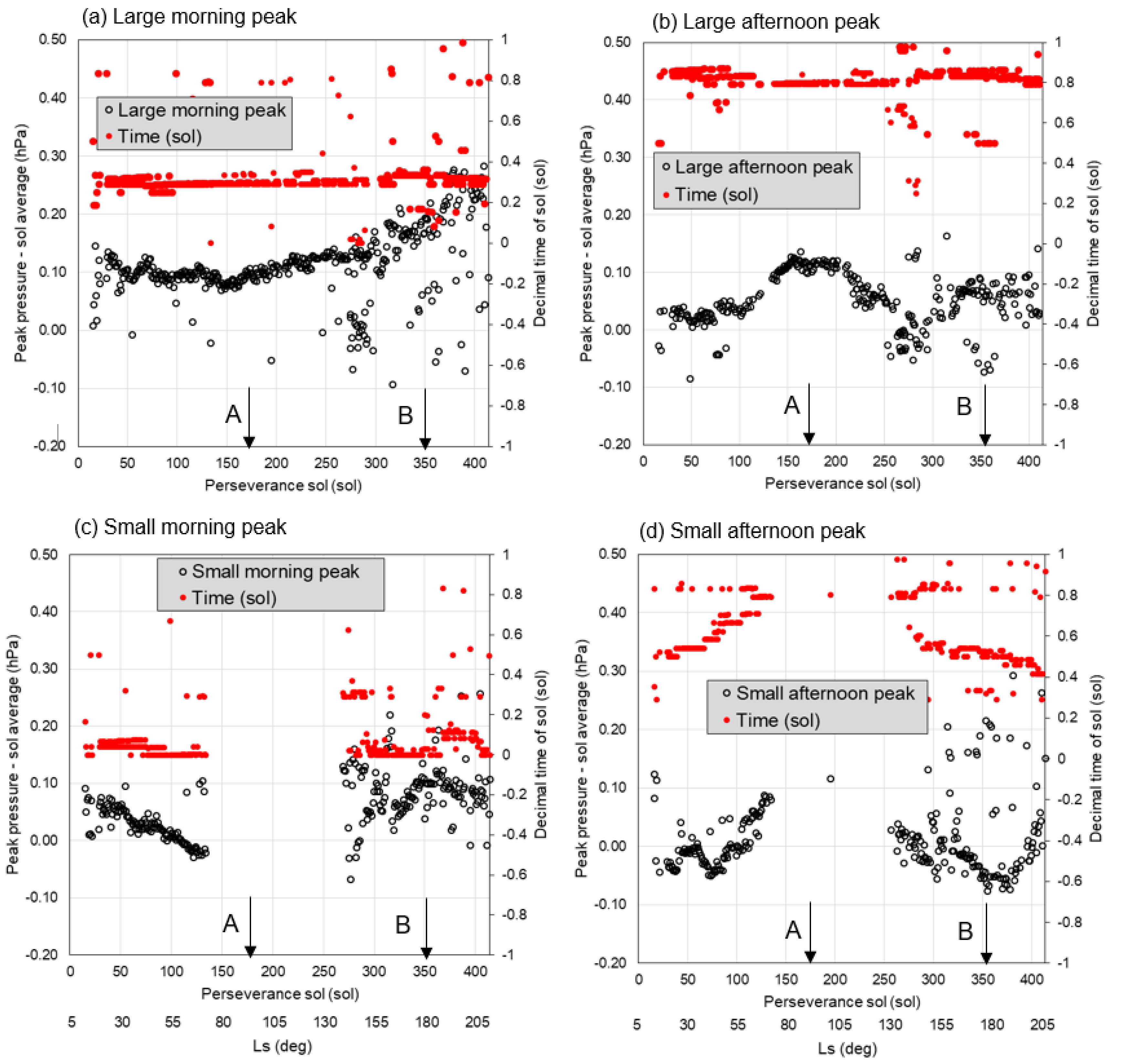
(a) Large morning peak
Large morning peak
Time (sol)
Peak pressure - sol average (hPa)
Decimal time of sol (sol)
Perseverance sol (sol)
A
B
(b) Large afternoon peak
Large afternoon peak
Time (sol)
Peak pressure - sol average (hPa)
Decimal time of sol (sol)
Perseverance sol (sol)
A
B
(c) Small morning peak
Small morning peak
Time (sol)
Peak pressure - sol average (hPa)
Decimal time of sol (sol)
Perseverance sol (sol)
Ls (deg)
A
B
(d) Small afternoon peak
Small afternoon peak
Time (sol)
Peak pressure - sol average (hPa)
Decimal time of sol (sol)
Perseverance sol (sol)
Ls (deg)
A
B

Figure 9.

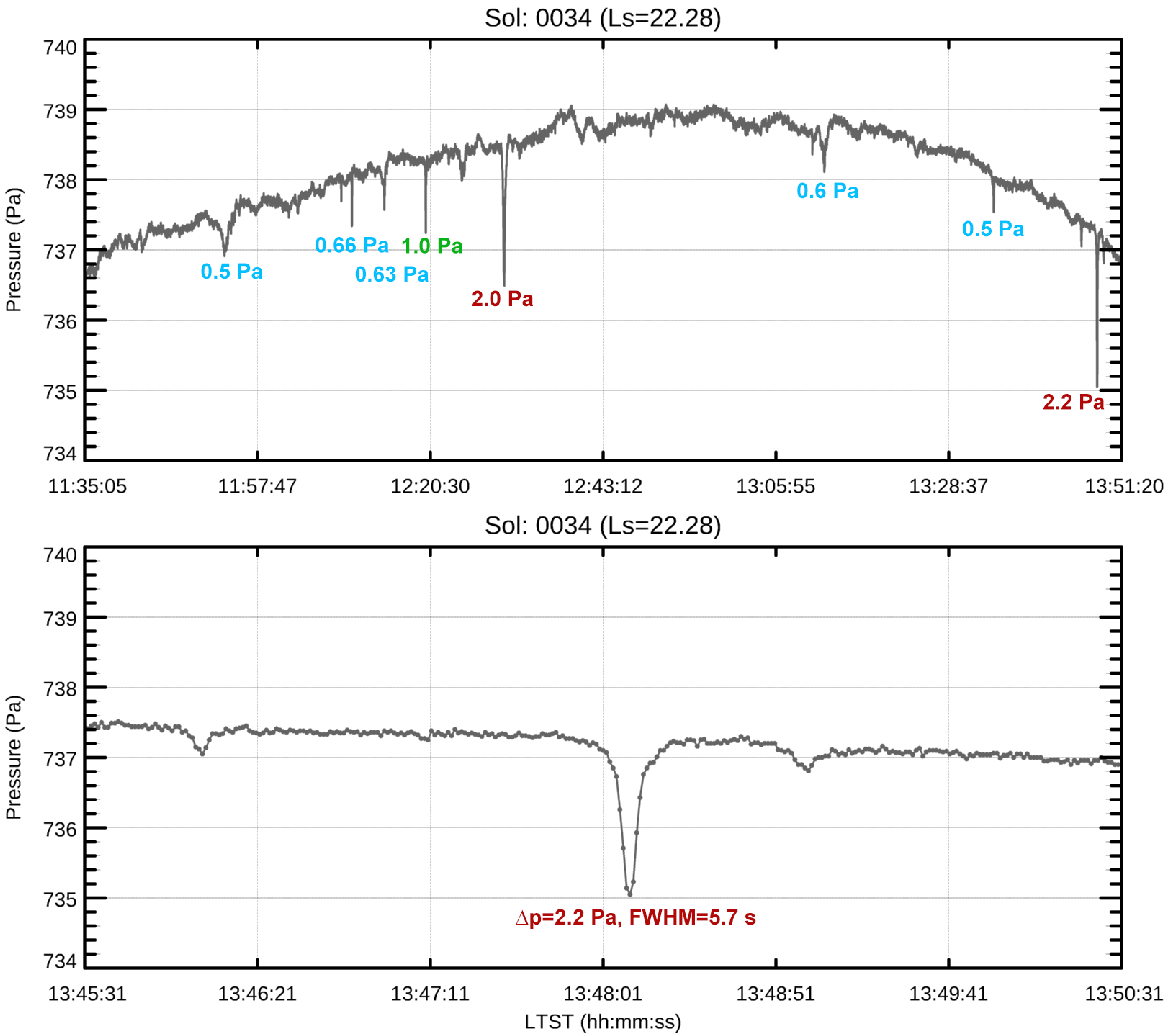

Sol: 0034 (Ls=22.28)
Pressure (Pa)
740
739
738
737
736
735
734
0.5 Pa
0.66 Pa
1.0 Pa
0.63 Pa
2.0 Pa
0.6 Pa
0.5 Pa
2.2 Pa
11:35:05
11:57:47
12:20:30
12:43:12
13:05:55
13:28:37
13:51:20
Sol: 0034 (Ls=22.28)
Pressure (Pa)
740
739
738
737
736
735
734
Δp=2.2 Pa, FWHM=5.7 s
13:45:31
13:46:21
13:47:11
13:48:01
13:48:51
13:49:41
13:50:31
LTST (hh:mm:ss)

Figure 10.

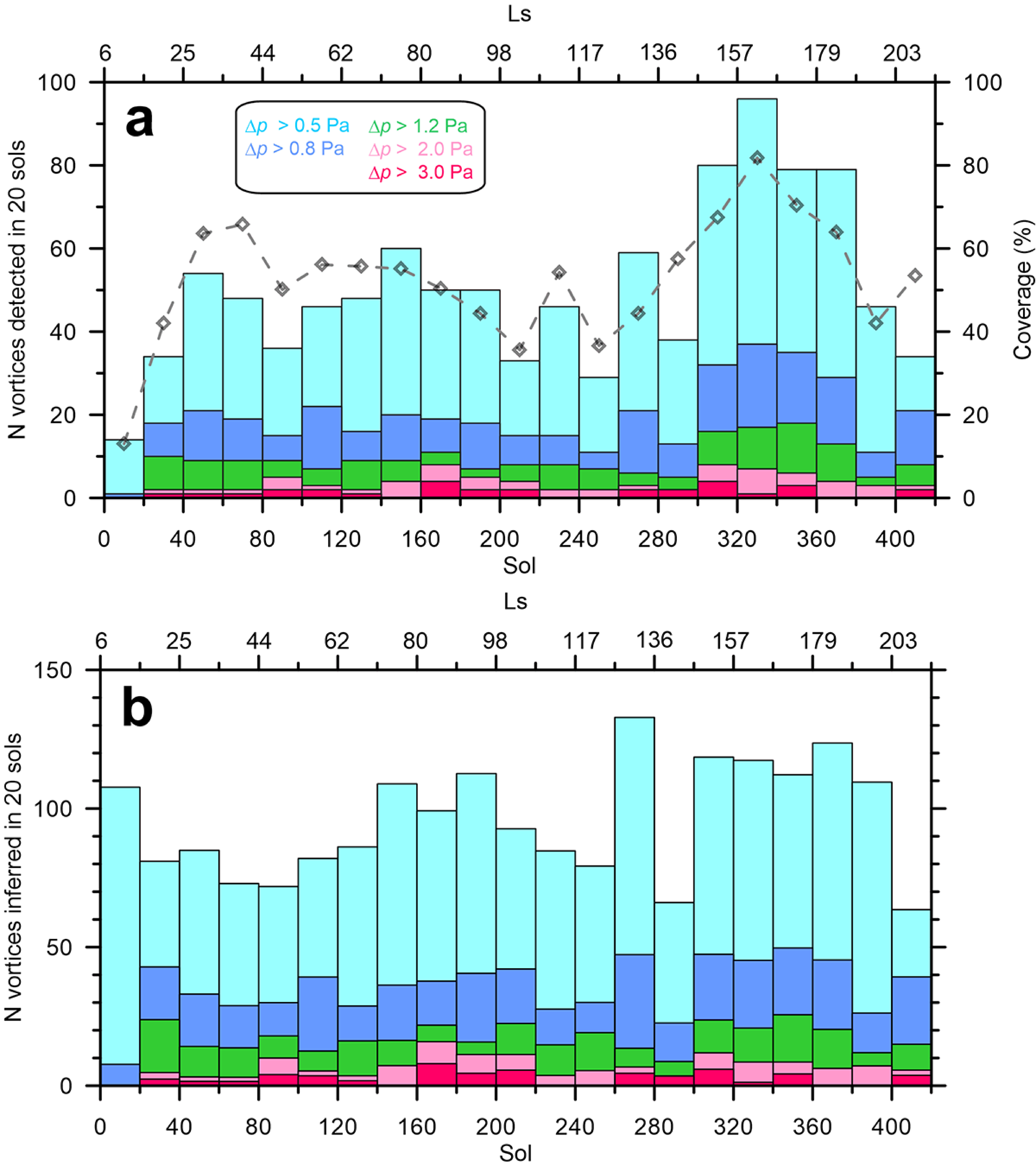

a
b
Ls
Sol
N vortices detected in 20 sols
N vortices inferred in 20 sols
Coverage (%)
Δp > 0.5 Pa
Δp > 0.8 Pa
Δp > 1.2 Pa
Δp > 2.0 Pa
Δp > 3.0 Pa

Figure 11.

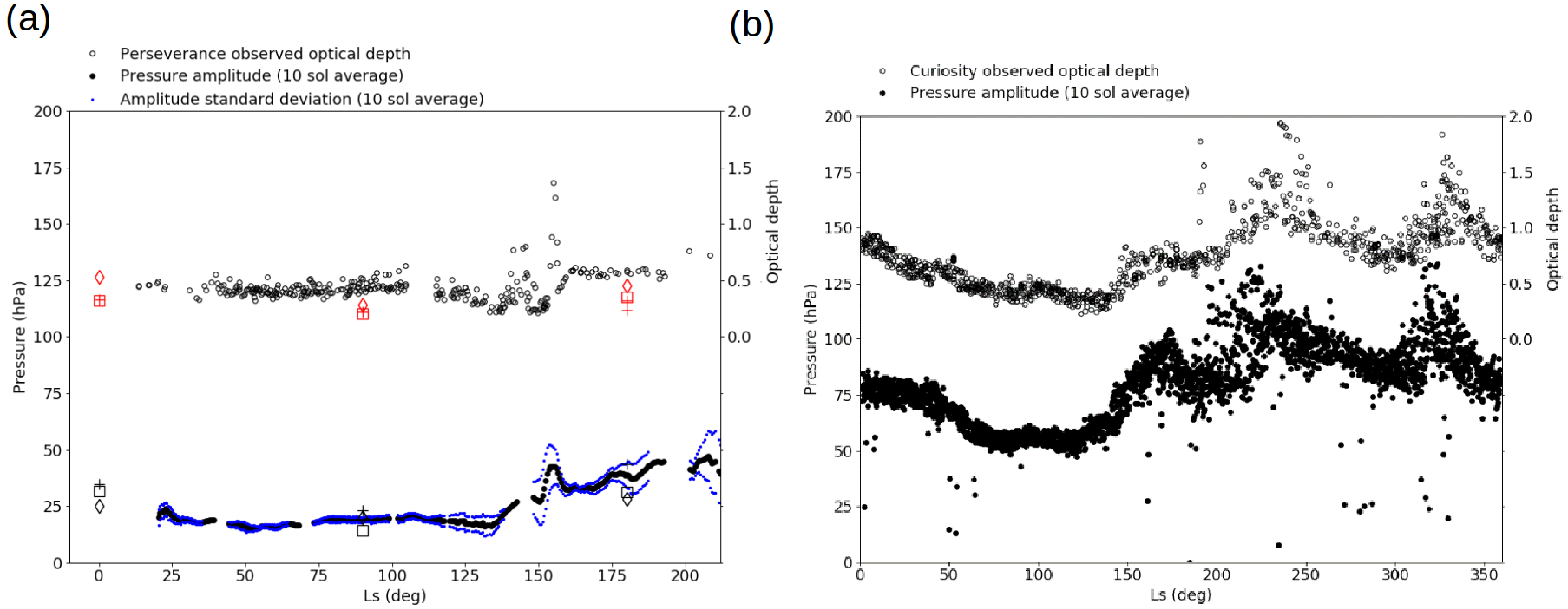
(a)
Perseverance observed optical depth
Pressure amplitude (10 sol average)
Amplitude standard deviation (10 sol average)
Pressure (hPa)
Optical depth
Ls (deg)
(b)
Curiosity observed optical depth
Pressure amplitude (10 sol average)
Pressure (hPa)
Optical depth
Ls (deg)

Figure 12.

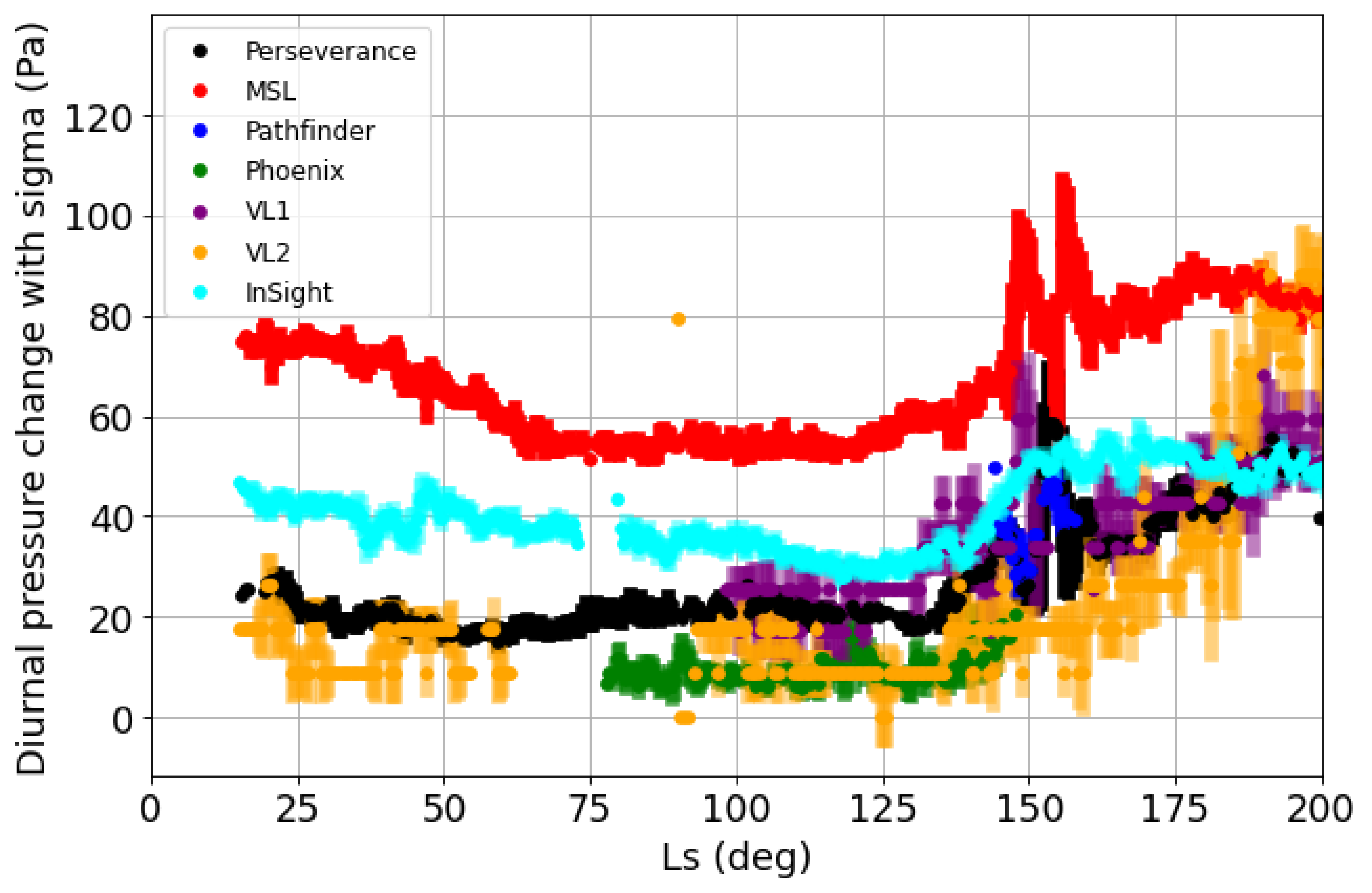

Perseverance
MSL
Pathfinder
Phoenix
VL1
VL2
InSight
Diurnal pressure change with sigma (Pa)
Ls (deg)
0
20
40
60
80
100
120
0
25
50
75
100
125
150
175
200

Figure 13.

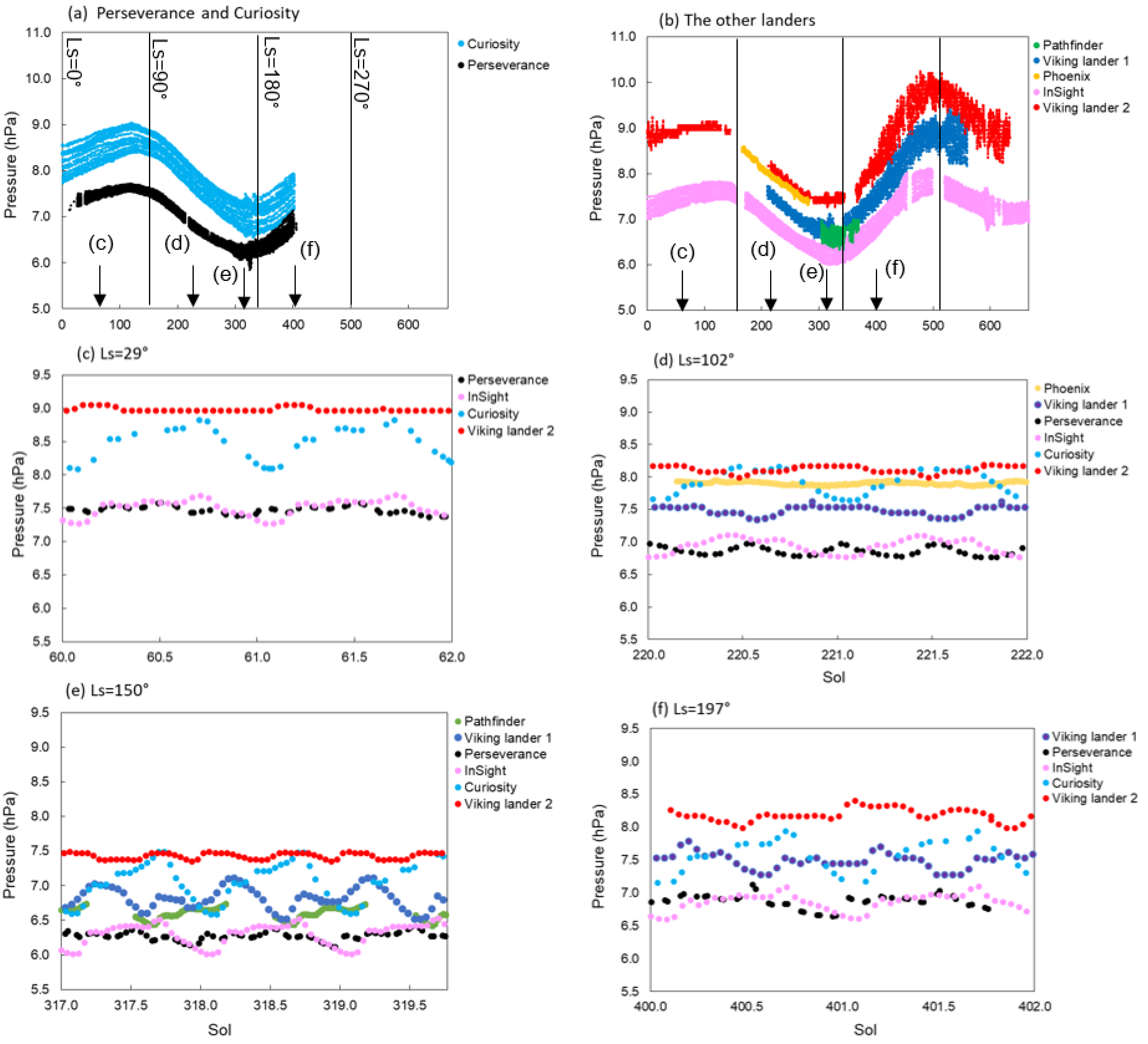

(a) Perseverance and Curiosity
(b) The other landers
(c) Ls=29°
(d) Ls=102°
(e) Ls=150°
(f) Ls=197°
Ls=0°
Ls=90°
Ls=180°
Ls=270°
Curiosity
Perseverance
Pathfinder
Viking lander 1
Phoenix
InSight
Viking lander 2
Pressure (hPa)
Sol

Figure 14.

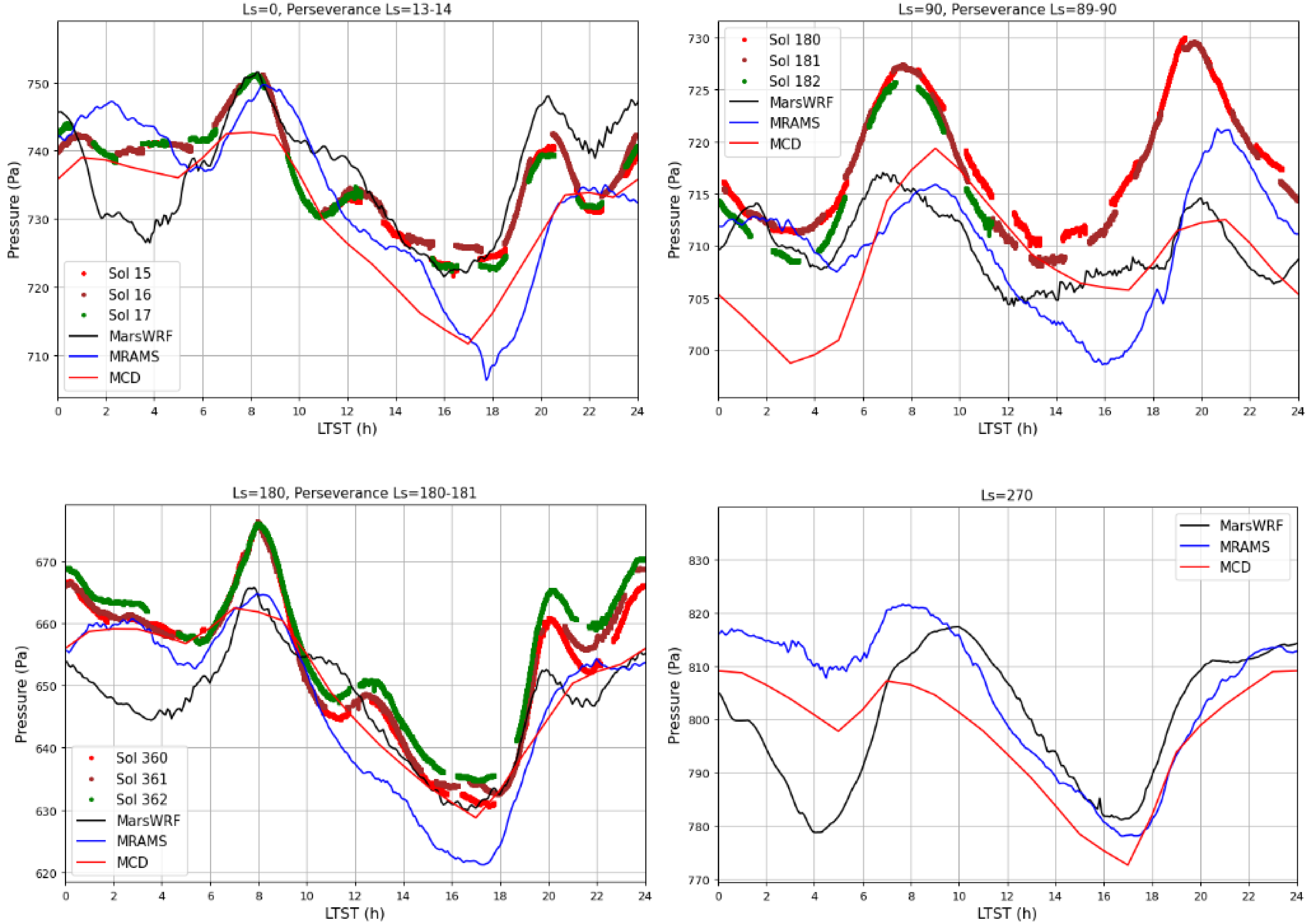

Ls=0, Perseverance Ls=13-14
Ls=90, Perseverance Ls=89-90
Ls=180, Perseverance Ls=180-181
Ls=270
Pressure (Pa)
LTST (h)
Sol 15
Sol 16
Sol 17
Sol 180
Sol 181
Sol 182
Sol 360
Sol 361
Sol 362
MarsWRF
MRAMS
MCD

Perseverance MEDA Atmospheric Pressure Observations - Initial Results

Ari-Matti Harri[1*], Mark Paton[1], Maria Hieta[1], Jouni Polkko[1], Claire Newman[2], Jorge Pla-Garcia[3], Joonas Leino[1], Terhi Mäkinen[1], Janne Kauhanen[1], Iina Jaakonaho[1], Agustin Sánchez-Lavega[4], Ricardo Hueso[4], Maria Genzer[1], Ralph Lorenz[5], Mark Lemmon[6], Alvaro Vicente-Retortillo[3], Leslie K. Tamppari[7], Daniel Viudez-Moreiras[3], Manuel de la Torre-Juarez[7], Hannu Savijärvi[1], Javier A. Rodríguez-Manfredi[3], German Martinez[8]

[1]Finnish Meteorological Institute, Helsinki, Finland
[2]Aeolis Research, Chandler, AZ, USA
[3]Centro de Astrobiología (INTA-CSIC), Madrid, Spain
[4]UPV/EHU, Bilbao, Spain
[5]Johns Hopkins Applied Physics Laboratory, Laurel, MD, USA
[6]Space Science Institute, College Station, TX, USA
[7]Jet Propulsion Laboratory/California Institute of Technology, Pasadena, CA, USA
[8]Lunar and Planetary Institute, Houston, TX, USA

Key Points:

- The atmospheric pressure observations by Perseverance Rover have proved to be of excellent quality fulfilling expectations
- Jezero crater pressure exhibits significant differences to other Martian areas likely due to varying regional geography and solar forcing
- Overall, the diurnal and seasonal atmospheric pressure cycles at Jezero Crater follow an anticipated pattern of pressure variation

*P.O. Box 503, 00101 Helsiki, Finland

Corresponding author: Ari-Matti Harri, `Ari-Matti.Harri@fmi.fi`

Abstract

The Mars2020 Perseverance Rover landed successfully on the Martian surface on the Jezero Crater floor (18.44°N, 77.45°E) at Martian solar longitude, L_s, ∼5 in February 2021. Since then it has produced highly valuable environmental measurements with a versatile scientific payload including the MEDA (Mars Environmental Dynamics Analyzer) suite of environmental sensors. One of the MEDA systems is the PS pressure sensor system which weighs 40 grams and has an estimated absolute accuracy of better than 3.5 Pa and a resolution of 0.13 Pa. We present initial results from the first 414 sols of Martian atmospheric surface pressure observations by the PS whose performance was found to meet its specifications. Observed sol-averaged atmospheric pressures follow an anticipated pattern of pressure variation in the course of the advancing season and are consistent with data from other landing missions. The observed diurnal pressure amplitude varies by ∼2-5 % of the sol-averaged pressure, with absolute amplitude 10-35 Pa in an approximately direct relationship with airborne dust. During a regional dust storm, which began at L_s 135° the diurnal pressure amplitude roughly doubles. The diurnal pressure variations were found to be remarkably sensitive to the seasonal evolution of the atmosphere. In particular analysis of the diurnal pressure signature revealed diagnostic information likely related to the regional scale structure of the atmosphere. Comparison of Perseverance pressure observations to data from other landers reveals the global scale seasonal behaviour of Mars' atmosphere.

Plain Language Summary

The Mars2020 Perseverance Rover successfully arrived at Mars in February 2021. It landed during an early Martian spring afternoon in a crater north of Mars' equator called Jezero crater. The rover is equipped with meteorological instruments that have so far produced extensive and valuable data for understanding the Martian atmosphere. One of the meteorological instruments is an accurate and precise pressure sensor. The pressure sensor has revealed large changes in the pressure over the seasons that are related to large changes in the actual mass of the Martian atmosphere. This is in line with seasonal pressure changes measured during previous Mars missions and can be explained as the freezing of the atmosphere onto the Martian poles and its subsequent thaw. On a shorter time scale the pressure sensor revealed complex pressure changes over a Martian day. These variations are thought to be related to atmospheric dust whose ubiquitous nature is known to have a strong influence on the Martian climate. As the seasons progressed the daily pressure variations morphed to exhibit different patterns likely related to the large-scale regional changes in the atmosphere. Comparison of Perseverance pressure observations to other landers revealed the global nature of the atmosphere.

1 Introduction

The Mars2020 Perseverance Rover landed successfully on the Martian surface on the Jezero Crater floor (18.44°N, 77.45°E) at the Martian solar longitude, $L_s, 5°$ in February 2021. Since then, it has produced highly valuable environmental measurements with a versatile scientific payload including the MEDA (Mars Environmental Dynamics Analyzer) suite of environmental sensors (Rodriguez-Manfredi et al., 2021). One of the MEDA sensor systems is the pressure sensor (PS) whose observations and initial results utilizing the data acquired during the first 414 sols of the mission ($L_s 5 - 212°$) will be addressed in this manuscript.

Martian atmospheric investigations through spacecraft observations began in the early to middle 1960s as reported by, *e.g.*, Kliore et al. (1969, 1973) and later by Kieffer et al. (1973, 1977); Snyder and Moroz (1992); Zurek (1992); Zurek et al. (1992a). Surface pressure of the atmosphere was firstly estimated using remote sensing methods, both ground based by *e.g.* (Young, 1969) and from spacecraft starting from Mariner as reported by, *e.g*, (Kliore et al., 1965). The Viking landers in 1974-77 provided the first time series of *in situ* atmospheric observations that turned out to be a treasure trove of data covering multiple Martian years (Kieffer et al., 1977; Tillman et al., 1979; Zurek, 1978, 1981). Thereafter Mars Pathfinder (M. P. Golombek et al., 1999; Schofield et al., 1997), the Phoenix lander (Taylor et al., 2008; Savijärvi & Määttänen, 2010), the Mars Science Laboratory aka Curiosity Rover (Gómez-Elvira et al., 2012), the InSight lander (M. Golombek et al., 2020) and the Perseverance Rover (Rodriguez-Manfredi et al., 2021) have continued *in situ* investigations of the Martian atmosphere including accurate atmospheric pressure observations.

During the years of *in situ* and remote observations, Martian atmospheric observations have been accompanied and supplemented by increasingly sophisticated and varied modeling efforts in a range of spatial and temporal scales already since late 1960s (Leovy & Mintz, 1969; Pollack et al., 1981, 1990; Haberle et al., 1993; Barnes et al., 1993; Forget et al., 1999; Richardson et al., 2007; Savijärvi & Kauhanen, 2008; Newman et al., 2017; Richardson & Newman, 2018; Newman et al., 2019). Pressure observations from surface stations have prompted investigations of the CO2 cycle and its connection to the poles, ice and dust e.g. Guo et al. (2009); Kahre and Haberle (2010). The characacterisation of pressure changes due to large scale circulations (Wilson & Hamilton, 1996; Basu et al., 2004) and local meteorology (Toigo & Richardson, 2003; Rafkin et al., 2016) have been predicted and characterised using computer models.

Data assimilation using orbital data is an important activity to enable realistic predictions using atmospheric models and verifying the physics (Rogberg et al., 2010; Lee et al., 2011; Montabone et al., 2014). Better understanding of the behaviour of the Martian atmosphere can help develop better predictions e.g. Battalio and Lora (2021). A network of surface pressure stations could could be key to characterising fast evolving weather systems and dust lifting events (Newman et al., 2021). Our current understanding of the Martian atmosphere and its processes is still understandably far less detailed than our understanding of our own terrestrial atmosphere, but the Martian atmospheric phenomena are presently clearly much better understood than those of any other solar system atmospheres.

Some of the earlier Martian landing vehicles have operated at similar latitudes or elevations to Perseverance, resulting in similarities in terms of climate zone or annual mean atmospheric pressure. Figure 1 shows the locations of Martian landing vehicles with Martian topography, giving a clear idea of the differences in the altitude and type of terrain of the landing sites. In terms of longitude, however, Perseverance seems to be relatively isolated, which has implications when comparing to data from other landed missions. Perseverance observations also have particular significance because they mean that for the first time, we have four *in situ* sets of meteorological observations being carried out at the same time at different locations on the Martian surface (including observations by MSL, InSight, Perseverance, and also China's Zhurong rover, data from which are not currently publicly available). We will present several interesting initial discoveries based on these facts, in addition to the independent Perseverance pressure observations.

In addition to this article there are two companion articles in this journal utilizing the pressure data focusing on atmospheric dynamics (Sánchez-Lavega et al., 2023) and small-scale thermal vortices (Hueso et al., 2023).

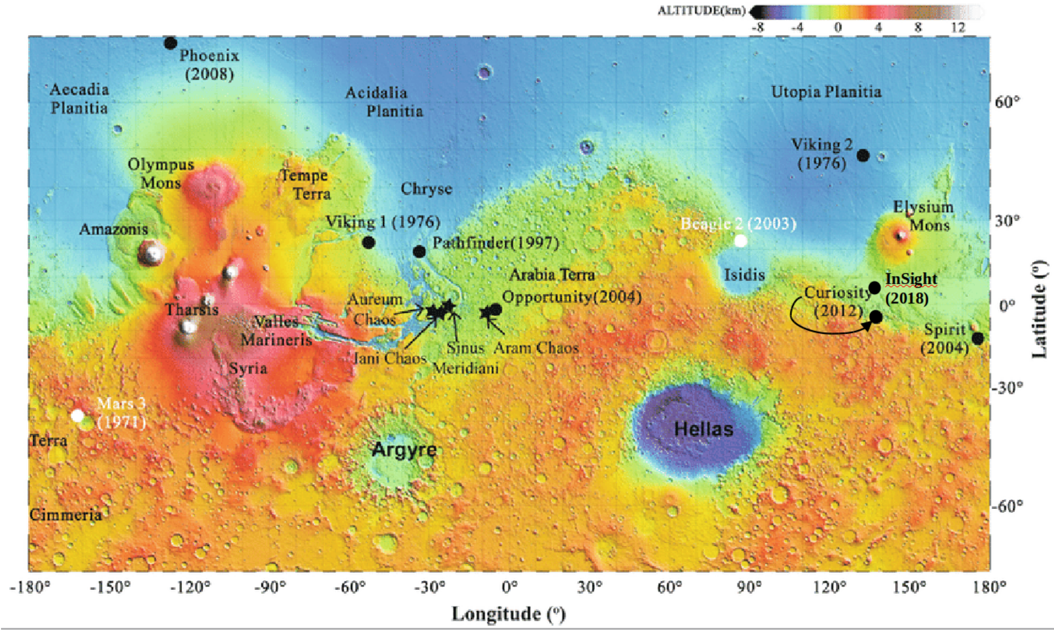

Figure 1. Landing sites of the seven spacecraft having provided *in situ* atmospheric data depicted on a topographic map of Mars (NASA JPL, 2021).

2 Brief MEDA PS device specification and performance

Instrument description. The Perseverance pressure measurement device (MEDA PS) is based on the silicon-micro-machined pressure sensor head (Barocap®) and transducer technology developed by Vaisala Inc. The Barocap® version used by MEDA PS is optimized for the Martian near-surface atmospheric pressure. Changing ambient pressure is changing the sensor head capacitance by varying the distance of the sensor head capacitor plates. Besides being pressure dependent, the Barocap® capacitance is also sensitive to temperature, and thus accurate temperature measurements close to the sensor head are necessary. The supporting housekeeping temperature measurements are provided by Vaisala's Thermocap® sensor heads.

MEDA PS consists of two transducers, each having its controlling ASIC (application specific integrated circuit) and 8 channels containing the Barocap sensor heads, Thermocap sensor heads and constant reference capacitors. Two types of Barocap sensors are used: the NGM type with high stability and relatively long warm-up time and the less stable but faster RSP2M type as a backup. Hence, the primary sensor for scientific investigations is the NGM type Barocap on transducer 1 channel 8 and the secondary sensor the RSP2M Barocap on transducer 1 channel 6. We provide a calibrated pressure reading for both sensor heads in the DER and CAL type data products in the PDS archive (Rodriguez-Manfredi & de la Torre Juarez, 2021) that are optimal for most investigations.

Calibration and performance. MEDA PS has been calibrated at the Finnish Meteorological Institute (FMI) laboratories over the expected operational pressure and temperature ranges. The calibration has been performed in stable temperatures from -45°C to +55°C and stable pressure points ranging from 0 hPa to 14 hPa, which extend well beyond the pressure and temperature ranges prevailing within the electronics compartment housing the MEDA PS on Mars itself. Cali-

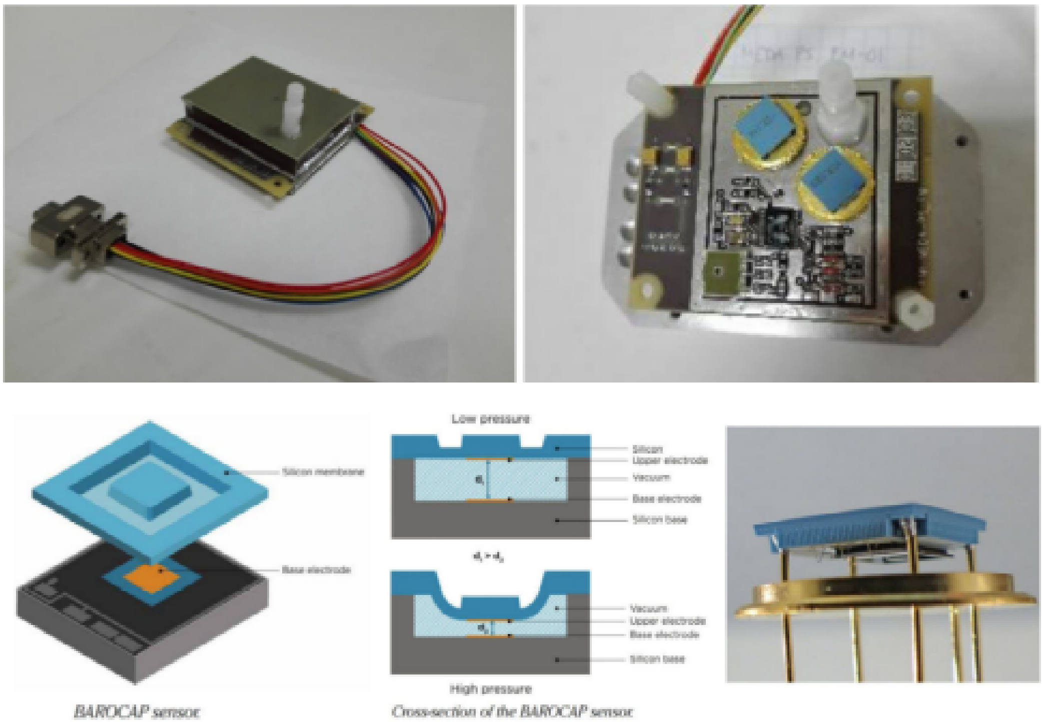

Figure 2. MEDA PS device within its Faraday cage made out of thin conductive foil (ltop eft pane) and the instrument with its pressure sensor heads and part of the electronics visible without the Faraday cover (top right pane). The structure of the silicon micromachined sensor head is shown on the lower row.

bration measurements were also performed in changing pressure and temperature conditions. The Barocap sensors are known to have small changes in the temperature dependence or sensor offset when introduced to a new electrical and thermal environment, and thus calibration checks were performed at all stages after the sensor-level calibration. The calibration checks were performed after integration to the MEDA electronics compartment (MEDA ICU), during the final rover-level thermal vacuum test, during the interplanetary cruise and soon after landing on Mars. The RSP2M Barocaps are also periodically cross-checked against the primary Barocap for possible drift compensation.

The estimated MEDA PS uncertainty based on the sensor- and rover-level measurements was analyzed to be better than 3.5 Pa. This includes the effects of the short-term repeatability, environmental effects and the pressure reference accuracy. The resolution of the primary Barocap, restricted mostly by the electronics noise, is 0.13 Pa in nominal measurement mode, and 0.1 Pa in high-resolution mode, as determined in sensor-level measurements. According to the test data, the time response of MEDA PS is equal to or less than 1 s, having almost no effect on the measurements at the nominal sampling rate of 1 Hz. The effect of the warm-up time of the NGM Barocaps has been removed by the calibration.

The system resources required by the whole MEDA PS package are dimensions $62\times50\times17$ mm, mass 43 g and power consumption less than 15 mW. The MEDA PS detailed specification available before the launch of the Perseverance Rover is described in detail by (Rodriguez-Manfredi et al., 2021). The MEDA PS is located inside the MEDA Instrument Control Unit (ICU) in the rover body, with a filter-protected tube connecting it to the outside environment and conveying ambient pressure to be measured. The MEDA PS device is depicted in Figure 2 illustratating the pressure sensor head and its encapsulation of the full pressure device in a Faraday cage giving shielding against electromagnetic interference.

During the first 414 Martian sols of Perseverance operations MEDA PS has been functioning as expected. The temperature dependence of the Barocap sensors was checked and corrected at the beginning of the operations against the primary Barocap, which is known to be very stable based on the test data. In the first drift offset check performed after 150 sols, the drift of the secondary Barocap was less than 0.3 Pa and slightly larger for the other RSP2M Barocaps.

3 MEDA PS observation strategy and pressure data coverage

MEDA has been designed for flexible operations that are being conducted according to the scheduling by the Perseverance rover. MEDA measures for five minutes at the top of each hour in local mean solar time (LMST) in every mission sol, other than during exceptional circumstances. In addition, on average, MEDA is operating continuously for every other hour. That enables us to generate data sets with averaged pressure measurements approximately at 1-hour intervals, as well as data sets with pressure observations at 1 second intervals for a period of one hour or a few hours in a row for *e.g.* turbulence-related studies. There are also periods, when MEDA is only able to measure for five minutes per hour (or sometimes fifteen or twenty minutes per hour) or is doing no measurements at all for a few hours, due to Perseverance resource allocation reasons.

In the present investigations we use data sets with 1-hour intervals. The 1-hour data sets are not complete but they do have gaps due to scheduling of Perseverance and MEDA operations. Figure 3 illustrates how well the observed data sets cover each Perseverance sol. in the average about 50-70 % of the 24 hour of a sol throughout the season with some periods having 100 % coverage and few sols have

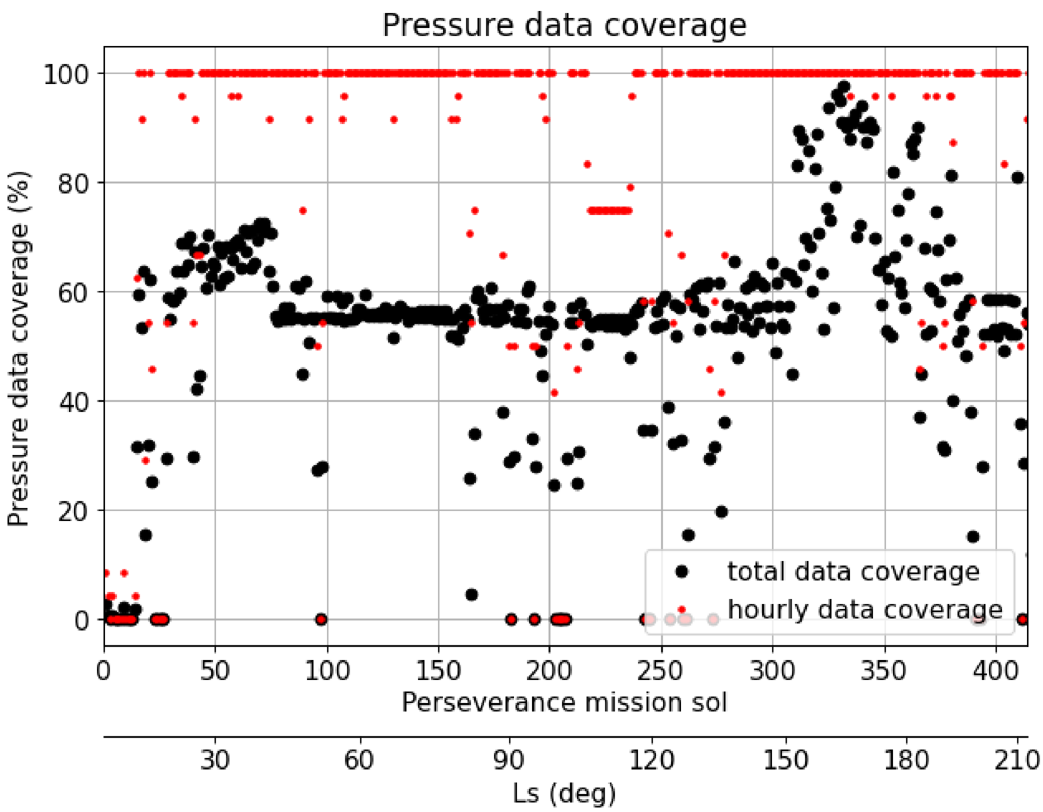

Figure 3. The coverage of atmospheric pressure observations made by the MEDA PS instrument. The black dots depict the overall percentage of pressure readings once per second in a sol, red dots the percentage of the pressure readings available at 1-hour intervals.

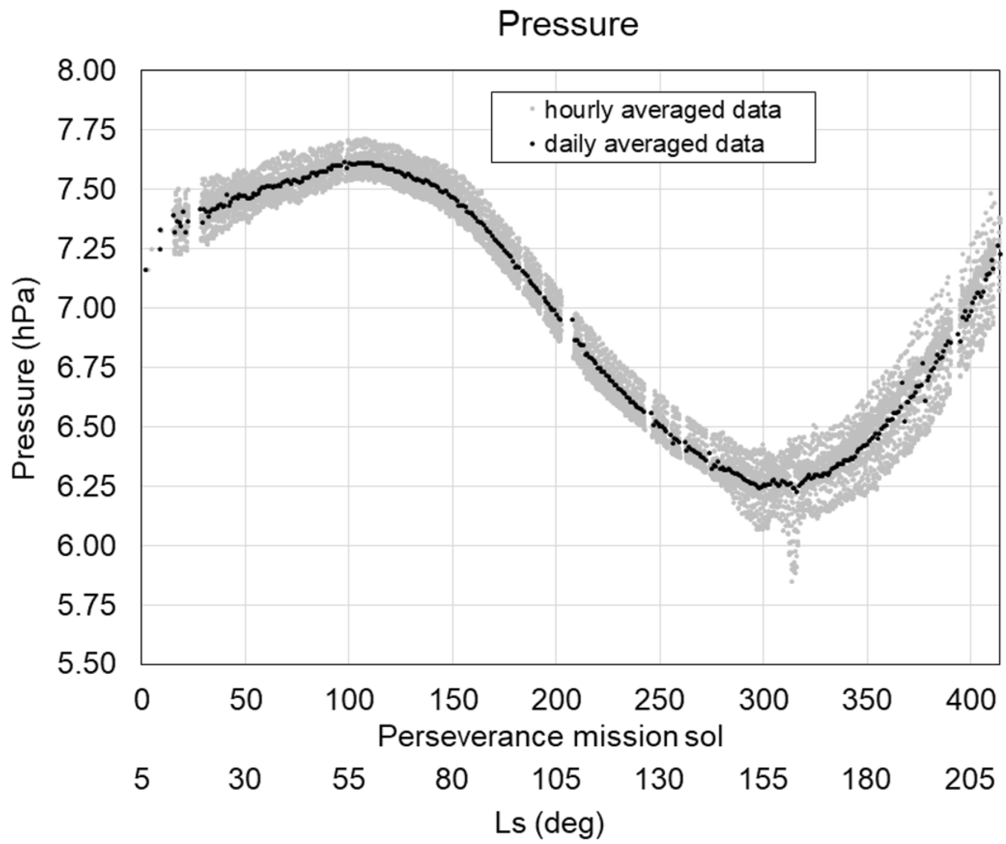

Figure 4. The sol averaged pressure data and the diurnal pressure amplitude (approximate total peak-to-peak range based on observations once per hour) for Perseverance during the period of the first 414 sols corresponding to approximately solar longitude range of L_s $5 - 212°$.

no pressure data at all. The gaps in the 1-hour data set take place more or less randomly around the 24 hour Martian sol. The data coverage of this level allows good characterisation of both the diurnal and seasonal variations in the pressure.

4 Changes in Jezero crater atmospheric pressure with seasonal cycle

The condensation and sublimation of CO2 in the polar regions during winter and spring causes planetwide seasonal variations in the surface pressure, which were first detected by the Viking landers as reported by, *e.g.*, Kieffer et al. (1977); Tillman et al. (1979). The seasonal CO2 cycle, which is largely controlled by the polar heat balance (Paige & Ingersoll, 1985, e.g.,), can clearly be seen in the seasonal variation of daily average surface pressure.

This is nicely demonstrated at the Jezero crater site by the Perseverance Rover measurements. The daily averaged atmospheric surface pressure during the first 414 sols of the Perseverance mission is depicted in Figure 4. The figure also includes the range of diurnal pressure variation plotted on both sides of the average pressure line with a gray color. Hence the gray area illustrates the approximate total range of diurnal pressure variation around the average pressure of a sol. The minimum pressure peak at around Ls 153 shown in Figure 4 was likely caused by a regional dust storm (Lemmon et al., 2022).

In seasonal-to-annual time scales the CO2 condensation-sublimation cycle at the polar regions gives rise to a seasonal pressure variation on the order of as much as 30 % of the local surface pressure (Kieffer et al., 1977; Tillman et al., 1979, e.g.,). The observed sol-averaged atmospheric pressure during the 414 first Perseverance sols, from the landing time at early Northern springtime to Northern fall, follows an anticipated pattern of total pressure variation in the course of the advancing season. The data has the first maximum in late spring roughly on Perseverance sol 110 and a minimum on sol 310, whereas by the Perseverance sol 414 (corresponding to approximately L_s 212°) the atmospheric pressure is climbing higher than the first maximum toward the annual maximum. When comparing Perseverance with concurrent observations by the Curiosity Rover and the Insight lander as well as with the historical Viking Landers data, we can see distinct differences in the amplitude of the seasonal pressure variations that are due to different surface elevations.

The sol-averaged MEDA PS atmospheric pressure data together with the hourly-averaged pressure depicted in Figure 4 is nicely showing the evolution of the atmospheric pressure over first 414 Perseverance sols at the Jezero crater site. In the beginning of the data set the pressure is going down during the Northern spring and summer seasons and turning to an increasing leg during the late summer. The diurnal amplitude, shown approximately by the gray area in Figure 4, shows a clear increase during periods with increased amounts of airborne dust starting approximately from Perseverance sol 270 and staying high until sol 414 (when our investigation period ends). There seems to be a direct relationship between the range of diurnal pressure variation and the amount of airborne dust as has been earlier discovered by, *e.g.*, Zurek (1978, 1981); Paige and Ingersoll (1985).

The seasonal dependence of the Martian atmospheric pressure drives the atmosphere to the extent that about one third of the mass of the Martian atmosphere is deposited on the polar caps during Northern and Southern winters and evaporated back to the atmosphere during summertime. This results in the characteristic atmospheric pressure pattern having two local maxima and minima during a Martian year, with the maxima occurring approximately at solar longitudes L_s 60° and L_s 260°. This pattern can clearly be seen in Figure 5, which compares the sol-averaged pressure of Perseverance with Curiosity Rover, Insight Lander, Viking Landers and the Pathfinder mission. Table 1 gives the basic characteristics of each mission.

Investigations of the seasonal pressure cycle together with observations from other Martian landing missions enhance our understanding of the CO2 cycle, the annual heat balance of the polar caps and the global scale atmospheric circulation of Mars (Paige & Ingersoll, 1985; Guo et al., 2009). Major drivers behind the seasonal variation are solar radiation and surface and subsurface thermal properties (Wood and Paige, 1992). Atmospheric dust loading and regional circulation will influence short scale variations (Haberle et al., 1993; Hess et al., 1980). The annually averaged atmospheric pressure is largely depending on the elevation of the site and hence the atmospheric pressures are differing between observation sites (Hess et al., 1980; Richardson & Newman, 2018).

In order to investigate the relative evolution of the pressure cycle at different latitudes figures 5 (c) and 5 (d) show the differences in pressure between the Perseverance landing site and the other four landers, excluding Pathfinder. In figures 5 (c) and (d) a more negative pressure signifies a higher pressure compared to Perseverance. The results from MCD data shown in figure 5 (d) tracks in the evolution of the results for the observational data shown in figure 5 (c). For Curiosity there

Table 1. Essential characteristics of seven Martian lander missions performing atmospheric observations. The elevations are based on MOLA data (Smith et al., 2001)

Vehicle	Lat (°N)	Lon (°E)	Elevation (km)	Climate Zone	Operational (years)	Platform Type
Viking lander 1	22	-48	-3.6	North subtropics	1976-82	Stationary
Viking lander 2	48	134	-4.4	North mid-latitudes	1976-80	Stationary
Mars Pathfinder	19	-34	-3.7	North subtropics	1997	Stationary
Phoenix	68	-126	-4.1	North polar regions	2008	Stationary
Curiosity	-4.6	137	-4.5	Equatorial regions	2012-	Mobile
InSight	4.5	136	-2.6	Equatorial regions	2020-	Stationary
Perseverance	18	77	-2.6	North subtropics	2021-	Mobile

are two sets of lines in figure 5 (c). These correspond to years 2 and 3 of the mission with year 3 being at a higher elevation which explain the difference in the mean pressure. There are a number of interesting dip or hump-like features over timescales of 100-200 sols in figure 5 (c) and (d) that need explaining.

The dips and humps in the season pressures in figure 5 (c) and (d) are most likely connected to latitude dependant processes that include the orographic, i.e. the large difference in elevation between the northern and southern hemisphere, and the dynamical effects on the pressure cycle (Hourdin et al., 1993). Regarding the orographic effect, during northern hemisphere winter a large mass of cool air is trapped in the low elevation of the northern hemisphere basin. In the winter a low atmospheric scale height traps a large portion of the atmosphere. The result is a higher winter maximum at higher latitudes in the northern hemisphere in winter. For example the heights of the winter and summer pressure peaks for Viking landers 1 is much more symmetric than for Viking lander 2. We will not cover dynamical effect here, which is related to the winds, as it apparently has little influence at the equatorial and middle latitudes considered here. An explanation of the dynamical effect can be found in Hourdin et al. (1993).

The greatest dip seen is for the Viking lander 2 in 5 (d) which is at a latitude of 48°N. This results from the pressure observed by Viking lander 2 increasing more rapidly than the pressure observed by Perseverance most likely due to the orographic effect. For the other landers the, except maybe for Curiosity, the pressure differences in figures 5 (c) and (d) are fairly level indicating the pressures at these landing site increase more or less at the same rate.

A shallow but distinct dip can be seen for Curiosity in figures 5 (c) and (d) over the spring-summer time period. A possible reason for a dip at this time of year

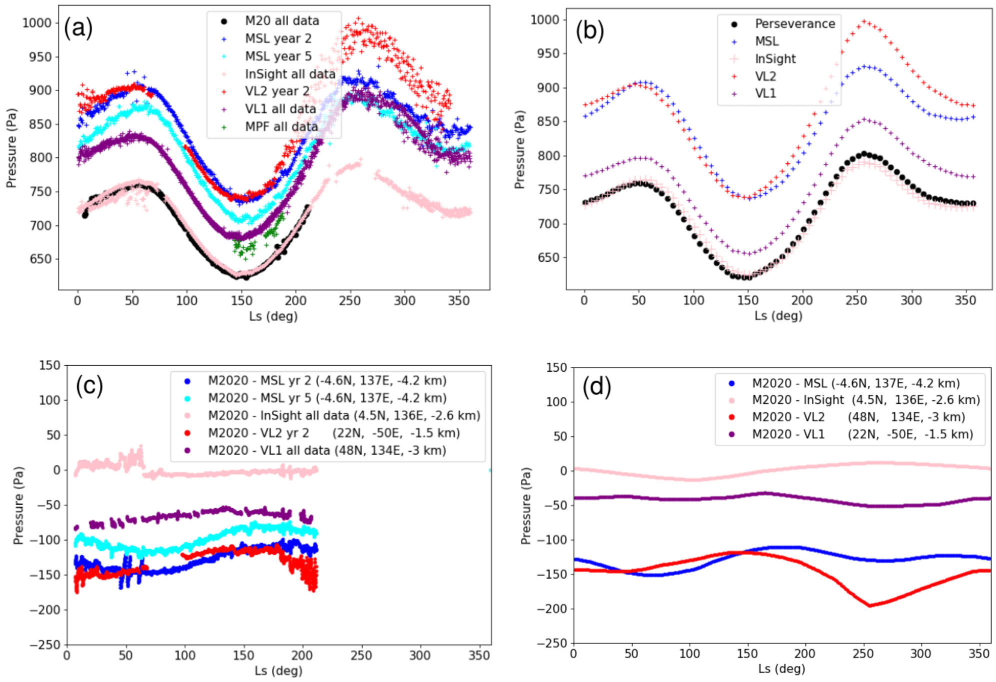

Figure 5. Comparisons of pressure between different lander missions. The top row shows the sol averaged observed pressure data, and the bottom row sol-averaged pressure data by different lander missions subtracted from Perseverance pressures. The left column shows results from the observations while on the right are the same results from the Mars Climate Database.

is that the cold air trapped in the northern hemisphere trapped during the winter is now being released as it is the summer. This lowers the pressure faster at the Perseverance landing site than at the Curiosity landing site, which is located near the equator in the southern hemisphere. This would result a relative increase in the pressure between Curiosity and Perseverance as seen in figure 5 (c) and (d). Both plots for Curiosity exhibit a dip around the summer solstice indicating that the process driving the evolution of the pressure, i.e. the dip, is not related to the change in elevation.

There are shallow dips and and troughs in the data for other landers in figures 5 (c) and (d) but these are less obvious and probably cannot be interpreted with much certainty. For example there appears to be a small dip in the MCD data for InSight in figure 5 (d). This might be expected because InSight is located at a more southerly latitude than Perseverance with InSight being less sensitive to the ejection of summer time air from the northern basin than Perseverance. Interestingly this dip cannot be seen in Figure 5 (c) perhaps suggesting some other process or mechanism is masking the effect in the observations or limits with the model.

5 Diurnal atmospheric pressure and small scale atmospheric phenomena

In situ pressure observations by several landed missions have shown that the Martian atmospheric surface pressure is composed of variations over several time scales and amplitudes. They include, *e.g.*, the overarching seasonal CO2 cycle, regional-scale perturbations caused by planetary waves and thermal tides, including their interactions with topography, hydrostatic adjustment flows, and baroclinic and barotropic disturbances. Small scale eddies and disturbances, e.g. convective vortices are a usual cause of the shortest pressure variations of the order of a few tens of seconds (Harri et al., 2014, e.g.). If the vortices carry an optically distinguishable dust load they are called dust devils.

Thermal tides driven by solar irradiation cause distinct detectable diurnal pressure variations and are especially significant at low latitudes. In the Martian thin atmosphere the thermal tides - and hence the range of diurnal pressure variation - are much larger than in Earth's atmosphere due to the relatively stronger solar forcing at the surface (Zurek, 1982; Kieffer et al., 1992).

At the Jezero crater site measured by Perseverance rover the diurnal atmospheric pressure range seems to be approximately 20 Pa during the first 270 sols of the mission and thereafter during mission sols 270-414 extending to roughly 40 Pa. The wider range of diurnal pressure is likely due to increased amounts of airborne dust measured by Perseverance. Several earlier investigations have found the direct relationship between the amount of airborne dust and the range of diurnal pressure variation as shown by, *e.g.*, Zurek (1981, 1982); Guzewich et al. (2016).

The Perseverance in situ pressure observations show variations ranging from microscale to seasonal scale as has been observed by earlier *in situ* pressure measurements of Viking (Soffen, 1976; Soffen, 1977), Pathfinder (M. P. Golombek et al., 1999), Phoenix (Taylor et al., 2008) and Curiosity missions (Harri et al., 2014; Haberle et al., 2014). The advancing Martian season has a clear signature in the atmospheric pressure as clearly manifested by Figure 6 depicting the diurnal pressure variation by data stacked in steps of 10 sols. It shows the gradual increase of the observed Perseverance pressure levels during the Northern spring until approximately sol 110, then gradual decrease bypassing the Northern midsummer (Ls 90) until sol 320, and thereafter again showing increasing pressure until the last sol (414) of this investigation when the season advances further into the Northern fall. The data of this investigation covers only 60 % of the Martian year, but this kind of seasonal dependence will be seen throughout the Martian year.

When inspecting the structure of diurnal pressure, 2-4 peaks appear in the data on each sol in Figure 6. A clear evolution of the peaks can be seen in the stacked diurnal pressure data. During Northern summer (Figure 6, second row from top) diurnal pressure exhibits two distinct and regular peaks, one in the morning around 6-7 AM and the other one around 8-9 PM LTST. During the Northern spring (Figure 6, top row) and fall (Figure 6, lowest rows) this summertime regular pattern is broken into more like four separate peaks whose amplitudes vary along with advancing season.

It seems that during springtime - at the start of the mission, Perseverance sols 0-150 - smaller peaks are superimposed on the larger peaks. These smaller peaks disappear between about sols 150 and 250 (Northern summertime) and return around sol 300 in early Northern fall. The wintertime has not yet come during the first 414 Perseverance sols. The features in the plots give clues on the behaviour of regional atmospheric dynamics and circulation patterns in the Martian atmosphere (Read & Lewis, 2004, e.g.).

The largely repeatable two-peak shape of the daily surface pressure profile especially during the Northern summertime (Figure 6) is likely due to the strong semi-diurnal thermal tidal component as indicated in Figure 7. Abundant amount of airborne dust is one cause responsible for amplified semi-diurnal tidal component as shown by, e.g., (Zurek, 1981; Newman et al., 2021). Similar two-peak structure was also discovered during Pathfinder mission Schofield et al. (1997).

The harmonic components – principal components - of daily pressure variations sheds light on our understanding on the atmospheric phenomena behind the complex structure of daily pressure cycle. The principal components of the atmospheric diurnal pressure variation can be revealed by decomposing the pressure observations through Fourier transformation. The estimated diurnal, semi-, ter- and quad-diurnal amplitudes are represented by the first four components of the resulting series representation, respectively, as shown in Figure 7 together with the Perseverance optical thickness observations.

The Fourier transformations shown in Figure 7 were calculated using a fast Fourier transform (FFT) scheme. The input data series was created by generating hourly bins of observations from a window of three sols to get at least one observation per hour. In case of multiple observations per hour the bin value was achieved by averaging. The middle sol of the three-sol window was the one that was assigned the calculated amplitudes and phases. When using this procedure it was assumed that the three consecutive sols were sufficiently similar for calculating the principal components. The analysis was performed by sliding the three-sol window over the first 414 sols of Perseverance observations.

The principal components of the Perseverance diurnal pressure variation seem to be smaller than those measured by the Curiosity rover at Gale crater where tidal forcing is stronger due to the location close to the equator and also due to the fact that, at Curiosity's longitude sector, eastward and westward modes are expected to interact constructively (Wilson and Hamilton, 1996; Haberle et al., 2013; Harri et al., 2014).

In the light of the strong semi-diurnal component shown in Figure 7 during the Northern summer (sols 150-250), the prevailing stable 2-peak diurnal pressure cycle may be due to the strong summertime tidal forcing by relatively high amount of regional airborne dust creating a strong and stable semidiurnal component (Figure 7, top panel). This situation resembles that in the terrestrial tropics, where diurnal

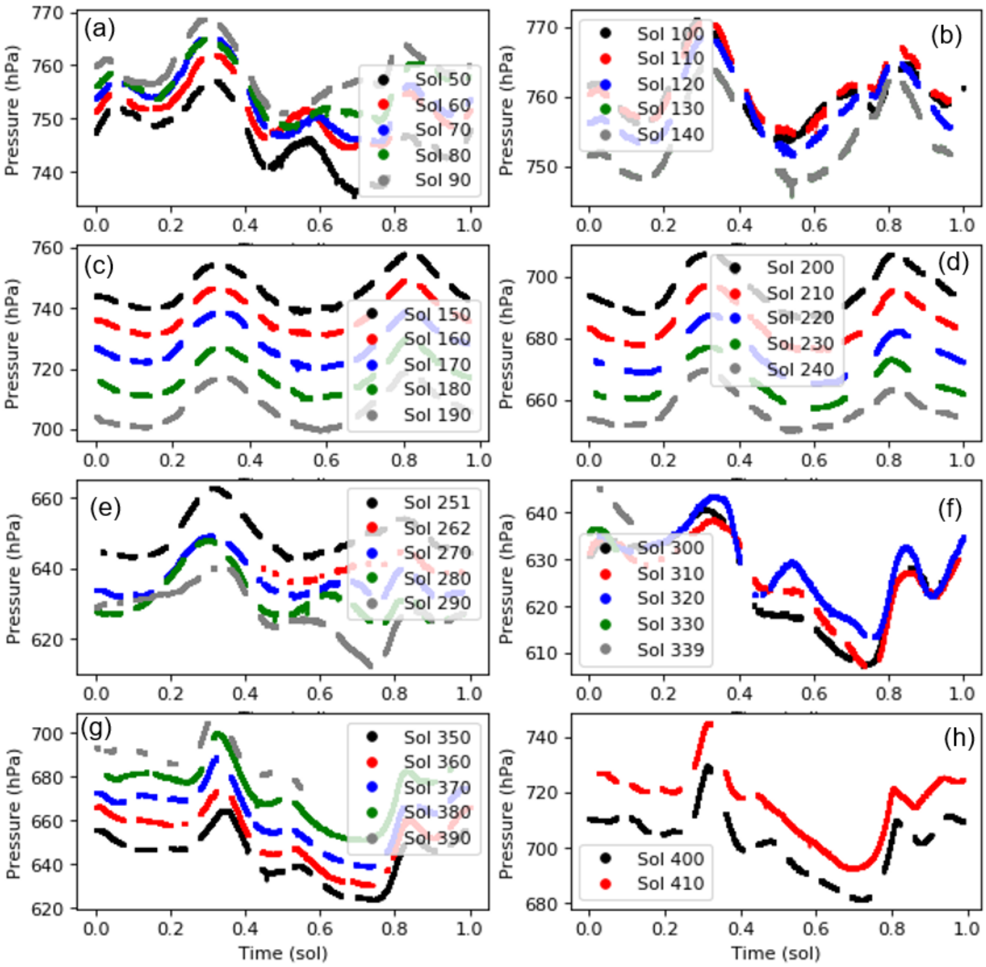

Figure 6. Evolution of diurnal pressure variation in steps of 10 sols covering the first 414 Perseverance sols during the advancing season. Each figure shows data averaged over five sols centered on the sol number shown, except the last on the bottom right (pane h).

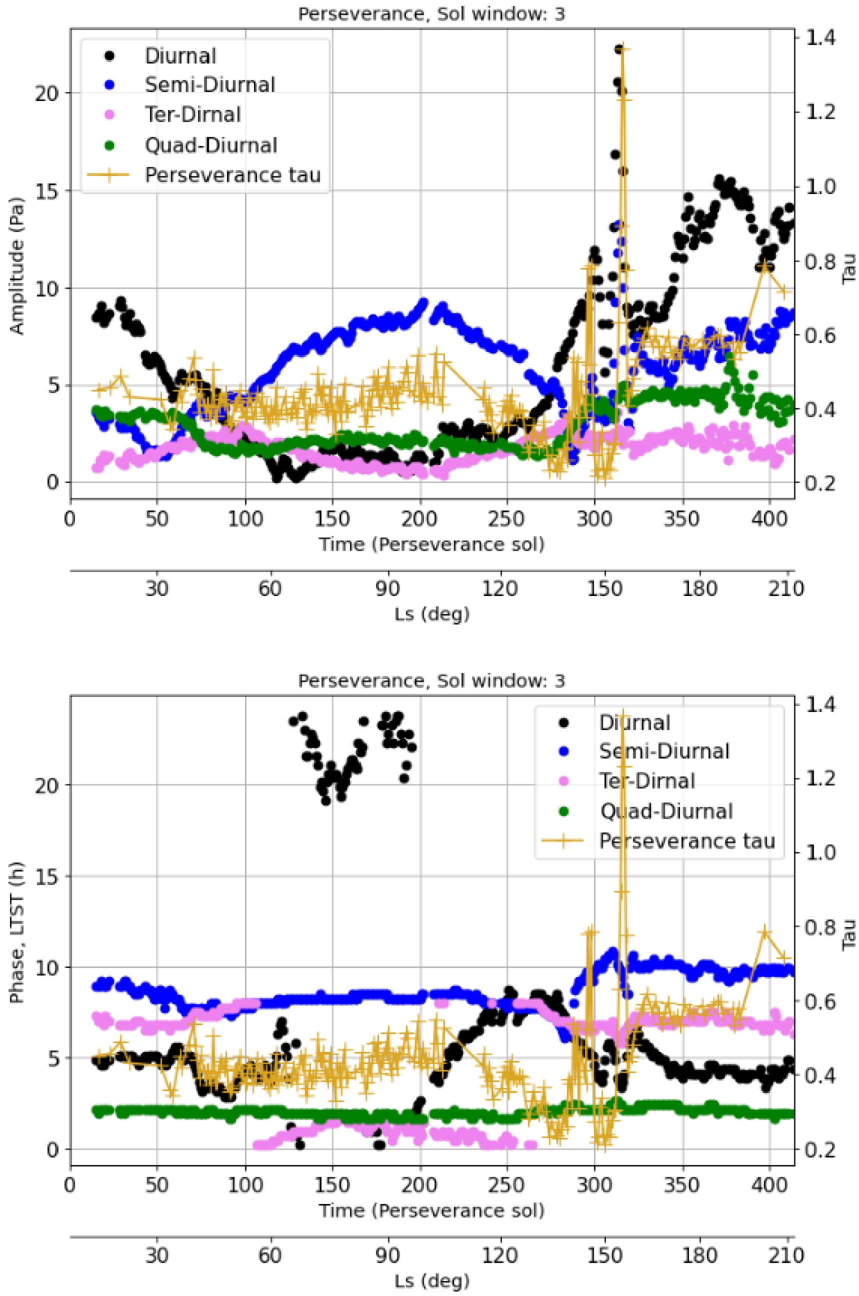

Figure 7. The amplitude and phase of the first four harmonic components of diurnal pressure calculated using FFT for all Perseverance sols. A running averaging window of three sols was used in the calculations. The amplitudes (top pane) and phases (lower pane) are illustrated in different colors (left axis). On the amplitude plot also the optical thickness observed by Perseverance is also shown (right axis).

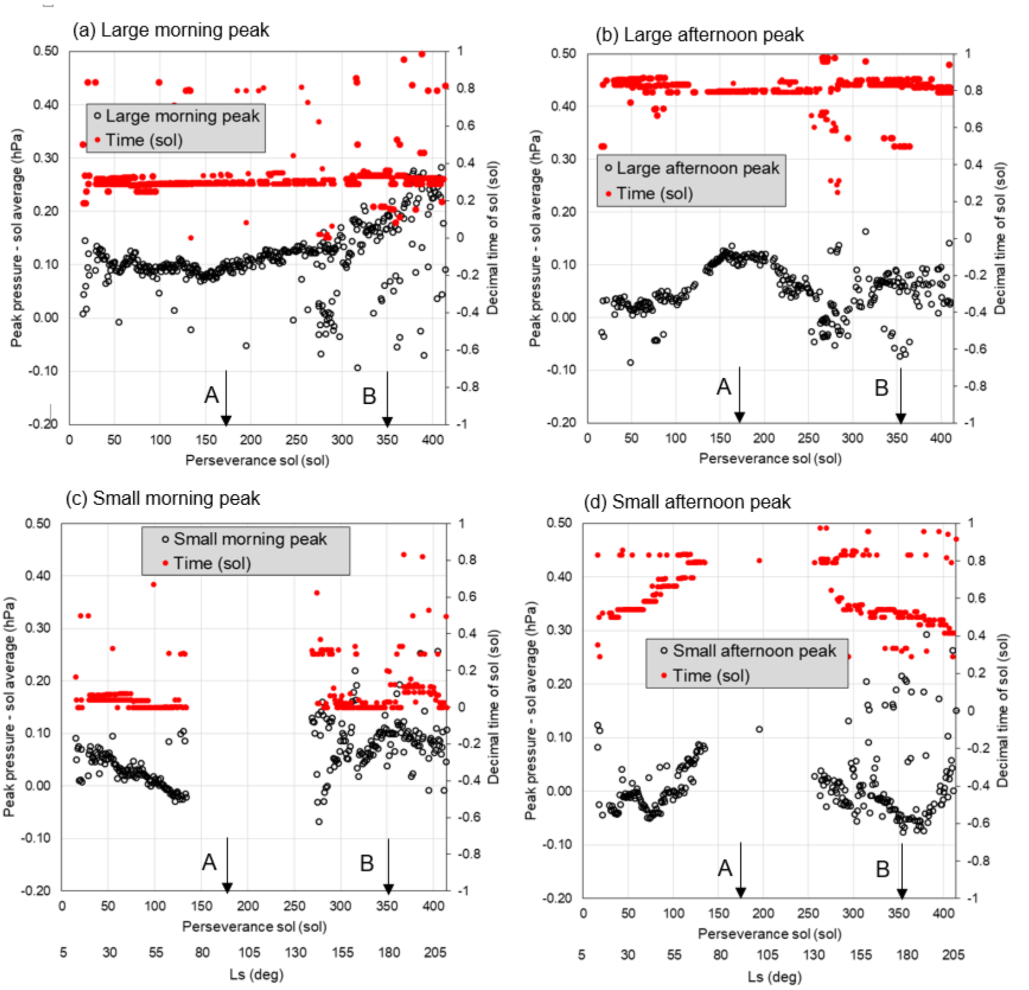

Figure 8. Black circles show the peak pressure minus sol averaged pressure. The time of occurrence of the peaks is also shown in red. The time has an uncertainty on it of plus or minus half an hour. The scatter in the points arises from relatively small fluctuations in flat regions of the data, *e.g.* in the dips between the peaks. The letters 'A' and 'B' point to midsummer (L_s 90° and fall L_s 180°, respectively.

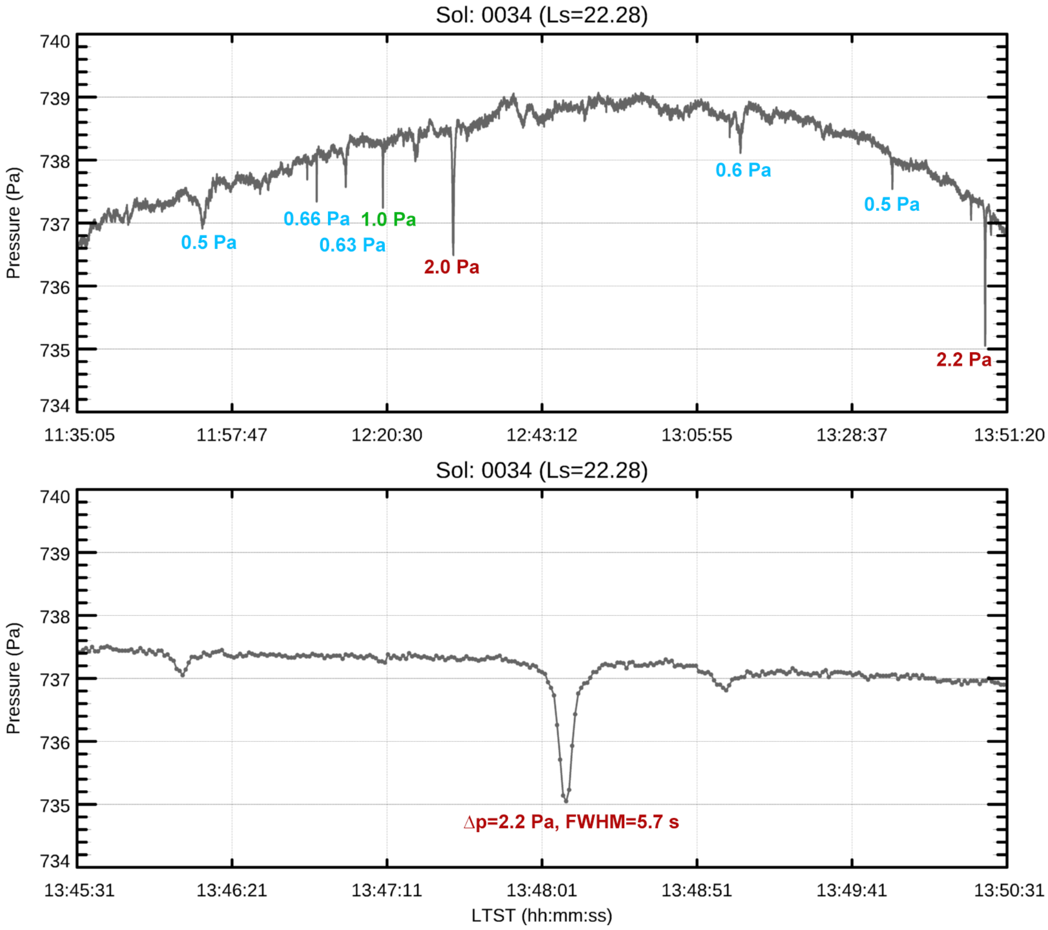

Figure 9. An example of vortex activity detected in pressure data over a 1.5 hour period around noon during the Perceverance mission sol 34. The upper pane displays vortex activity that can be seen as downward spikes in pressure with the depth of some spikes indicated. The lower pane zooms in on the deepest spike (2.2 Pa) to show a more detailed spike structure indicating also the full width at half maximum (FWHM) of the spike.

pressure has two distinct peaks, too – one in the morning and one in the evening. In the terrestrial tropics this is due to high-altitude ozone, whereas in northern late spring and early summer on Mars this may be due to the ever-present airborne dust getting heated by solar irradiation (Read and Lewis, 2001).

The semidiurnal tidal component at Jezero crater seems to be strong during Perseverance's Northern summer. This may be due to the fact that regional atmospheric dust load is relatively high at that time, which would amplify the semidiurnal component - assisted by the strong solar forcing at the Northern summer. Optical depth maps retrieved from the Mars Climate Database, based on data sets generated by Montabone et al. (2015), seem to support our inference. The maps from the MCD suggest that during the summer Perseverance is on the western edge of a patch of elevated optical depth that stretches over several 10s of degrees of longitude to the west. Later on in the year the optical depth at the latitude of Perseverance is more homogeneous.

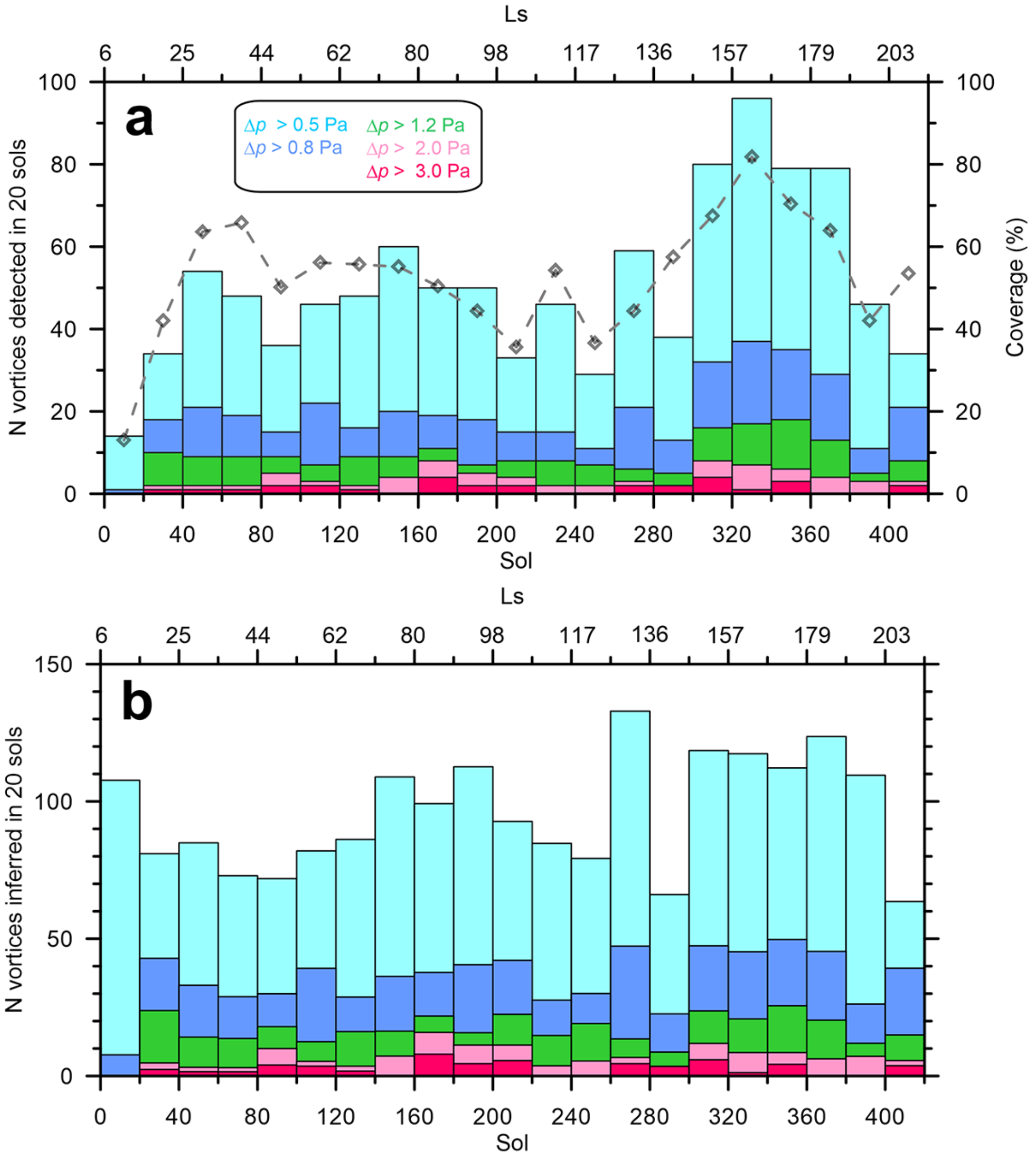

Figure 10. Assessment of the number of vortices by Perceverance through atmospheric pressure drops as a function of sol. (a) Number of vortices actually detected in intervals of 20 sols (left axis). The rhombs show the coverage of MEDA pressure data in each time interval (right axis). (b) Number of vortices that would have been detected if MEDA data would have been measured continuously. In both panes the intensity of the pressure drops is indicated by color coding as explained in the legend.

The seasonal evolution of diurnal pressure and its pattern of variation is shown in Figure 6. We found that during the Northern summertime a fairly stable pattern of two peaks was prevailing in diurnal pressure variation, but that was broken into four peaks during the spring and fall. Now, we can study further the evolution of the daily pressure pattern by analyzing the peaks and their evolution with the advancing season (Figure 8). This is done by subtracting the average pressure of the sol of interest from maximum pressure to get the peak amplitude and also noting the local time of occurrence.

Figure 8 shows the peak pressures relative to the daily-averaged sol pressure and the time that the peaks occur. As can be seen in Figures 6 and 8 there is one large peak both in the morning and in the afternoon that persist in the daily pressure data. These are clearly illustrated in the top row of Figure 8. The time these peaks occur remains steady throughout sols 50 to 400 in the data. Their magnitude varies with the large morning peak increasing after about sol 150. The large afternoon peak reaches a maximum around sol 150.

Figure 6 shows small morning and afternoon peaks prevailing during Northern springtime and fall. They are also depicted in Figure 8, where it can be seen (bottom row) that the small morning peak occurs at the same time each sol but the magnitude decreases until about sol 140 and then the peaks disappear. They reappear around sol 270 but appear to fluctuate in magnitude before settling down to a near constant value around sol 360. In Figure 8 (lower right) the small afternoon peaks appear to increase in magnitude before disappearing around sol 140. They then reappear around sol 260 and decrease in magnitude with the advancing sols.

These interesting morning and afternoon peak variations illustrated by Figures 6 and 8 could be a manifestation of local circulation phenomena causing pressure variation, which is then superposed with the strong semidiurnal pressure mode. During the Northern summer the semi-diurnal thermal tide (as shown by the semi-diurnal pressure variation) is at its strongest, which creates a stable diurnal pressure variation with one distinct large peak in the morning and another one in the afternoon. During the Northern spring and fall the semidiurnal mode of the thermal tide is weaker than in summer. Hence the stable situation is broken resulting in the creation of two additional small peaks, one preceding the large morning peak and another preceding the large afternoon peak.

This kind of pressure peak structure riding on top of the diurnal pressure variation is possibly caused by local effects due to the more complex topography of Jezero crater as compared, *e.g.*, to the topographically more simple and flat region of the Pathfinder and Viking Lander sites (Soffen, 1976; Schofield et al., 1997), where such peaks are not so clearly visible. On the other hand, at the Curiosity rover site additional peaks are also seen in the diurnal pressure variation, which is likely due to the fact that Gale crater is also a topographically complex site (Harri et al., 2014; Haberle et al., 2014). Variations in the thermal tide could also introduce multiple oscillations into the observed surface pressure. Schofield et al. (1997) suggest interference effects between the westward tide and the eastern travelling topographically induced Kelvin mode could produce surface pressure observations with two minima and two maxima per sol.

A highly interesting atmospheric phenomenon regularly observed in pressure data are convective vortices - called dust devils when raising surface dust in the atmosphere (Zurek, 1982; Ferri et al., 2003, e.g.). These rotating small scale atmospheric phenomena are investigated in this journal issue by (Hueso et al., 2023) using Perseverance pressure observations. Vortices appear as pressure drops in MEDA data, some times in bursts of activity as displayed by Figure 9 and 10 based on the investigations by Hueso et al. (2023). These pressure drops are most likely caused by passages of thermal vortices. Some of these events can be identified as dust devils when observing with additional MEDA radiative sensors able to infer the presence of dust, and by other instruments onboard Perseverance such as rover cameras. In the context of the Aeolian environment of Jezero, thermal vortices were discussed by Newman et al. (2022). These studies provide the overall abundance of vortices at Jezero, their daily cycle of activity, which peaks roughly at local noon, with some seasonal variation in the transition from summer to fall, the frequency of vortices that carry dust and are therefore dust devils, and establish the link between vortex activity and the thermal gradient of the near surface atmosphere.

An interesting aspect of vortex activity at Jezero revealed originally by the work of Hueso et al. (2023)) is the nearly constant activity with little seasonal variation during the period of observation of this investigation. This is demonstrated by Figure 10 showing the statistics of detected and estimated amount of vortices during the period of the first 414 Perseverance sols. This allows us to estimate (Figure 10) that about 100 thermal vortices with pressure drops exceeding 0.5 Pa during a 20 sol period are dwelling in the Perseverance neighbourhood throughout the first 414 Perseverance sols. Thus the vortex activity at Jezero seems to be nearly constant through the first 414 Perseverance sols. Apparently solar forcing varying considerably from springtime to fall has not significantly affected the generation of vortices. It is interesting to see whether this pattern will hold through the upcoming Northern wintertime with decreasing thermal forcing.

Martian atmospheric small scale turbulence and dynamics can be investigated using Perseverance observations accompanied by additional Perseverance measurements. These phenomena are studied in an accompanying paper in this journal issue by Sánchez-Lavega et al. (2023).

6 Perseverance diurnal pressure compared with other landing sites and modeling results

Atmospheric diurnal pressure variation is affected by *e.g.* the strength of thermal tide, regional and local geography and amount of airborne dust and hence some local atmospheric phenomena can be partially explained by studying diurnal pressure variation (Zurek, 1982; Zurek et al., 1992b; Haberle et al., 2014; Harri et al., 2014, e.g.). The diurnal pressure amplitude – minimum to maximum range – as a function of solar longitude for both Perseverance and Curiosity rovers is depicted in Figure 11 including the measured optical depth. Additionally results by regional models MWRF (squares) and MRAMS (plus-signs), as well as values by Mars Climate Database (diamonds) are shown. Furthermore, an uncertainty corridor of two standard deviations is drawn on the pressure amplitude by smoothing over a few sols. The standard deviation of the diurnal pressure range is calculated over 10 sols and it is then drawn on both sides of the curve. Thus the width of the uncertainty shown is thus twice the standard deviation.

The diurnal pressure variation exhibits a clear amplitude increase with the increasing amount of the atmospheric dust, which was reported by Curiosity pressure observations (Haberle et al., 2013; Harri et al., 2014). This phenomenon has been discovered also earlier by, *e.g.* Zurek (1978, 1982); Tillman (1988); Kahre and Haberle (2010). Actually, this is considered as a manifestation of how the Martian atmospheric conditions are intertwined with the airborne dust to such extent that atmospheric diurnal pressure observations could even be used to infer the amount of dust afloat *e.g.* (Zurek, 1981; Guzewich et al., 2016).

Figure 11 shows that the observed daily amplitudes in pressure are similar to those predicted by two atmospheric models that cover Jezero crater at km scale

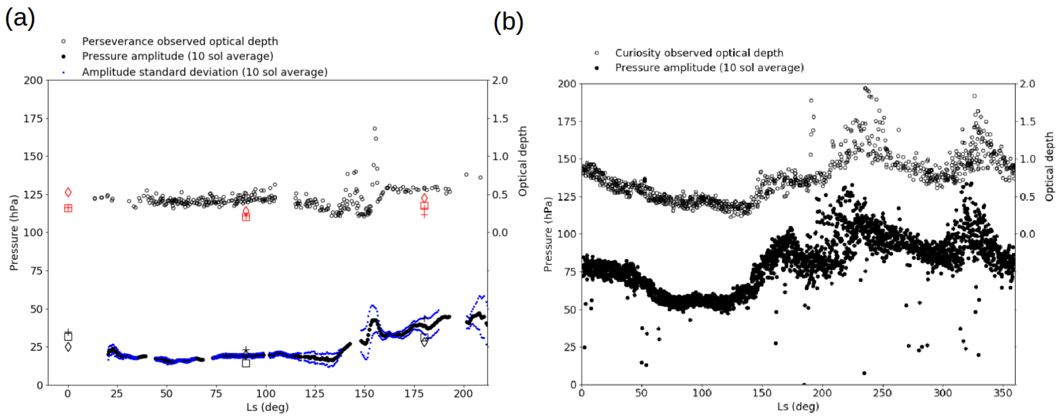

Figure 11. Diurnal pressure amplitude – minimum to maximum range – as a function of solar longitude (black dots, left axis) and the optical depth (small black spheres, right axis). The plots in (a) includes Perseverance pressure (MEDA PS) and optical thickness (M2020 Mastcam-Z) data during the first 414 Perseverance sols and in (b) all Curiosity pressure (REMS-P) and optical thickness (MSL Mastcam) data until Perseverance mission time. The depicted diurnal pressure range is a 10-sol moving average in both plots. The Perseverance plot also includes a 2-sigma belt around the diurnal pressure with the standard deviation (sigma) calculated from the 10 sols for each average point. Additionally results by regional models MWRF (squares) and MRAMS (plus-signs), as well as values by Mars Climate Database (diamonds) are shown.

resolution (MRAMS and MarsWRF). The amplitude predicted by MRAMS is usually slightly higher and MarsWRF slightly lower, for the Ls with data available. The models use TES optical depth zonally averaged over previous non dust storm years (Pla-Garcia et al., 2020) (Newman et al., 2021). As to the MCD values for the location of Perseverance (18°N, 77°E) the optical depth used in these models is similar to those observed by Perseverance. Note that the pressure amplitude in the MCD, which has a resolution of order several hundred km, is also similar to that observed by Perseverance.

It is interesting to compare the average amplitude of diurnal pressure variation – minimum to maximum value – at different locations and for varying Martian altitudes and terrain. The Martian atmospheric pressure has some interannual variation, but it appears to be sufficiently small to the extent that the atmospheric pressure at each landing site seems to be behaving largely in a similar fashion from year to year as shown by, *e.g.*, Tillman (1988); Tillman et al. (1994). This interannual similarity justifies qualitative and also somewhat quantitative comparison of pressure by different landing missions even if they are not observed at the same time, but rather in different Martian years. This applies especially to diurnal pressure variation that is being largely driven by thermal tide, local geography and regional atmospheric flows.

Figure 12 depicts the daily pressure amplitude during the first 414 sols of the Perseverance mission with concurrently observed daily pressure amplitudes of the Insight and Curiosity missions, as well as that of historical Viking Landers, Pathfinder and Phoenix mission data at matching solar longitudes. Basic characteristics of those seven Martian missions are shown in Table 1 including the climate zones and geographical locations (also in Figure 1) of those missions.

It can be readily seen in Figure 12 that the daily pressure amplitude of Perseverance, Viking Lander 1 and Pathfinder are quite similar, which is likely caused by the fact that they are at similar latitudes and experience similar thermal tides. The tides also have a distinct pattern in longitude too, though, due to interference by the large-scale topography although this does not seem to be a factor here. A regional dust storm like in the case of Viking Lander 1 starting on around L_s 200° increases the amplitude. In the case of Pathfinder the amplitude variation increases considerably as a function of the Martian season (Schofield et al., 1997). The diurnal pressure amplitude seems to be highest at the Curiosity and Insight landing areas, which are located close to the equator and hence have the strongest thermal tides. On the other hand, Phoenix observations have the lowest diurnal pressure amplitude as expected due to the weaker thermal tide occurring at such high latitudes.

Basic characteristics of those seven Martian missions are shown in Table 1 including the climate zones and geographical locations (also in Figure 1) of those missions. It is to be noted that similarities on some of those characteristics allow interesting considerations to be made. Insight and Perseverance have a very similar altitude above the Martian geoid, which allows for direct comparison of the sol-averaged pressure data including the pressure variation with advancing Martian season. This is the most direct possibility for comparisons. As to the longitudinal location, Perseverance seems to be relatively isolated from the other landed missions. When inspecting the latitudinal location, Perseverance shares the same climate zone – North subtropics – with the Pathfinder and Viking 1 landers and is similarly able to feel the additional effects of baroclinic disturbances through the mesoscale small pressure variations that these disturbances cause at the surface. The same applies also to the traveling low- and high-pressure systems – typical both on Mars and the Earth - causing pressure variations in a 2–5 sols time range especially in the wintertime subtropics and low midlatitudes (James et al., 1992).

The shape of diurnal pressure variation at different Martian landing sites in four periods evenly separated over the first 414 Perseverance sols are shown in Figure 13. In each case, two sols of data are shown figure 13 (top left) shows clearly that the diurnal pressure amplitude observed by Curiosity in Gale crater is larger by a factor of 2-3 than for Perseverance in Jezero crater. The diurnal pressure amplitude observed by some other landing missions (Figure 13, top right) – Pathfinder, Viking Landers, Insight - is also smaller than what Curiosity has observed. The large amplitude of pressures observed by Curiosity has been shown by using atmospheric models to arise from the influence of a daily cycle of heating on the large slopes of Gale crater, such that warming of air causes mass to flow out of the crater in order to maintain hydrostatic balance along the slopes (Richardson and Newman, 2018). Perseverance observations indicate that the diurnal pressure range at the Jezero crater is smaller by a factor of 2-3, somewhat smaller amplitude than measured by Insight, about the same amplitude than calculated from historical observations of Viking lander 1 and 2 and, however, somewhat larger than diurnal pressure range measured by the Phoenix mission.

In the two lower rows of Figure 13 (panes c-f), approximately two sols for each lander at four solar longitude values marked in panes a-b are shown. Perseverance can be seen to have a similar mean pressure to InSight. This is likely due the similar elevations of around -2.6 km. The diurnal pressure patterns are similar in amplitude but slightly out of phase between Perseverance and InSight, most likely due to the 59° difference in longitude, i.e. the thermal tide will pass over Insight and then over Perseverance four hours later. Also note that the diurnal patterns for Curiosity and InSight, separated by only one degree of longitude, are similar except that Curiosity has a greater diurnal amplitude.

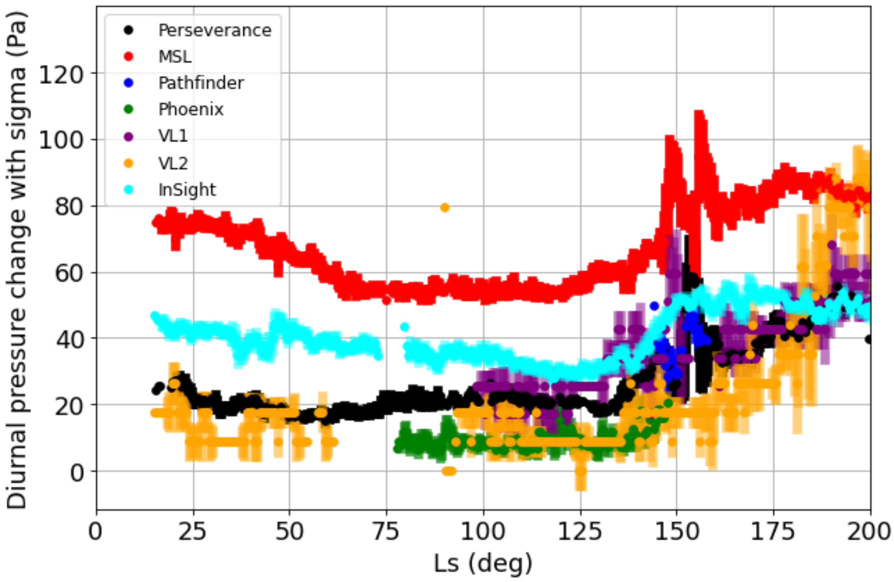

Figure 12. Diurnal pressure amplitude – minimum to maximum value – during the first 414 sols of the Perseverance mission with concurrently observed diurnal pressure amplitude of Insight and Curiosity missions, as well as that of historical Viking Landers, Pathfinder and Phoenix mission data on matching solar longitude range. Each diurnal pressure point is a moving 3-sol central average. The thickness of the curves represent the value of 2 standard deviations calculated over seven sols around each average diurnal pressure point.

At the Viking lander 2 site the daily pressure amplitude approaches similar levels to those observed by Curiosity only in the second half of the year, i.e. in the winter, as can be seen in figure 13 (b). The diurnal pressure amplitudes for the landers at high latitudes, i.e. Phoenix and Viking lander 2, during the northern hemisphere summer are small because of the weak thermal tide (Zhao et al., 2015). Curiosity and InSight latitudes (Table 1) are close to the equator and both have consistent daily pressures amplitudes throughout the year suggesting little variation in the thermal tide conditions at these latitudes.

Regional atmospheric modeling efforts are needed to expand the value of the *in situ* observations. This was done by running MarsWRF and MRAM models (Pla-Garcia et al., 2021) at the Perseverance site on solar longitude values of L_s 270°, 90°, 180° and 270°. Figure 14 illustrates these results together with *in situ* Perseverance observations at L_s 0°, 90°, 180° as well as data points acquired from the Mars Climate Database MCD (LMD-Jussieu, 2021).

MarsWRF and MRAMS simulate Jezero crater at high resolution. MarsWRF is a mesoscale nest embedded inside a global model model and MRAMS is a mesoscale model. Overall, MarsWRF and MRAMS as well as the lower-resolution MCD do fairly well compared to the actual *in situ* pressure observations. MarsWRF seems to reproduce the dip at 1700 better than MRAMS in Figure 14. MarsWRF reproduces the main features quite well except the small peaks at noon in the Northern springtime (L_s 0°, Figure 14a) and fall (L_s 180°, Figure 14c) where it generates a shoulder-like feature instead. The average pressure in Figure 14a for MarsWRF is generally good but in the Northern summertime (L_s 90°, Figure 14b) and fall (Figure 14c) the average pressure is too low. The height of the peaks in Figure 14b

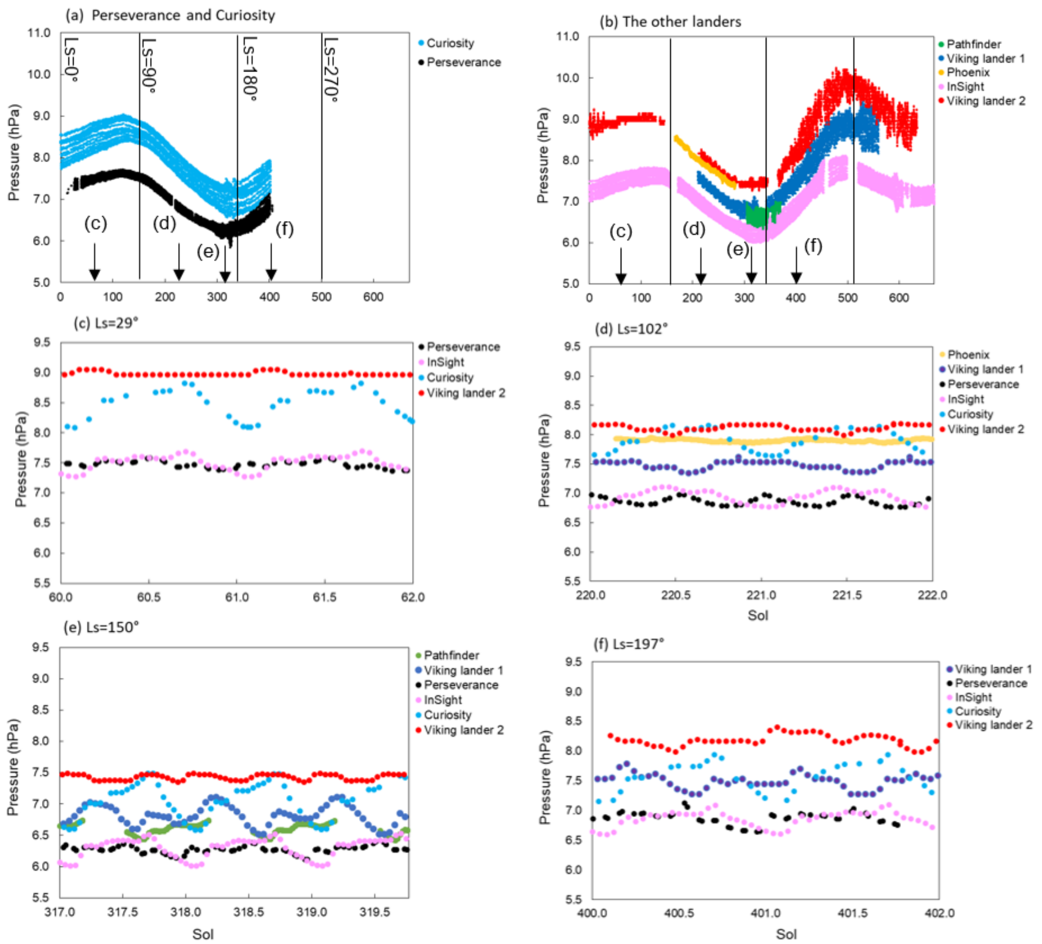

Figure 13. Diurnal pressure range of the Perseverance Rover compared over seasons with the diurnal pressure ranges observed by the Curiosity Rover, Insight Lander, Viking Lander 2 and Pathfinder (top row). Detailed diurnal pressure variation over 2-sol periods on these five surface missions is depicted at four solar longitudes evenly covering the first 414 sols of Perseverance operations. The lander data is plotted against the yearly sol, i.e. midnight on sol 1 corresponds to Ls=0° at the prime meridian, with midnight offset at each landing site depending on their longitude. The 2-sol periods were chosen in (c) to (f) over periods that avoided gaps in the lander data.

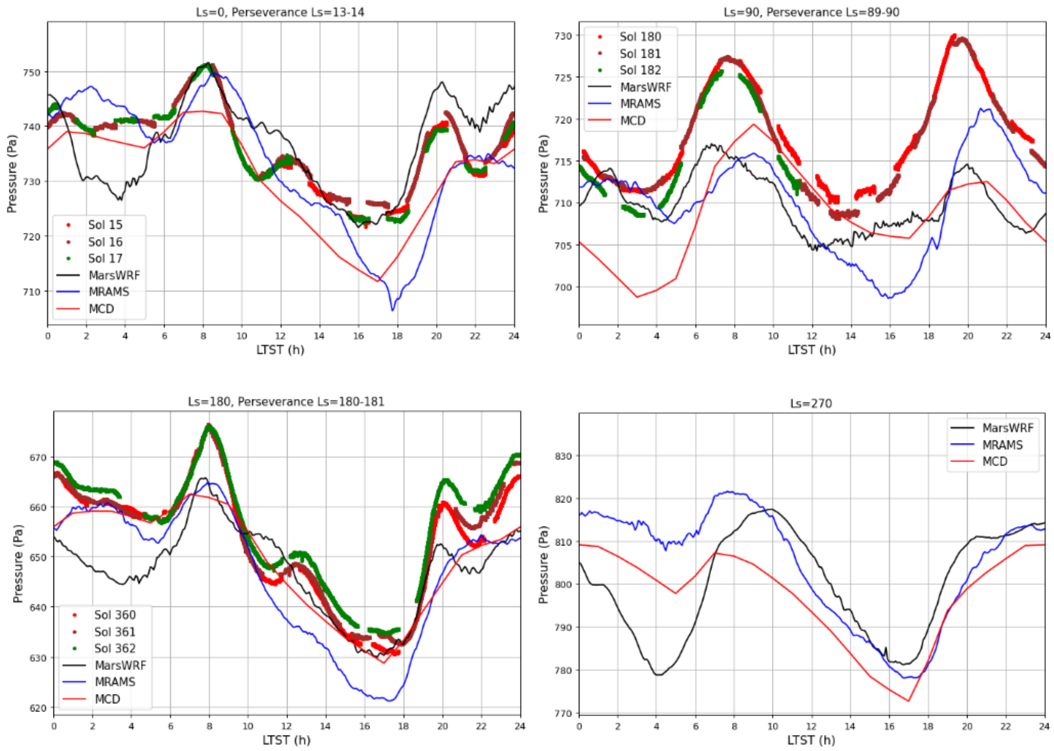

Figure 14. Diurnal pressure variation modeled by atmospheric models that simulate Jezero at km grid spacing MarsWRF, MRAMS and also the same data points from Mars Climate Database at solar longitude L_s 0°, 90°, 180° and 270°, which are depicted in panes a) to d). Around the solar longitude 0, 90 and 180 Perseverance pressure observations from three sols are added (Perseverance has no data as yet at L_s 270°).

are too low in the MarsWRF data. MCD is roughly producing in the average similar results to Mars WRF and MRAMS.

MRAMS matches the average pressure level quite well in Figure 14a if it was not for the big dip at 1700. It is not clear if it reproduces the peaks at 2200 and midnight. The occurrence of the peaks in the MRAMS data seems to be delayed by about 2 hours. Like MarsWRF MRAM does not reproduce the small peak at noon. MRAMS reproduces the height of the two big peaks in Figure 14b but they are on average too low. The timing of the peaks seems to be delayed by about 2 hours in Figure 14b. Overall, it seems to be the case that state-of-the-art regional atmospheric models succeed fairly well in producing diurnal pressure variation at the Jezero crater region. Then, understandably, reproducing through modeling the small peaks in diurnal pressure variation caused largely by the local geography and atmospheric flow conditions proves to be challenging.

The distinct oscillations in the observed surface pressure are expected to be primarily due to the thermal tides and their interactions with the Martian topography, e.g. Wilson and Hamilton (1996). Oscillations in the pressure could also include contributions of the local crater circulations that are especially important for deep craters like Gale crater (Tyler and Barnes, 2015; Wilson, 2017). In addition hydrostatic adjustment has been shown to be important in amplification of the amplitude of the diurnal pressure variation (Richardson and Newman, 2018).

This complex structure in the pressure signal was anticipated by Pla-Garcia et al. (2020). This is demonstrated in a distinct fashion in figure 14. A more comprehensive modeling study is needed, but the Perseverance pressure observations support the initial regional atmospheric modeling results at the Perseverance site made with the Mars WRF and MRAMS models as well as the data provided by MCD.

Jezero crater does not seem to have a similarly strong amplification from hydrostatic adjustment as is the case at the Gale crater based on the observations by the Curiosity rover (Harri et al., 2014; Newman et al., 2021). A plausible reason for this is the fact that compared to the Gale crater, the Jezero crater is shallow and wide resulting in relatively weaker amplification effect on the diurnal pressure variation amplitude. In addition the thermal tide at the Gale crater is stronger at most times of year than at Jezero crater because it is closer to the subsolar point for most of the year.

Combining the atmospheric regional modeling with *in situ* pressure observations proves to be highly useful – it adds the value of the observations by expanding their effect beyond the actual point of observation and sheds more light on the physical and meteorological processes behind the Martian atmospheric phenomena. The physics and implementation of the models themselves can also be modified to better address the actual atmosphere.

7 Summary and discussion

The Mars2020 Perseverance Rover landed successfully onto the Martian surface on the Jezero Crater floor (18°N, 77°E) at the Martian solar longitude L_s 5° in February 2021. Since then it has produced highly valuable environmental measurements with a versatile scientific payload including a suite of environmental sensors MEDA (Mars Environmental Dynamics Analyzer). One of the MEDA sensor systems is MEDA PS pressure device weighing 40 grams.

The Martian atmospheric pressure observations by MEDA PS have proved to be of excellent quality fulfilling expectations with the estimated overall uncertainty being equal or better than 3.5 Pa and the resolution about 0.13 Pa. The system resources required by the whole MEDA PS package are dimensions being 62×50×17 mm, mass 40g and power consumption less than 15 mW.

This paper presents initial results of the first 414 sols of Martian atmospheric surface pressure observations by the MEDA PS device whose performance was found to fulfill the specification. Observations controlled by the Perseverance resources allocation schedule cover approximately 50 – 70 % of the Perseverance operational time.

The atmospheric pressure measurement device (MEDA PS) is based on the silicon-micro-machined pressure sensor head (Barocap®) and transducer technology developed by Vaisala Inc. The Barocap® version used by MEDA PS is optimized for the Martian near-surface atmospheric pressure. The transducer electronics and required electromagnetic shielding and mechanical support structures were developed by Finnish Meteorological Institute (FMI).

The MEDA PS pressure device is making measurements continuously with 1 Hz frequency in average for every other hour according to the operational schedule by the Persevereance Rover. That enables us to generate data sets with averaged pressure measurements approximately at 1-hour intervals, as well as data sets with pressure observations at 1 second intervals for one or a few hours in a row for short time scale studies. In this work we use data sets with 1-hour intervals. The 1-hour data sets are not complete but they do have some gaps due to scheduling of Perseverance and MEDA operations. However, the available data coverage allows good characterisation of both the diurnal and seasonal variations in the pressure.

The seasonal-to-annual time scales the CO2 condensation-sublimation cycle of the Martian atmosphere is nicely demonstrated at the Jezero crater site by the Perseverance Rover measurements.The observed sol-averaged atmospheric pressure during the 414 first Perseverance sols from the landing time at early Northern springtime to Northern fall follow an anticipated pattern of total pressure variation in the course of the advancing season. The data has the first maximum in late spring roughly on the Perseverance sol 110 and minimum on sol 310, whereas by the Perseverance sol 414 corresponding to approximately L_s 212° the atmospheric pressure is climbing higher than the first maximum toward the seasonal maximum. When comparing Perseverance with concurrent observations by the Curiosity Rover and the Insight lander as well as with the historical Viking Landers data, we can see distinct differences with the amplitude of the seasonal pressure variation that are due to different surface elevations.

When comparing pressure observations of the seven Martian landing missions on different locations on Mars the first part of seasonal atmospheric pressure cycle measured by Perseverance seems to follow the seasonal increase and decrease in the atmospheric pressure as expected. The visible bias between the landers' pressure observations is largely due to different landing elevations. Detailed investigation reveals that during L_s $0 - 170°$ the Perseverance pressure looks to be decreasing somewhat more slowly than the pressure measured by the historical Viking landers. However, Insight exhibits similar kind of slow pressure decrease and hence this could be due to a regional occurrence possibly related with the regional topography or variability in large scale atmospheric flows.

The observed diurnal pressure amplitude is ranging roughly within 2 -5 % of the sol-averaged pressure with the absolute amplitude (10 – 35 hPa) not having a direct relationship with the sol-averaged pressure. The optical thickness varying with the amount of airborne dust seems to affect considerably the diurnal pressure amplitude. The increase of optical thickness from 0.5 to 0.8 around sols 130-160 seems to raise the diurnal pressure amplitude from approximately 20 hPa to 35 hPa. Regional atmospheric models seem to give roughly similar results on the average diurnal pressure amplitude, when Perseverance -like airborne dust conditions are assumed.

It appears to be evident that the range of diurnal atmospheric pressure varies considerably with location on Mars. The Perseverance diurnal pressure variation seem to be smaller than those measured by the Curiosity rover at Gale crater where tidal forcing is stronger due to the location close to the equator and also due to the fact that at Curiosity's longitude sector eastward and westward modes are expected to interact constructively. Comparison with pressure observations at other Martian sites it looks that also regional and local geography also play a role in the range of observed diurnal pressure variation.

When inspecting the structure of diurnal pressure, 2-4 small peaks appear in the data on each sol (Figure 6). A clear evolution of the peaks can be seen in the stacked diurnal pressure data. During Northern summer (Figure 6, second row from top) diurnal pressure exhibits two distinct and regular peaks, one in the morning around 6-7 AM and the other one around 8-9 PM LTST. During the Northern spring (Figure 6, top row) and fall (Figure 6, lowest rows) this summertime regular pattern is broken into more like four separate peaks whose amplitudes vary along with advancing season.

During Northern springtime - at the start of the mission, Perseverance sols 0-150 - it appears that smaller peaks are superimposed on the larger peaks. These smaller peaks disappear between about sols 150 and 250 (Northern summertime) and return around sol 300 in early fall. The wintertime has not yet come during the first 414 Perseverance sols. The features in the plots give clues on the behaviour of regional atmospheric dynamics and circulation patterns in the Martian atmosphere

The daily surface pressure profile seems to exhibit a largely repeatable two-peak shape during the Northern summertime (Figure 6). This is probably mostly due to the strong semi-diurnal thermal tidal component, which seems to be the case as illustrated in Figure 7.

MEDA PS observations allow us to estimate that about 100 thermal vortices with ¿ 0.5 Pa pressure drops during a 20 sol period throughout the first 414 Perseverance sols. Based on this analysis, the vortex activity at Jezero crater in the vicinity of Perseverance seems to be nearly constant with little seasonal variation. Apparently solar forcing varying considerably from springtime to fall has not affected the frequency of occurrence of thermal vortices. It is interesting to see whether this pattern will hold through the upcoming Northern wintertime.

Through *in situ* pressure observations and regional atmospheric modeling results a distinct local circulation pattern including nighttime katabatic and daytime upslope flows over the boundary of the Jezero crater was discovered. This circulation amplifies the diurnal pressure variation.

For comparison, the Gale crater diurnal pressure amplitude measured by the Curiosity Rover is much larger (50 to 120 hPa) than at the Jezero crater. This may be due to the fact that Gale is smaller and deeper than Jezero resulting in a stronger diurnal pressure cycle due to hydrostatic adjustment. On the plateaus with more gentle local circulation the diurnal pressure variation based on Viking Lander observations is weaker than at the Gale crater and about the same as given by Perseverance observations. On the other hand Insight diurnal pressure is higher than that of Perseverance during Northern springtime and summer but assumes roughly the same level during fall. Apparently the behavior of local diurnal pressure is affected by a mixture of solar forcing on the surface, airborne dust, regional geography and atmospheric wave activity.

The observed diurnal pressure variation seems to have a significant seasonal dependence. During Northern summer diurnal pressure displays two distinct and regular peaks, one in the morning around 6-7 AM and the other one around 8-9 PM LTST. This regular pattern is likely caused by the interaction of strong thermal tide and the seasonally varying airborne dust causing an amplified semi-diurnal component. During the Northern fall and spring this summertime regular pattern is broken into four separate peaks whose amplitudes vary along with advancing season.

The seasonal form of the diurnal pressure variation was investigated through regional atmospheric modeling by Mars WRF and MRAMS limited area models using the modeling results described in Pla-Garcia et al. (2020). The modeling results were compared with actual MEDA PS observations at solar longitude values L_s 0°, 90° and 180°, as well as with the MCD data. In the summertime (midsummer L_s 90°) the modeling results match very well with the shape and two-peak pattern of diurnal pressure cycle, but they underestimate the average pressure level. These modeling results showed the importance of the boundary fields for the regional models in getting pressure levels correct. Also the complexity of the diurnal pressure signal especially during the springtime and fall was revealed.

Overall, the modeling data seems to fit surprisingly well with the Perseverance pressure observations. Mars WRF and MRAMS have higher resolution than the relatively coarse MCD and hence these models pick up the local daily pressure variation better than MCD. But even the MCD seems to work surprisingly well, which is an excellent indication of the capabilities of current Martian atmospheric modeling tools. The modelling data indicates that they are correctly modelling the large-scale forcing of the main components of the daily pressure curves.

These modeling efforts underlined the clear need to investigate more in detail the diurnal pressure cycle as a superposition of the thermal tide, regional and local crater circulations and of various barotropic and baroclinic wave forms with seasonal dependence. These differences between the models and the observations inform us about the needs and areas to focus on in improving atmospheric models.

8 Open Research

The observational data used for this work is available in Planetary Data System (PDS) at the web site https://pds.nasa.gov/. MEDA instrument data is available in the PDS Atmospheres node in https://doi.org/10.17189/1522849 (Rodriguez-Manfredi & de la Torre Juarez, 2021).

Acknowledgments

Ari-Matti Harri, Mark Paton, Maria Hieta and Jouni Polkko are thankful for the Finnish Academy grant number 310509. Agustín Sánchez-Lavega and Ricardo Hueso were supported by Grant PID2019-109467GB-I00 funded by MCIN/AEI/10.13039/501100011033/ and by Grupos Gobierno Vasco IT1742-22.

References

Barnes, J. R., Pollack, J. B., Haberle, R. M., Leovy, C. B., Zurek, R. W., Lee, H., & Schaeffer, J. (1993). Mars atmospheric dynamics as simulated by the NASA Ames General Circulation Model, 2, transient baroclinic eddies. *J. Geophys. Res.*, *98*, 3125–3148.

Basu, S., Richardson, M. I., & Wilson, R. J. (2004, November). Simulation of the Martian dust cycle with the GFDL Mars GCM. *Journal of Geophysical Research (Planets)*, *109*(E11), E11006. doi: 10.1029/2004JE002243

Battalio, J. M., & Lora, J. M. (2021, August). Annular modes of variability in the atmospheres of Mars and Titan. *Nature Astronomy*, *5*, 1139-1147. doi: 10.1038/s41550-021-01447-4

Ferri, F., Smith, P. H., Lemmon, M., & Rennó, N. O. (2003, December). Dust devils as observed by Mars Pathfinder. *Journal of Geophysical Research (Planets)*, *108*(E12), 5133. doi: 10.1029/2000JE001421

Forget, F., Hourdin, F., Fournier, R., Hourdin, C., Talagrand, O., Collins, M., ... Huot, J.-P. (1999, October). Improved general circulation models of the Martian atmosphere from the surface to above 80 km. *J. Geophys. Res.*, *104*, 24155-24176. doi: 10.1029/1999JE001025

Golombek, M., Williams, N., Warner, N. H., Parker, T., Williams, M. G., Daubar, I., ... Sklyanskiy, E. (2020, October). Location and Setting of the Mars InSight Lander, Instruments, and Landing Site. *Earth and Space Science*, *7*(10), e01248. doi: 10.1029/2020EA001248

Golombek, M. P., Bridges, N. T., Moore, H. J., Murchie, S. L., Murphy, J. R., Parker, T. J., ... Wilson, G. R. (1999, April). Overview of the Mars Pathfinder Mission: Launch through landing, surface operations, data sets, and science results. *J. Geophys. Res.*, *104*(E4), 8523-8554. doi: 10.1029/98JE02554

Gómez-Elvira, J., Armiens, C., Castañer, L., Domínguez, M., Genzer, M., Gómez, F., ... Martín-Torres, J. (2012, September). REMS: The Environmental Sensor Suite for the Mars Science Laboratory Rover. *Space Sci. Rev.*, *170*, 583-640. doi: 10.1007/s11214-012-9921-1

Guo, X., Lawson, W. G., Richardson, M. I., & Toigo, A. (2009, July). Fitting the Viking lander surface pressure cycle with a Mars General Circulation Model. *Journal of Geophysical Research (Planets)*, *114*(E7), E07006. doi: 10.1029/2008JE003302

Guzewich, S. D., Newman, C. E., de la Torre Juárez, M., Wilson, R. J., Lemmon, M., Smith, M. D., ... Harri, A. M. (2016, April). Atmospheric tides in Gale Crater, Mars. *Icarus*, *268*, 37-49. doi: 10.1016/j.icarus.2015.12.028

Haberle, Houben, H. C., Hertenstein, R., & Herdtle, T. (1993, June). A boundary-layer model for Mars - Comparison with Viking lander and entry data. *J. Atmos. Sci.*, *50*, 1544-1559. doi: 10.1175/1520-0469(1993)050⟨1544:ABLMFM⟩2.0.CO;2

Haberle, R. M., Gómez-Elvira, J., de la Torre Juárez, M., Harri, A.-M., Hollingsworth, J. L., Kahanpää, H., ... Teams, R. S. (2014). Preliminary interpretation of the rems pressure data from the first 100 sols of the msl mission. *Journal of Geophysical Research: Planets*, *119*(3), 440-453. Retrieved from `https://agupubs.onlinelibrary.wiley.com/doi/abs/10.1002/2013JE004488` doi: https://doi.org/10.1002/2013JE004488

Harri, A. M., Genzer, M., Kemppinen, O., Kahanpää, H., Gomez-Elvira, J., Rodriguez-Manfredi, J. A., ... REMS/MSL Science Team (2014, January). Pressure observations by the Curiosity rover: Initial results. *Journal of Geophysical Research (Planets)*, *119*(1), 82-92. doi: 10.1002/2013JE004423

Hess, S. L., Ryan, J. A., Tillman, J. E., Henry, R. M., & Leovy, C. B. (1980, March). The annual cycle of pressure on Mars measured by Viking landers 1 and 2. *Geophys. Res. Lett.*, *7*, 197-200. doi: 10.1029/GL007i003p00197

Hourdin, F., Le van, P., Forget, F., & Talagrand, O. (1993, November). Meteorological Variability and the Annual Surface Pressure Cycle on Mars. *Journal of Atmospheric Sciences*, *50*(21), 3625-3640. doi: 10.1175/1520-0469(1993)050⟨3625:MVATAS⟩2.0.CO;2

Hueso, R., Newman, C. E., del Río-Gaztelurrutia, T., Munguira, A., Sánchez-Lavega, A., Toledo, D., ... Lepinette-Malvite, A. (2023). Convective vortices and dust devils detected and characterized by mars 2020. *Journal of Geophysical Research: Planets*, *128*(2), e2022JE007516. Retrieved from `https://agupubs.onlinelibrary.wiley.com/doi/abs/10.1029/2022JE007516` (e2022JE007516 2022JE007516) doi: https://doi.org/10.1029/2022JE007516

James, P. B., Kieffer, H. H., & Paige, D. A. (1992). The seasonal cycle of carbon dioxide on Mars. In H. H. Kieffer, B. M. Jakosky, C. W. Snyder, & M. S. Matthews (Eds.), *Mars* (p. 934-968). University of Arizona Press.

Kahre, M. A., & Haberle, R. M. (2010, June). Mars CO_2 cycle: Effects of airborne dust and polar cap ice emissivity. *Icarus*, *207*, 648-653.

Kieffer, H. H., Chase, S. C., Miner, E. D., Munch, G., & Neugebauer, G. (1973). Preliminary report on infrared radiometric measurements from the Mariner 9 spacecraft. *J. Geophys. Res.*, *78*, 4291–4312.

Kieffer, H. H., Jakosky, B. M., Snyder, C. W., & Matthews, M. S. (Eds.). (1992). *Mars*. University of Arizona Press.

Kieffer, H. H., Martin, T. Z., Peterfreund, A. R., Jakosky, B. M., Miner, E. D., & Palluconi, F. D. (1977). Thermal and albedo mapping of Mars during the Viking primary mission. *J. Geophys. Res.*, *82*, 4249–4291.

Kliore, A., Cain, D. L., Fjeldbo, G., Seidel, B. L., Sykes, M. J., & Woiceshyn, P. M. (1973, March). Some Recent Results of Mariner 9 Occultation Measurements of Mars. In *Bulletin of the american astronomical society* (Vol. 5, p. 298).

Kliore, A., Cain, D. L., Levy, G. S., Eshleman, V. R., Fjeldbo, G., & Drake, F. D. (1965, September). Occultation Experiment: Results of the First Direct Measurement of Mars's Atmosphere and Ionosphere. *Science*, *149*(3689), 1243-1248. doi: 10.1126/science.149.3689.1243

Kliore, A., Fjeldbo, G., Seidel, B. L., & Rasool, S. I. (1969, December). Mariners 6 and 7: Radio Occultation Measurements of the Atmosphere of Mars. *Science*, *166*(3911), 1393-1397. doi: 10.1126/science.166.3911.1393

Lee, C., Lawson, W. G., Richardson, M. I., Anderson, J. L., Collins, N., Hoar, T., & Mischna, M. (2011, November). Demonstration of ensemble data assimilation for Mars using DART, MarsWRF, and radiance observations from MGS TES. *Journal of Geophysical Research (Planets)*, *116*(E11), E11011. doi: 10.1029/2011JE003815

Lemmon, M. T., Smith, M. D., Viudez-Moreiras, D., de la Torre-Juarez, M., Vicente-Retortillo, A., Munguira, A., ... Apestigue, V. (2022). Dust, sand, and winds within an active martian storm in jezero crater. *Geophysical Research Letters*, *49*(17), e2022GL100126. Retrieved from `https://agupubs.onlinelibrary.wiley.com/doi/abs/10.1029/2022GL100126` (e2022GL100126 2022GL100126) doi: https://doi.org/10.1029/2022GL100126

Leovy, C. B., & Mintz, Y. (1969). Numerical simulation of the atmospheric circulation and climate of Mars. *J. Geophys. Res.*, *26*, 1167–1190.

LMD-Jussieu. (2021). *Mcd - mars climate database.* Retrieved from `http://www-mars.lmd.jussieu.fr/` (Accessed = 2022-8-26)

Montabone, L., Forget, F., Millour, E., Wilson, R. J., Lewis, S. R., Cantor, B., ... Wolff, M. J. (2015). Eight-year climatology of dust optical depth on mars. *Icarus*, *251*, 65-95. (Dynamic Mars) doi: https://doi.org/10.1016/j.icarus.2014.12.034

Montabone, L., Marsh, K., Lewis, S. R., Read, P. L., Smith, M. D., Holmes, J., ... Pamment, A. (2014). The mars analysis correction data assimilation (macda) dataset v1.0. *Geoscience Data Journal*, *1*(2), 129-139. Retrieved from https://rmets.onlinelibrary.wiley.com/doi/abs/10.1002/gdj3.13 doi: https://doi.org/10.1002/gdj3.13

Newman, C., Bertrand, T., Battalio, J., Day, M., De La Torre Juárez, M., Elrod, M. K., ... Zorzano, M.-P. (2021, May). Toward More Realistic Simulation and Prediction of Dust Storms on Mars. In *Bulletin of the american astronomical society* (Vol. 53, p. 278). doi: 10.3847/25c2cfeb.726b0b65

Newman, C., Juárez, M., Pla-García, J., Wilson, R., Lewis, S., Neary, L., ... Rodriguez-Manfredi, J. (2021, 02). Multi-model meteorological and aeolian predictions for mars 2020 and the jezero crater region. *Space Science Reviews*, *217*. doi: 10.1007/s11214-020-00788-2

Newman, C. E., Gómez-Elvira, J., Marin, M., Navarro, S., Torres, J., Richardson, M. I., ... Bridges, N. T. (2017, July). Winds measured by the Rover Environmental Monitoring Station (REMS) during the Mars Science Laboratory (MSL) rover's Bagnold Dunes Campaign and comparison with numerical modeling using MarsWRF. *Icarus*, *291*, 203-231. doi: 10.1016/j.icarus.2016.12.016

Newman, C. E., Hueso, R., Lemmon, M. T., Munguira, A., Álvaro Vicente-Retortillo, Apestigue, V., ... Guzewich, S. D. (2022). The dynamic atmospheric and aeolian environment of jezero crater, mars. *Science Advances*, *8*(21), eabn3783. Retrieved from https://www.science.org/doi/abs/10.1126/sciadv.abn3783 doi: 10.1126/sciadv.abn3783

Newman, C. E., Lee, C., Mischna, M. A., Richardson, M. I., & Shirley, J. H. (2019, January). An initial assessment of the impact of postulated orbit-spin coupling on Mars dust storm variability in fully interactive dust simulations. *Icarus*, *317*, 649-668. doi: 10.1016/j.icarus.2018.07.023

Paige, D. A., & Ingersoll, A. P. (1985, June). Annual Heat Balance of Martian Polar Caps: Viking Observations. *Science*, *228*(4704), 1160-1168. doi: 10.1126/science.228.4704.1160

Pollack, J. B., Haberle, R. M., Schaeffer, J., & Lee, H. (1990). Simulations of the general circulation of the Martian atmosphere 1. polar processes. *J. Geophys. Res.*, *95*, 1447–1473.

Pollack, J. B., Leovy, C. B., Greiman, P. W., & Mintz, Y. (1981). A Martian general circulation experiment with large topography. *J. Atmos. Sci.*, *38*, 3–29.

Rafkin, S. C. R., Pla-Garcia, J., Kahre, M., Gomez-Elvira, J., Hamilton, V. E., Marín, M., ... Vasavada, A. (2016, December). The meteorology of Gale Crater as determined from Rover Environmental Monitoring Station observations and numerical modeling. Part II: Interpretation. *Icarus*, *280*, 114-138. doi: 10.1016/j.icarus.2016.01.031

Read, P., & Lewis, S. (2004). *The martian climate revisited - atmosphere and environment of a desert planet.* Springer.

Richardson, M. I., & Newman, C. E. (2018, December). On the relationship between surface pressure, terrain elevation, and air temperature. Part I: The large diurnal surface pressure range at Gale Crater, Mars and its origin due to lateral hydrostatic adjustment. *Planet. Space Sci.*, *164*, 132-157. doi: 10.1016/j.pss.2018.07.003

Richardson, M. I., Toigo, A. D., & Newman, C. E. (2007). PlanetWRF: A general purpose, local to global numerical model for planetary atmospheric and climate dynamics. *J. Geophys. Res.*, *112*, 9001. doi: 10.1029/2006JE002825

Rodriguez-Manfredi, J. A., de la Torre Juárez, M., Alonso, A., Apéstigue, V., Arruego, I., Atienza, T., ... MEDA Team (2021, April). The Mars Environmental Dynamics Analyzer, MEDA. A Suite of Environmental Sensors for the Mars 2020 Mission. *Space Sci. Rev.*, *217*(3), 48. doi: 10.1007/s11214-021-00816-9

Rodriguez-Manfredi, J. A., & de la Torre Juarez, M. (2021). *Mars 2020 meda bundle dataset.* (NASA. Retrievable from https://doi.org/10.17189/1522849)

Rogberg, P., Read, P. L., Lewis, S. R., & Montabone, L. (2010, August). Assessing atmospheric predictability on Mars using numerical weather prediction and data assimilation. *Quarterly Journal of the Royal Meteorological Society*, *136*(651), 1614-1635. doi: 10.1002/qj.677

Savijärvi, H., & Kauhanen, J. (2008, April). Surface and boundary-layer modelling for the mars exploration rover sites. *Quarterly J. Royal Met. Soc.*, *134*, 635-641. doi: 10.1002/qj.232

Savijärvi, H., & Määttänen, A. (2010, August). Boundary-layer simulations for the Mars Phoenix lander site. *Quarterly J. Royal Met. Soc.*, *136*, 1497-1505. doi: 10.1002/qj.650

Schofield, J. T., Barnes, J. R., Crisp, D., Haberle, R. M., Larsen, S., Magalhaes, J. A., ... Wilson, G. (1997, December). The Mars Pathfinder Atmospheric Structure Investigation/Meteorology. *Science*, *278*, 1752. doi: 10.1126/science.278.5344.1752

Smith, D. E., Zuber, M. T., Frey, H. V., Garvin, J. B., Head, J. W., Muhleman, D. O., ... Sun, X. (2001, October). Mars Orbiter Laser Altimeter: Experiment summary after the first year of global mapping of Mars. *J. Geophys. Res.*, *106*(E10), 23689-23722. doi: 10.1029/2000JE001364

Snyder, C. W., & Moroz, V. I. (1992). Spacecraft exploration of Mars. In H. H. Kieffer, B. M. Jakosky, C. W. Snyder, & M. S. Matthews (Eds.), *Mars* (p. 71-119). University of Arizona Press.

Soffen, G. A. (1976, December). Scientific results of the Viking missions. *Science*, *194*, 1274-1276. doi: 10.1126/science.194.4271.1274

Soffen, G. A. (1977, September). The viking project. *J. Geophys. Res.*, *82*, 3959-3970. doi: 10.1029/JS082i028p03959

Sánchez-Lavega, A., del Rio-Gaztelurrutia, T., Hueso, R., Juárez, M. d. l. T., Martínez, G. M., Harri, A.-M., ... Mäkinen, T. (2023). Mars 2020 perseverance rover studies of the martian atmosphere over jezero from pressure measurements. *Journal of Geophysical Research: Planets*, *128*(1), e2022JE007480. Retrieved from `https://agupubs.onlinelibrary.wiley.com/doi/abs/10.1029/2022JE007480` (e2022JE007480 2022JE007480) doi: https://doi.org/10.1029/2022JE007480

Taylor, P. A., Catling, D. C., Daly, M., Dickinson, C. S., Gunnlaugsson, H. P., Harri, A.-M., & Lange, C. F. (2008, July). Temperature, pressure, and wind instrumentation in the Phoenix meteorological package. *J. Geophys. Res.*, *113*, 0. doi: 10.1029/2007JE003015

Tillman, J. E. (1988, August). Mars global atmospheric oscillations - Annually synchronized, transient normal-mode oscillations and the triggering of global dust storms. *J. Geophys. Res.*, *93*, 9433-9451. doi: 10.1029/JD093iD08p09433

Tillman, J. E., Henry, R. M., & Hess, S. L. (1979, June). Frontal systems during passage of the Martian north polar HOOD over the Viking Lander 2 site prior to the first 1977 dust storm. *J. Geophys. Res.*, *84*, 2947-2955. doi: 10.1029/JB084iB06p02947

Tillman, J. E., Johnson, N. C., Guttorp, P., & Percival, D. B. (1994). Erratum: "The Martian annual atmospheric pressure cycle: Years without great dust storms" [J. Geophys. Res., 98(E6), 10,963-10,971 (1993]. *J. Geophys. Res.*, *99*, 3813-3814. doi: 10.1029/94JE00232

Toigo, A. D., & Richardson, M. I. (2003, November). Meteorology of proposed Mars Exploration Rover landing sites. *Journal of Geophysical Research (Planets)*, *108*(E12), 8092. doi: 10.1029/2003JE002064

Wilson, R. J., & Hamilton, K. (1996, May). Comprehensive model simulation of thermal tides in the Martian atmosphere. *Journal of Atmospheric Sciences*, *53*(9), 1290-1326. doi: 10.1175/1520-0469(1996)053⟨1290:CMSOTT⟩2.0.CO;2

Young, L. D. G. (1969, November). Interpretation of High-Resolution Spectra of Mars. I. CO_2 Abundance and Surface Pressure Derived from the Curve of

Growth. *icarus*, *11* (3), 386-389. doi: 10.1016/0019-1035(69)90070-0

Zurek, R. W. (1978, August). Solar heating of the Martian dusty atmosphere. *Icarus*, *35*, 196-208. doi: 10.1016/0019-1035(78)90005-2

Zurek, R. W. (1981, January). Inference of dust opacities for the 1977 Martian great dust storms from Viking Lander 1 pressure data. *Icarus*, *45*, 202-215. doi: 10.1016/0019-1035(81)90014-2

Zurek, R. W. (1982, June). Martian great dust storms - an update. *Icarus*, *50*, 288-310. doi: 10.1016/0019-1035(82)90127-0

Zurek, R. W. (1992). Comparative aspects of the climate of Mars: an introduction to the current atmosphere. In H. H. Kieffer, B. M. Jakosky, C. W. Snyder, & M. S. Matthews (Eds.), *Mars* (p. 799-817). University of Arizona Press.

Zurek, R. W., Barnes, J. R., Haberle, R. M., Pollack, J. B., Tillman, J. E., & Leovy, C. B. (1992a). Dynamics of the atmosphere of Mars. In H. H. Kieffer, B. M. Jakosky, C. W. Snyder, & M. S. Matthews (Eds.), *Mars* (p. 835-934). University of Arizona Press.

Zurek, R. W., Barnes, J. R., Haberle, R. M., Pollack, J. B., Tillman, J. E., & Leovy, C. B. (1992b). Dynamics of the atmosphere of Mars. In H. H. Kieffer, B. M. Jakosky, C. W. Snyder, & M. S. Matthews (Eds.), *Mars* (p. 835–934). University of Arizona Press.